Synthesis and characterization of 3,3”-dihydroxy-[1,1’:4’,1”-terphenyl]-4,4”-dicarboxylic acid derivatives as precursors for functionalized Co-MOF-74-III materials

A dissertation submitted in accordance with the requirements for the degree

Magister Scientiae

in the

Department of Chemistry

Faculty of Natural and Agricultural Science

at the

University of the Free State

by

Annelmie Crause

Supervisor

Dr. E.H.G. Langner

January 2017

Acknowledgements

First and foremost, praise and thanks to God, the Almighty, for His showers of blessings throughout my studies and in completing this research successfully. I would like to thank my family, friends and colleagues for their support, friendship and guidance throughout this period. Special thanks must be made to the following people:

My supervisor: Dr. E.H.G. Langner, for his guidance, leadership and kindness throughout the course of study. It has been a privilege to be your student.

My loving family, my father (James Crause), mother (Karien Crause) and sisters (Mariska Crause and Mare-Lise Badenhorst). Your love, guidance, support and PATIENCE over the years are the reason I am here today. If not for you, I would not have this opportunity. Thanks to my sister's husband (Danie Badenhorst) for the cacti, this gave some peaceful hours during the write-up process.

Physical Chemistry group: thank you ALL for your collegial support and guidance throughout this study and for always helping me when needed. Also, thank you for the laughter and fun throughout this study. To the coffee team (you know who you are) thank you for the time we have shared drinking coffee and eating cookies, it helped to clear my head and get the caffeine levels optimal. Behind every successful person there is a substantial amount of COFFEE…

I would like to acknowledge the Chemistry Department at UFS for the available facilities. A special thanks to the National Research Foundation at the University of the Free State for their financial support.

In memory of my late

grandfather, Walter Kruger

(18 March 1941 – 23 January 2015)

&

grandmother, Alta Kruger

(18 July 1946 – 16 September 2016)

~ You are forever present in my heart

Table of Contents

Abbreviations

MeOH	Methanol
EtOH	Ethanol
DCM	Dichloromethane
DMF	Dimethylformamide
MEMCl	Methoxyethoxymethoxy chloride
MEM	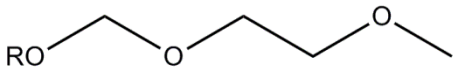
MOF	Metal-organic framework
THP	Tetrahydropyranyl
MOM	Methoxymethyl
IR	Infrared Spectroscopy
ASAP	Accelerated Surface Area and Porosity Analysis
NMR	Nuclear Magnetic Resonance
Boc	Tertbutyloxycarbonyl
TGA	Thermal Gravimetric Analysis
SEM	Scanning Electron Microscopy
CV	Cyclic Voltammetry
i_{pa}	Anodic peak current
i_{pc}	Cathodic peak current
E_{pa}	Anodic peak potential
E_{pc}	Cathodic peak potential
$E^{0\prime}$	Formal reduction potential
PSM	Post-synthetic modification
BET	Brunauer, Emmett and Teller
Fc	Ferrocene
FTIR	Fourier Transform Infrared Spectroscopy
PSM	Post-Synthetic Modification

List of Novel Compounds

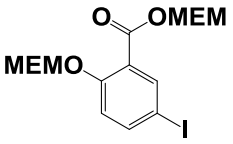

1

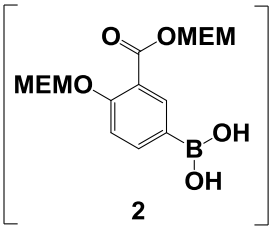

2

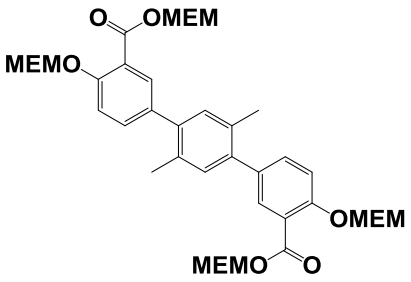

3

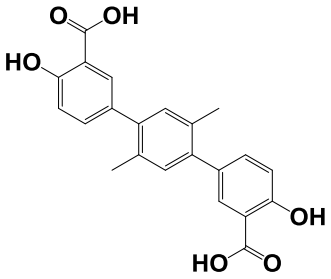

4

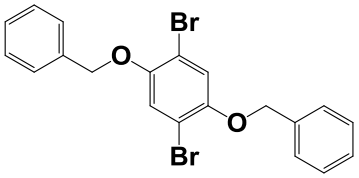

5

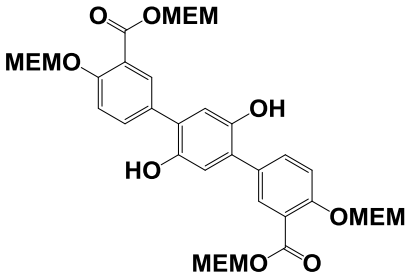

6

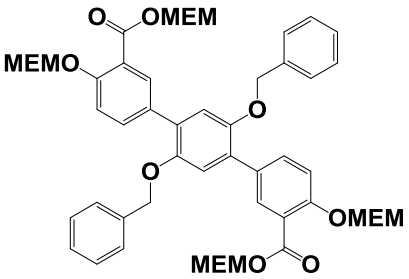

8

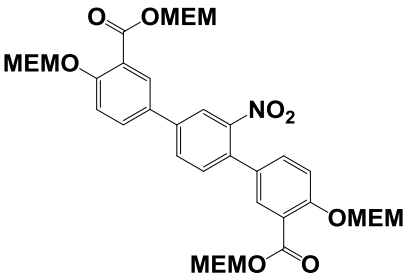

12

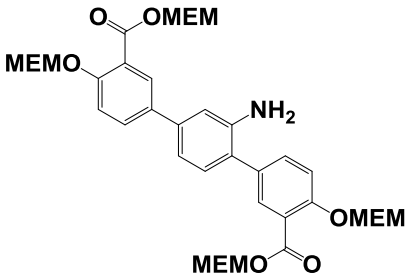

13

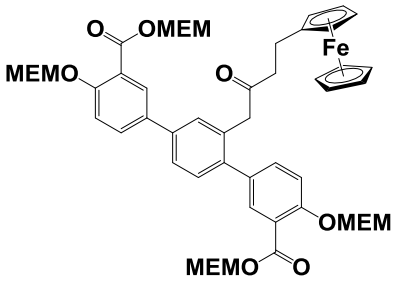

14

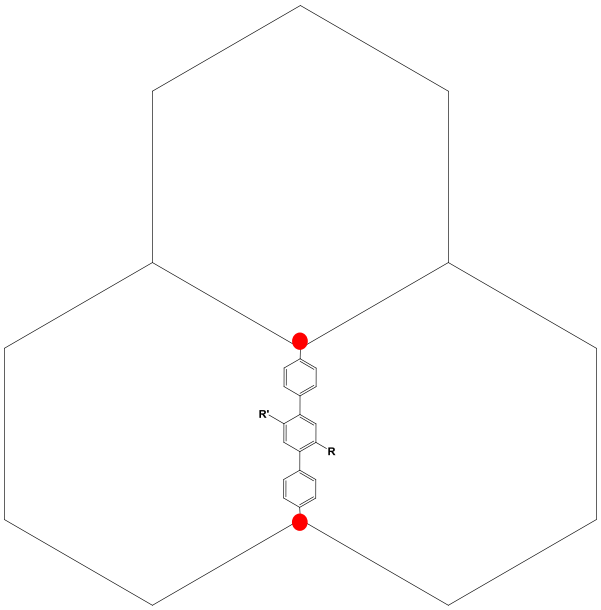

Co-MOF-74-III-Me, 15, where R = R' = CH_3

Co-MOF-74-III-OBn, 17, where R = R' = -O-CH_2-C_6H_5

Co-MOF-74-III-OH, 16, where R = R' = OH

Co-MOF-74-III-NHCOCH_2CH_2Fc, 18, where R = R' = -NHCO($CH_2)_2$Fc

Red = Co-metal center

Abstract

A series of new 4,4”-di[methoxyethoxymethoxy]-[1,1’:4’,1”-terphenyl]-3,3”-di[methoxy-ethoxymethoxycarbonyl] derivatives were synthesised as possible linkers for MOF-74-III derivatives. The following products were synthesised via Suzuki-Miyuara cross-coupling and characterized by a combination of FTIR and ^{1}H NMR spectroscopy as well as MS spectrometry: 4,4”-di[methoxyethoxymethoxy]-2’,5’-dimethyl-[1,1’:4’,1”-terphenyl]-3,3”-di[methoxyethoxy-methoxycarbonyl], (90 %); 4,4”-di[methoxyethoxymethoxy]-2’,5’-dihydroxy-[1,1’:4’,1”-terphenyl]-3,3”-di[methoxyethoxymethoxycarbonyl], (90 %); 4,4”-di[methoxyethoxy-methoxy]-2’,5’-bis-benzyloxy-[1,1’:4’,1”-terphenyl]-3,3”-di[methoxyethoxymethoxycarbonyl], (60 %) and 4,4”-di[methoxyethoxymethoxy]- 3’-[3-ferrocenylpropamide]-[1,1’:4’,1”-terphenyl]-3,3”-di[methoxyethoxymethoxycarbonyl], (70 %). Novel methods were developed for the syntheses of these linkers, with a different structural orientation than these found in literature. A generalized method, using methoxyethoxymethoxychloride (MEMCl), was developed for the protection of the hydroxy- and carbonyl-functionalities on these ligands Two MOF-74-III derivatives, Co-MOF-74-III-Me, and Co-MOF-74-III-NHCOCH$_2$CH$_2$Fc were successful synthesised from the methylated and ferrocene-containing linkers respectively.

Co-MOF-74-III-Me is mesoporous with a pore width of 32.6 Å. Co-MOF-74-III-Me and Co-MOF-74-III-NHCOCH$_2$CH$_2$Fc are both thermally stable up to 180 ^{o}C.

All the 4,4”-di[methoxyethoxymethoxy]-[1,1’:4’,1”-terphenyl]-3,3”-di[methoxyethoxy-methoxycarbonyl] derivatives showed irreversible redox couples for the carbonyl functionalities of the MEM-groups (-1500 mV vs. FcH/FcH^{+}). An additional redox couple (-2160 mV vs. FcH/FcH^{+}) was found for the amide functionality of the 4,4”-di[methoxyethoxymethoxy]- 3’-[3-ferrocenylpropamide]-[1,1’:4’,1”-terphenyl]-3,3”-di[methoxyethoxymethoxycarbonyl] ligand. Solid state cyclic voltammetry of Co-MOF-74-III-NHCOCH$_2$CH$_2$Fc, showed a redox couple (17 mV vs. FcH/FcH^{+}) for the ferrocenyl fragments on the linkers, detected because electron transfer through the mesoporous material was fast enough.

Keywords: Linkers; MOF-74-III; Suzuki-Miyuara cross-coupling; MEMCl; ferrocene; amide; protecting groups; redox couples; surface area; pore size.

Opsomming

ʻn Reeks 4,4”-di[metoksie-etoksiemetoksie]-[1,1’:4’,1”-trifeniel]-3,3”-di[metoksie-etoksiemetoksiekarboniel] derivate is as moontlike skakels vir MOF-74-III derivate gesintetiseer. Die volgende produkte is gesintetiseer via Suzuki-Miyuara kruiskoppeling en gekarakteriseer deur ‘n kombinasie van FTIR en ^{1}H KMR spektroskopie, sowel as MS spektrometrie: 4,4”-di[metoksie-etoksiemetoksie]-2’, 5’-dimetiel-[1,1’:4’,1”-trifeniel]-3,3”-di[metoksie-etoksiemetoksiekarboniel], (90 %); 4,4”-di[metoksie-etoksiemetoksie]-2’, 5’-dihidroksi-[1,1’:4’,1”-trifeniel]-3,3”-di[metoksie-etoksiemetoksiekarboniel], (90 %); 4,4”-di[metoksie-etoksiemetoksie]-2’, 5’-bis-bensieloksi-[1,1’:4’,1”-trifeniel]-3,3”-di[metoksieetoksie-metoksiekarboniel], (70 %);4,4”-di[metoksie-etoksiemetoksie]-3’-[3-ferroseniel-propaanamied]-[1,1’:4’,1”-trifeniel]-3,3”-di[metoksie-etoksiemetoksiekarboniel], (70 %). Nuwe metodes is ontwikkel vir die sintese van hierdie skakels, met ‘n ander strukturele oriëntasie as dié uit die literatuur. ‘n Algemene metode wat gebruik maak van metoksi-etoksimetoksichloried (MEMCl) is ontwikkel vir die beskerming van die hidroksi- en karboniel-funksionaliteite, op hierdie ligande. Twee MOF-74-III derivate, Co-MOF-74-III-Me en Co-MOF-74-III-NHCOCH$_2$CH$_2$Fc is suksesvol gesintetiseer vanaf die gemetileerde en ferroseen-bevattende ligande onderskeidelik.

Co-MOF-74-III-Me is mesoporeus met ‘n poriegrootte van 32.6 Å. Co-MOF-74-III-Me en Co-MOF-74-III-NHCOCH$_2$CH$_2$Fc, is buide termiese stabiel tot en met 180 ^{o}C.Al die 4,4”-di[metoksi-etoksimetoksi]-[1,1’:4’,1”-trifeniel]-3,3”-di[metoksie-etoksiemetoksie-karboniel] derivate het onomkeerbare redokskoppels getoon vir die karboniel-funksionaliteite van die MEM-groepe (-1500 mV vs. FcH/FcH^{+}). ʻn Bykomende redokskoppel (-2160 mV vs. FcH/FcH^{+}) was sigbaar vir die amiedfunksionaliteit van die 4,4”-di[metoksie-etoksiemetoksie]-3’-[3-ferrosenielpropaanamied]-[1,1’:4’,1”-trifeniel]-3,3”-di[metoksie-etoksiemetoksiekarboniel] ligand. Vastetoestand sikliese voltammetrie van Co-MOF-74-III-NHCOCH$_2$CH$_2$Fc, het ‘n redokskoppel (17 mV vs. FcH/FcH^{+}) getoon vir die ferrosenielfragmente op die skakels, waargeneem omdat elektronoordrag vinnig genoeg deur die mesoporeuse materiaal kon plaasvind.

Sleutelwoorde: Ligande; MOF-74-III; Suzuki-Miyuara Kruiskoppeling; MEMCl; ferroseen; amied; beskermings groepe; redoks koppels; oppervlakte area; porie grootte.

1 Introduction, Aims and Objectives

1.1 Introduction

Metal-organic frameworks (MOFs) are crystalline porous materials[7], synthesised by coordinating organic ligands with inorganic units. An almost endless number of possible combinations of organic and inorganic building blocks already gave rise to more than 20 000 different MOFs to date.[1] After coordination the organic linkers can be chemically adapted towards specific applications.[3] These could be "traditional" applications like gas storage and separation as well as catalysis. MOFs may also be used in biomedical applications as sensor materials and drug carriers.[2]

MOF-74 derivatives with their honeycomb-like structures[4], formed through the coordination of metal ions and dioxidoterephthalate ligands, have unsaturated (open) metal sites that can be varied without affecting the framework structure.[5] These open-metal sites are created when solvent molecules, coordinated to the metal centres during MOF-74 formation, are evacuated during activation.[10] Visitor molecules can bind to these sites, giving MOF-74 an advantage over other MOFs.[12] Although chemical changes to the organic ligands often yield new framework topologies in many MOFs, certain framework types, like MOF-74, are more tolerant towards alteration and change in the chemical nature of these linkers. The pores of the MOF-74 series are enlarged by insertion of phenylene groups into the backbone of the dioxidoterephthalate linkers.[6]

The backbone of the dioxidoterephthalate linker in the MOF-74-III variant consists of three phenylene rings[8], resulting in one dimensional channels with a diameter of 25 Å in the honeycomb topology. [9] Materials with pores wider than 20 Å are mesoporous, ideal for migration of large molecules in and out of the MOF-74-III pores during catalysis, gas separations and storage. This mesoporosity also ensures that bulky substituents on the linkers will not block the channels.

Except for giving a pore diameter of 25 Å, the dioxidoterephthalate linker with three phenylene rings has another advantage: tailorability. A shorter linker with only two phenylene rings has no tailorability, since changes on the phenylene rings will severely disrupt framework formation during MOF synthesis. A third, central phenylene ring provides good attachment sites for functional groups without affecting MOF formation. Longer linkers containing four or more phenylene rings, also allow this tailorability, but are synthesised by increasingly more complex routes. The dioxidoterephthalate derivatives with three phenylene rings are thus the most economical to synthesise.

In this study, linkers with a different substitution pattern for the hydroxy- and carboxylic acid functionalities than in previous studies, will be synthesised. This was never attempted before and, if successful, will reduce the cost of MOF-74-III synthesis.

1.2 Aims and Objectives

i) Synthesis of structural isomers with a different orientation for the hydroxy- and carboxyl functionalities (b) than those currently found in literature (a) will be attempted:

a) Literature:

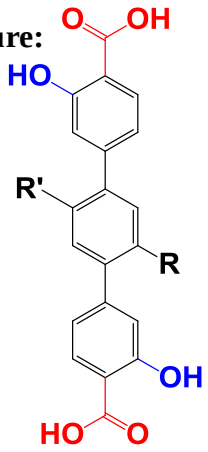

b) Proposed:

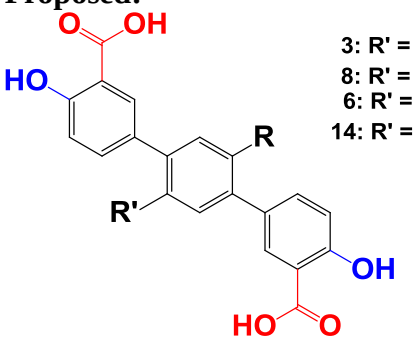

3: R' = R = CH_3
8: R' = R = -O-CH_2-C_6H_5
6: R' = R = OH
14: R' = H; R = -NHCO$(CH_2)_2$Fc

ii) Functionalization of the structural isomers as synthesised in (i) with amine-, hydroxy- and ferrocenyl functionalities. The amide- and hydroxy- functionalities will be used as anchoring sites for carboxylic acids, amides and benxyloxy-groups. Ferrocene derivatives are often employed in cancer therapy and as antioxidants, removing potentially harmful oxidizing agents from the body. Ferrocene derivatives are also used as catalysts for cross-coupling, hydrogenation, allylic substitution, hydroformylation and aldol reactions.[13] A ferrocenyl fragment will be anchored onto the dioxidoterephthalate linker to demonstrate the use of MOF-74-III as drug carrier.

iii) A generalized protection procedure, for the hydroxy- and carboxylic acid functionalities on the dioxidoterephthalate linkers, will be developed. Such a protecting group could reduce the number of synthesis steps and should be easy to introduce and remove.

iv) Characterization of the functionalized 4,4”-di[methoxyethoxymethoxy]-[1,1’:4’,1”-terphenyl]-3,3”-di[methoxyethoxymethoxycarbonyl] derivatives by Nuclear Resonance Spectroscopy (NMR), Fourier Transform Infrared (FTIR) Spectroscopy and Mass Spectrometry (MS).

v) Synthesis of Co-MOF-74-III derivatives from the four differently substituted (-CH_3, -OH, -OBn and -$NHCOCH_2CH_2Fc$) 4,4”-di[methoxyethoxymethoxy]-[1,1’:4’,1”-terphenyl]-3,3”-di[methoxyethoxymethoxycarbonyl] derivatives.

vi) Characterization of the Co-MOF-74-III derivatives by:

a. Accelerated Surface Area and Porosity Analysis (ASAP) to determine the surface area and pore size of the materials.

b. Thermogravimetric analysis (TGA) to determine the thermal stability and decomposition behaviour of the MOF derivatives.

c. Scanning Electron Microscopy (SEM) to view the morphology of the Co-MOF-74-III derivatives.

d. Powder X-Ray Diffraction Spectroscopy (PXRD) and/or Small-angle X-Ray Scattering Spectroscopy (SAXS) to determine the crystal structure.

vii) Liquid state electrochemical studies (cyclic voltammetry) on the new 4,4”-di[methoxy-ethoxymethoxy]-[1,1’:4’,1”-terphenyl]-3,3”-di[methoxyethoxymethoxycarbonyl] derivatives will reveal their redox properties. The redox properties of the ferrocene-containing Co-MOF-74-III derivative, determined with solid state cyclic voltammetry, will be compared to the redox properties of the ferrocene-containing organic linker prior to MOF synthesis.

1.3 References

1. H. Furukawa, K. E. Cordova, M. O'Keeffe, O. M. Yaghi, *Science*, **2013**, 341, 1230444, DOI: 10.1126/science.1230444.
2. N. Stock, S. Biswas, *Chem. Rev*., **2012**, 112, 933.
3. P.C. Banerjee, D.E. Lobo, R. Middag, W.K. Ng, M.E. Shaibani, M. Majumder, *Appl. Mater. Interfaces*, **2015**, 7, 3655.
4. T. Pham, K. A. Forrest, K. McLaughlin, J. Eckert, B. Space, *J. Phys. Chem. C*, **2014,** 118, 22683.
5. T.G. Glover, G.W. Peterson, B.J. Schindler, D. Britt, O.M. Yaghi, *Chemical Engineering Science*, **2011**, 66, 163.
6. J.L.C. Rowsell, O.M. Yaghi, *Microporous and Mesoporous Materials*, **2004**, 73, 3.
7. S. Zuluaga, E. M. A. Fuentes-Fernandez, K. Tan, C. A. Arter, J. Li, Y. J. Chabal and T. Thonhauser, *J. Mater. Chem. A*, **2016**, 4, 13176.
8. H. Deng, S. Grunder, K. E. Cordova, C. Valente, H. Furukawa, M. Hmadeh, F. Gándara, A. C. Whalley, Z. Liu, S. Asahina, H. Kazumori, M. O'Keeffe, O. Terasaki, J. F. Stoddart, O. M. Yaghi; *Science*, **2012**, 336, 6084, pp. 1018.
9. A.M. Fracaroli; H. Furukawa; M. Suzuki; M. Dodd; S. Okajima; F. Gándara; J. A. Reimer; O. M. Yaghi; *J. Am. Chem. Soc*., **2014**, 136, 8863.
10. K. Lee, J.D. Howe, L.C. Lin, B. Smit, J.B. Neaton, *Chem. Mater*., **2015**, 27, 668.
11. A. L. Dzubak, L. Lin, J. Kim, A. Swisher, R. Poloni, S. N. Maximoff, B. Smit, L. Gagliardi, *Nature Chemistry*, **2012**, 4, 810.
12. T.G. Glover, G.W. Peterson, B.J. Schindler, D. Britt, O.M. Yaghi, *Chemical Engineering Science*, **2011**, 66, 163.
13. R. C. J. Atkinson, V. C. Gibson, N. J. Long, *Chem. Soc. Rev*., **2004**, 33, 313.

2 Literature Survey and Fundamental Aspects.

2.1 Metal-Organic Frameworks (MOFs)

MOFs, in general, have relatively large surface areas and porosities making them important candidates for nanoporous applications, such as gas storage, separation, and catalysis.[2.9] MOFs also show characteristics of outstanding crystallinity, enhanced adsorption capacity and tenability.[2] MOFs consist of metal ions coordinated to electron donating organic ligands, yielding tailorable structures and pores.[3] MOFs can be synthesised with a variety of topologies and chemical composition, as illustrated in Figure 2.1, p.5. Different combinations of starting material and reaction conditions are investigated in an attempt to optimize the characteristics of these MOFs.[4]

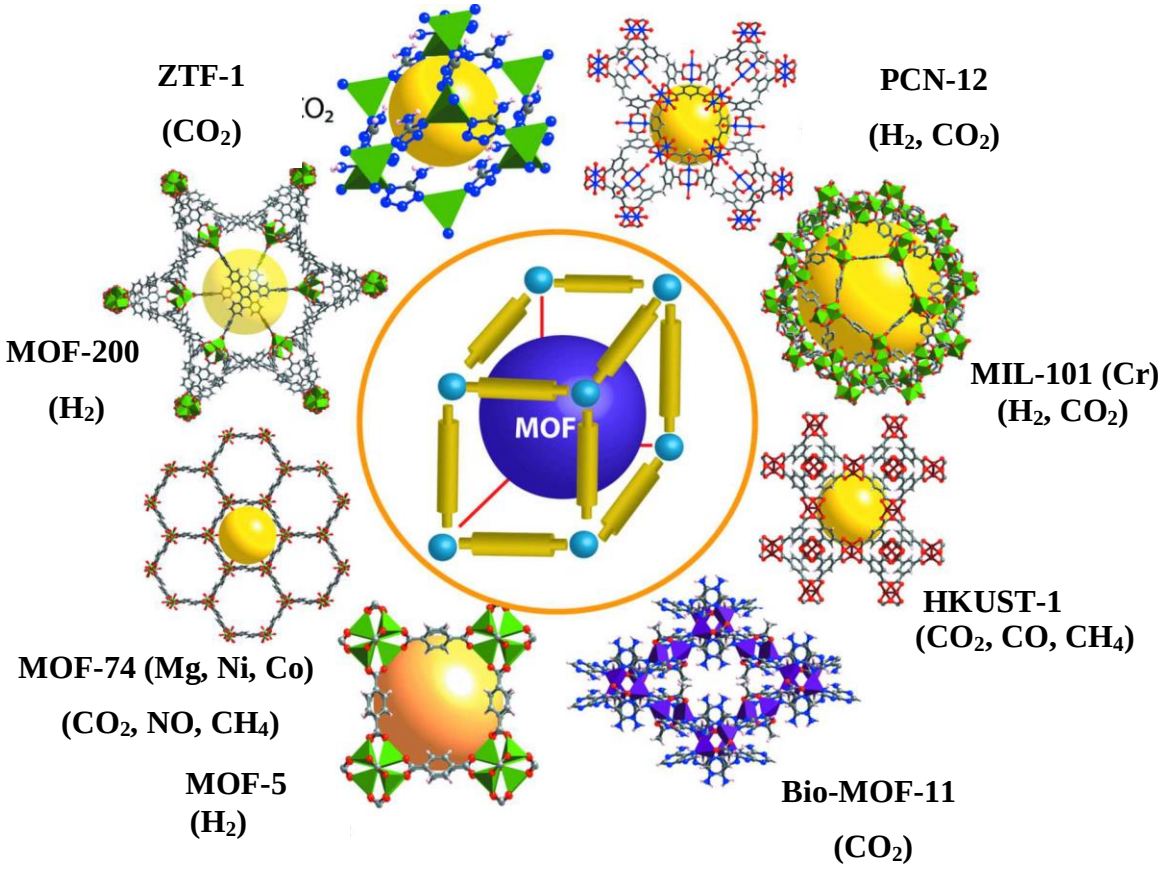

Figure 2.1: Illustration of different MOFs, containing a variety of topologies. The preferred gasses for high uptake are indicated for each structure. Reprinted (adapted) with permission from C. Dey, T. Kundu, B. P. Biswal, A. Mallick and R. Banerjee; *Acta Cryst.* (**2014**). B70, 3-10. Copyright 2014, International Union of Crystallography.

This study focuses on MOF-74. MOF-74, formed during the amalgamation of metal ions (+2 oxidation state) and 2,5-dioxido-1,4-benzenedicarboxylate (or similar) ligands. These MOFs have a honeycomb structure with a minimum pore width of 12 Å, Figure 2.2, p.6.[5]

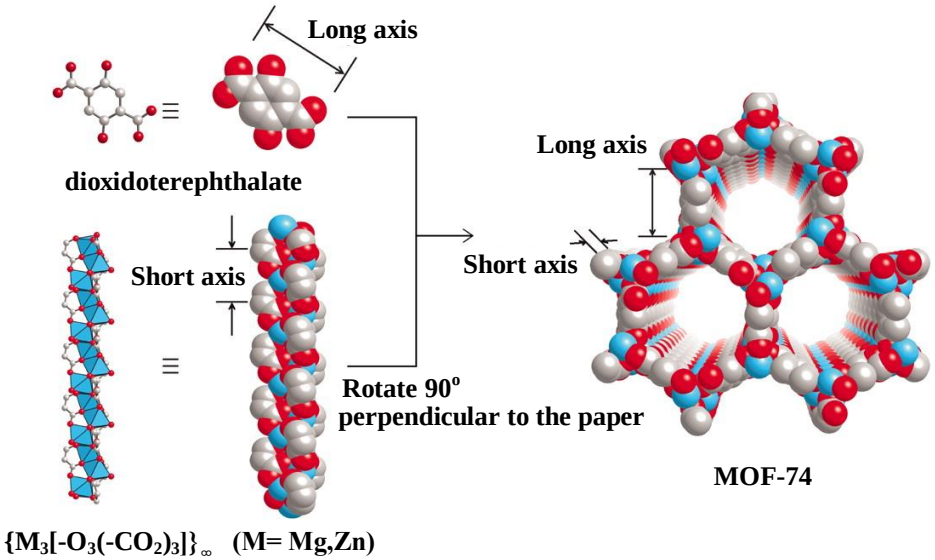

Figure 2.2: Typical synthesis of IRMOF-74, with dioxidoterephthalate (DOT) as a linker and a metal salt. Reprinted (adapted) with permission from Hexiang Deng, Sergio Grunder, Kyle E. Cordova, Cory Valente, Hiroyasu Furukawa, Mohamad Hmadeh, Felipe Gándara, Adam C. Whalley, Zheng Liu, Shunsuke Asahina, Hiroyoshi Kazumori, Michael O'Keeffe, Osamu Terasaki, J. Fraser Stoddart, Omar M. Yaghi; *Science* 25 May **2012**: Vol. 336, Issue 6084, pp. 1018-1023. Copyright 2016, The American Association for the Advancement of Science.

MOF-74 pore structure and functionality can be adapted for a particular application. The distinctive advantage of MOF-74 is that it contains unsaturated (open) metal sites that can be varied without affecting the framework structure.[6] Impregnated guest molecules binding to unsaturated metal centres are due to a delicate balance between hybridization of molecular orbitals, electrostatics, Pauli repulsion (sterics), and van der Waals (or dispersion) attraction.[2] Molecular conformation is the combination of electronic and steric effects. For example, the hydrogen bonds within C=O···H-N is favoured by the delocalization of the oxygen lone pair into the antibonding orbitals of the N-H bond, but disfavoured by Pauli repulsion between the lone pair and the N-H bonding orbital.[31] The electronic structure of Mg-MOF-74, with water molecules adsorbed in the pores, remains unchanged, indicating that there is no covalent bonding between the water molecules and the MOF but rather physisorption.[46] Hydrogen bonding of water to the open metal sites of the MOF-74, are of typical type $H_2(\sigma) \longrightarrow M(nd)$ charge transfer and $M(nd) \longrightarrow H_2(\sigma)$ "back bonding".[48]

The size and chemical environment of the MOF's pores are defined by the length and functionality of the organic linker units. A suitable choice of the starting material results in alteration of the materials properties. It's not only the significance of the building blocks but the way they are affixed.[7] One of the challenges in MOF synthesis is to get the pores sufficiently large enough to ensure that bulky organic, inorganic and biological molecules can be accommodated within the pores. By utilizing longer linkers, the dimensions of the pores should also increase,[26] thus the smallest MOF-74-I pore have dimensions of 14 Å by 10 Å, and was synthesised from the shortest possible linker, dioxidoterephthalate. Figure 2.3, p. 7, illustrates how the pore dimensions increase with an increase in linker length, with the largest pore dimensions, that of IRMOF-74-XI, being 98 Å by 85 Å, synthesised from a dioxidoterephthalte derivative containing eleven phenylene rings.

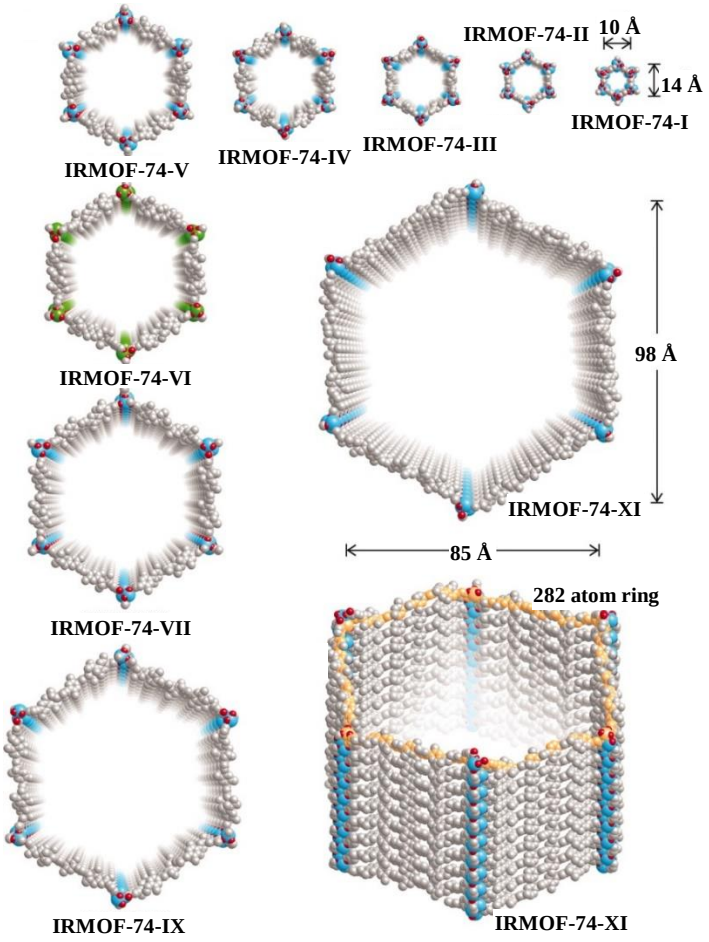

Figure 2.3: Illustrations of IRMOF-74 derivatives synthesised from organic linkers of different lengths and functionality. Reprinted (adapted) with permission from Hexiang Deng, Sergio Grunder, Kyle E. Cordova, Cory Valente, Hiroyasu Furukawa, Mohamad Hmadeh, Felipe Gándara, Adam C. Whalley, Zheng Liu, Shunsuke Asahina, Hiroyoshi Kazumori, Michael O'Keeffe, Osamu Terasaki, J. Fraser Stoddart, Omar M. Yaghi; *Science* 25 May **2012**: Vol. 336, Issue 6084, pp. 1018-1023. Copyright 2016, The American Association for the Advancement of Science.

2.2 Synthesis

In generating functionalized materials in open frameworks, the inclusion of chiral centres or reactive sites (like open metal sites) is advantageous.[7] For example, immobilization of functional groups/ sites, like Lewis basic nitrogen sites onto the MOF framework, not only improves acetylene uptake but also distinguishes between acetylene and other gasses.[50] The unpaired electrons of the metal centres can cause MOFs to have magnetic properties, in particular, Fe-MOF-74 shows a magnetic switching behaviour with guest molecules. The adsorption of O_2 can enhance the ferromagnetic coupling with 10 times, due to a superexchange interaction between the oxygen and Fe centre.[51] Due to the high surface area and unique structure of MOF-74, its metal oxide sites are preferred for supercapacitors and lithium ion batteries.[50] Magnesium and cobalt MOF-74 showed breakthrough adsorption of ammonia, this is due to the open metal sites acting as coordination sites.[6] Crafty changes to the coordinating organic ligands often yield new framework topologies, but certain framework types accommodate alteration and change in the chemical nature of these moieties.[7]

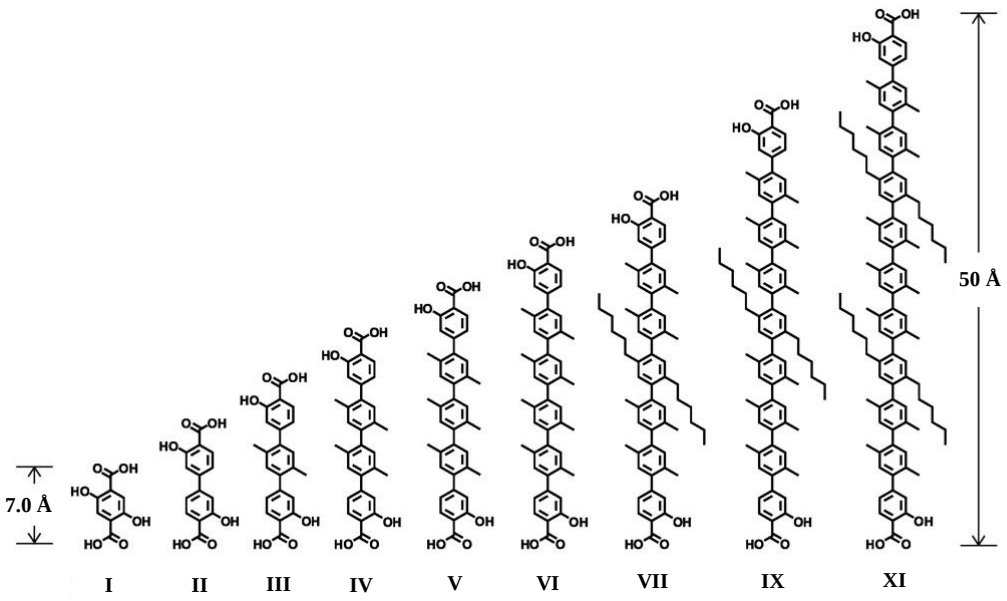

Figure 2.4: Crafty changes to the organic linkers resulting in different pore sizes of the resultant IRMOF-74. Reprinted (adapted) with permission from Hexiang Deng, Sergio Grunder, Kyle E. Cordova, Cory Valente, Hiroyasu Furukawa, Mohamad Hmadeh, Felipe Gándara, Adam C. Whalley, Zheng Liu, Shunsuke Asahina, Hiroyoshi Kazumori, Michael O'Keeffe, Osamu Terasaki, J. Fraser Stoddart, Omar M. Yaghi; *Science* 25 May **2012**: Vol. 336, Issue 6084, pp. 1018-1023. Copyright 2016, The American Association for the Advancement of Science.

By changing the length of the central linkers the pore size increases from 7.0 Å to 50 Å. Alkane chains can also be strategically attached to the phenyl rings in the centre of the linker, as

indicated in VII, IX and XI, Figure 2.4, p. 8. Other functional groups can also be added to the linkers to increase the functionality of MOF-74, which will increase the possible application of the specific MOF-74 derivatives.

2.2.1 Linkers

The field of post-synthetic modification (PSM) of MOFs are well studied. MOFs display excellent guest loading capacities[24] through physisorption abilities, but modification of linkers yield a chemical alteration which is more permanent than guest molecule physisorption.

The linker, containing three phenylene rings, makes modification of the linker much easier since the two outer phenylene rings contain the carboxylic acid and alcohol functionalities, resulting in similar topology than that of MOF-74-III, previously studied, with the central phenylene ring containing the modifications.

M-MOF-74 displays high H_2 adsorption capabilities, due to the interaction between open-metal sites and hydrogen.[5] PSM through loading guest molecules might cause an interaction between the open-metal sites, thus modification of the linker itself prohibits this interaction, resulting in a functionalized MOF-74 with open-metal sites.

A tried and trusted method for the synthesis of the organic linker M-MOF-74-III can be seen in Scheme 2.1, p. 10.[26]

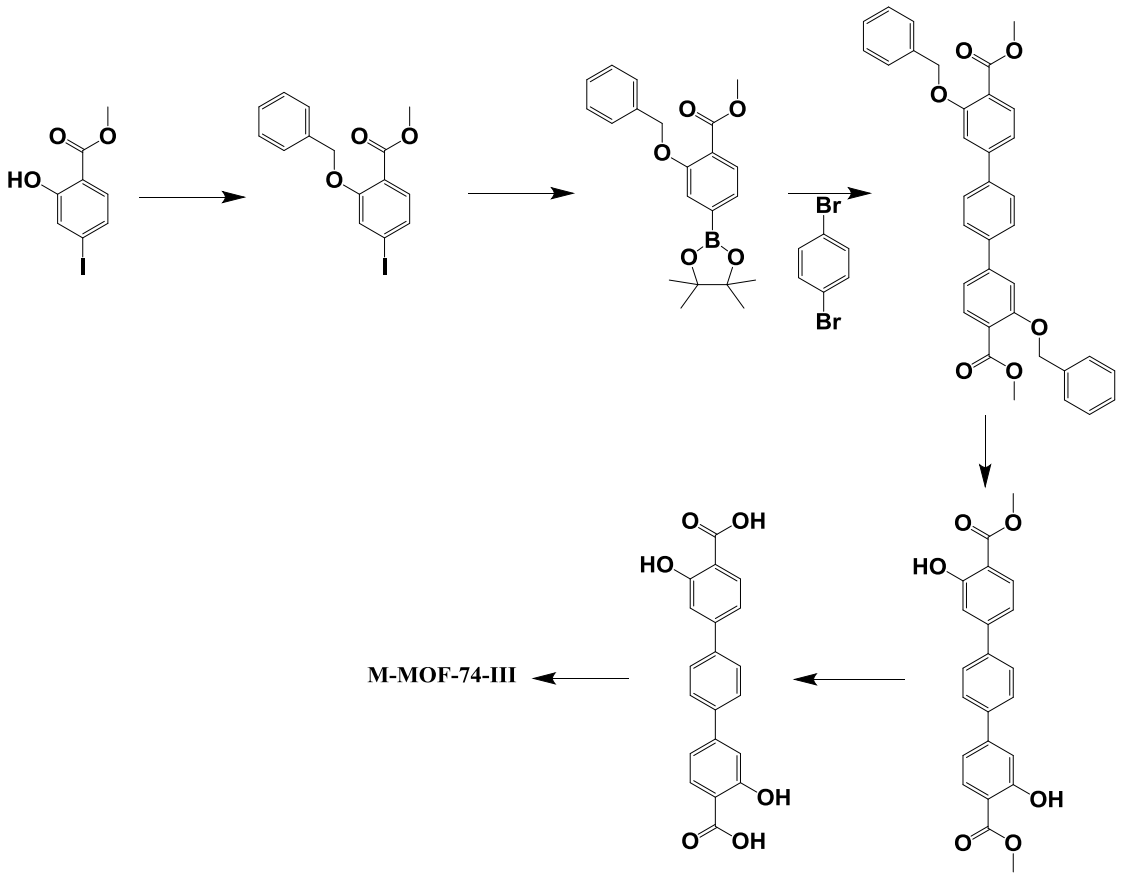

Scheme 2.1: Synthesis route for M-MOF-74-III from methyl-2-hydroxy-4-iodobenzoate.[26]

The first step in the synthesis process is the protection of the hydroxy-group, of methyl-2-hydroxy-4-iodobenzoate, with a benzyloxy-group. After protection, the only reactive site left on the molecule is the iodo-group. Through utilization of the appropriate cross-coupling reaction, this iodo-group can easily be substituted with a boronic ester functionality. The boronic ester functionality is then substituted with another phenyl-ring, forming an carbon-carbon bond.Finally coupled with another protected methyl-2-benzyloxy-4-iodobenzoate forming a carbon-carbon bond,and finally yielding a protected three phenylene linker. The final step in the synthesis of the organic linker is the deprotection of the benzyloxy-group, which is a bulky protecting group and can easily be removed, and lastly the methyl-group, which is a bit more difficult to remove. The deprotected three phenylene linkers are then ready to be reacted with the appropriate metal salt resulting in M-MOF-74-III.

2.2.1.1 Protection

In choosing a protecting group, there are a few requirements to keep in mind: the protecting group should react selectively to give a protected substrate which is stable in subsequent

reactions. After these reactions, selective removal of the protecting group using reagents that are unreactive to regenerated functional groups should give the desired product. This product should be easily separated from side-products, and the protecting group should not add new stereogenic centres to it. Do not use protecting groups with added functionality, to ensure minimal reactive sites.[8]

Hydroxy- and carboxylic acid groups play an important role in a variety of natural products. To synthesise these products in a laboratory often require a multitude of synthesis steps. To ensure that these functionalities remain intact throughout this long and tedious synthesis process, they need to be selectively protected.[9] Carboxylic acids are protected for several reasons, which include masking the acidic proton to avoid undesired side-reactions during base-catalysed reactions, avoiding nucleophilic addition reactions and improved molecule handling.[8]

Several groups exist for the protection of hydroxyl and carboxylic acid functionalities. One of these protecting group classes consists of acetyl-type groups including methoxymethyl (MOM), tetrahydropyranyl (THP), and methoxyethoxymethyl (MEM) ethers. These acetyl-type protecting groups are not only widely known for their stability towards strong basic and neutral reaction conditions, but also their excellent stability towards strong nucleophiles such as organometallic and hydride reducing agents.[10] The MEM-ether protecting group has several advantages, such as the easy introduction and handling.[11] Despite the several advantages of MEM-ethers as protecting groups, they also appear to help in separation of reaction mixtures by chromatography. This is due to the bulky ether chains containing oxygen atoms, causing the desired product to move slowly on a column. All the unprotected by-products will be separated from the desired protected product.[12]

2.2.1.2 Cross-coupling

There are many cross-coupling reactions that are used for C-N and C-C bond formation, e.g.

1. Heck cross-coupling[60]
2. Stille cross-coupling[60]
3. Shonagashira cross-coupling[61]
4. Suzuki cross-coupling[60]
5. Suzuki-Miyaura cross-coupling[62]
6. Hiyama cross-coupling[63]

Cross-coupling reactions utilizing transition metals transformed organic synthesis. Heck, Stille, Shonagashira and Suzuki-Miyuara cross-coupling reactions are some of the most important

carbon-carbon bond formation techniques. Suzuki and Miyuara reported the first coupling reactions utilizing a base and Pd(0) catalyst, in 1986.[14] The Suzuki-Miyuara cross-coupling reaction is the reaction that is utilized the most[15] and has advanced to be the most widely used carbon-carbon bond formation technique,[13] due to several advantages above other coupling reactions, which include: easy addition of a boron segment, controllable toxicity of by-products and a high tolerance for water.[16,17] Suzuki-Miyuara cross-coupling reactions make sp^2-sp^2 carbon-carbon bond formation possible between an aryl halide and organoboranes,[18] and is therefore extensively used in this study.

The catalytic cycle of the Suzuki-Miyaura cross-coupling reaction is similar to other coupling reaction mechanisms and includes oxidative addition, transmetallation and a reductive elimination step,[8] Figure 2.5, p. 13. There are one or more possible paths included in the reductive elimination step: heterolytic as well as homolytic or concerted α-elimination, *p*-elimination, 1,1-reductive elimination and dinuclear elimination.[19]

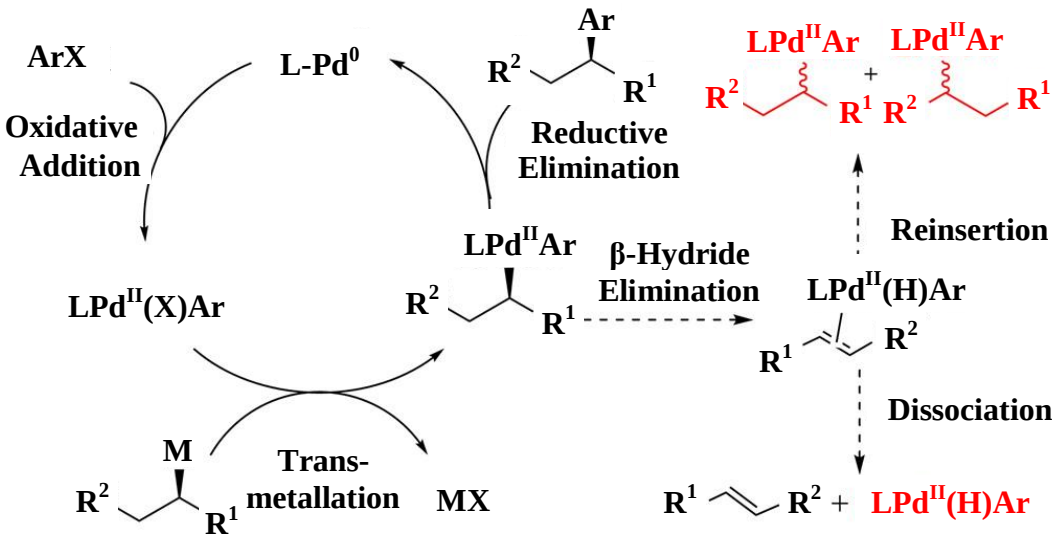

Figure 2.5: Catalytic cycle and possible side reactions (β-Hydride Elimination). Reprinted (adapted) with permission from Ling Li; Shibin Zhao; Amruta Joshi-Pangu; Mohamed Diane; Mark R. Biscoe; *J. Am. Chem. Soc.* **2014**, 136, 14027-14030. Copyright 2014, American Chemical Society.

The rate of the coupling reaction is determined by the nature of the organoboranes, aryl halide, the palladium catalyst and the base used in the coupling reaction.[8] Aryl halides with electron-withdrawing groups are more reactive in the oxidative addition step than aryl halides with electron-donating groups.[8] Aryl bromides and -iodides are often employed in the Suzuki-Miyuara cross-coupling reaction, but chlorides and triflates can also be used. When choosing triflates, it should be kept in mind that they are base sensitive and thermally labile.[11]

One disadvantage of the Suzuki-Miyuara cross-coupling reaction is that if the substrate has hydrogen in the β-position it may undergo β-hydride elimination, after transmetallation.[8] It may result in low yields of the desired product.[20]

The bidentate bis(diphenylphosphino)ferrocene ligand of the $PdCl_2$(dppf) catalyst enhances reductive elimination since its bite angle is large enough for the reactive species to move close to each other on the Pd(II) centre.[8] A common problem during homogeneous catalysis is the separation and recycling of the catalyst. With the Suzuki-Miyuara cross-coupling reaction, the catalyst is in the hydrophilic phase making separation of the catalyst easy since the organic products are insoluble in the water phase.[21] Palladium catalysts containing triphenylphosphine ligands, $Pd(PPh_3)_4$ and $(PPh_3)_2PdCl_2$, are able to generate a catalytically active $Pd(PPh_3)_2$ species *in situ*.[13]

It is important to choose the most appropriate base for a Suzuki-Miyuara reaction since it plays an important role in the transmetallation step of the catalytic cycle.[8] The addition of toxic thallium hydroxide to a Suzuki-Miyuara cross-coupling reaction of aryl halides allows the C-C bond formation at room temperature, which is not the case for aryl chlorides.[12]

Suzuki-Miyuara cross-coupling reactions work exceptionally well in polar solvents since they stabilize the substrate-palladium complex and enhance the reductive elimination step of the catalytic cycle.[13]

2.2.1.3 Adding functionality

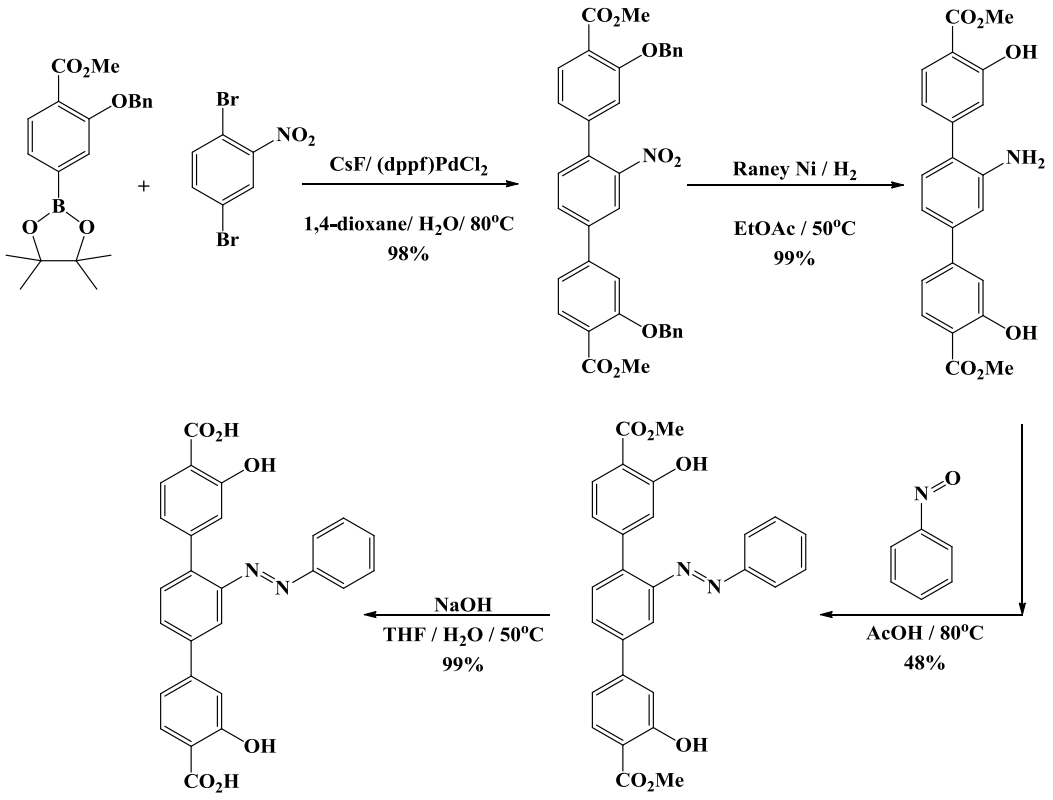

Scheme 2.2: Synthesis of organic linkers resulting in added functionality to the pores of IRMOF-74-III. Bn = Benzyl. Reprinted (adapted) with permission from Jonathan W. Brown, Bryana L. Henderson, Matthew D. Kiesz, Adam C. Whalley, William Morris, Sergio Grunder, Hexiang Deng, Hiroyasu Furukawa, Jeffrey I. Zink, J. Fraser Stoddart and Omar M. Yaghi; Chem. Sci., **2013**, 4, 2858–2864. *Science* 25 May 2012: Vol. 336, Issue 6084, pp. 1018-1023. Copyright 2016, Royal Society of Chemistry.

Recently MOF-74 derivatives were synthesised with azobenzene photoactive linkers, Scheme 2.2, p. 15. These MOFs have a one-dimensional hexagonal structure, with the azobenzene units pointing into the pores. The even distribution of the azobenzene units within the crystalline framework, resulted in improved photoswitching over previously designed MOFs.[39]

The synthesis in Scheme 2.2, p. 15, shows a Suzuki-Miyuara cross-coupling between 2,5-dibromonitrobenzene and the phenylboronic ester (1), employing $PdCl_2$(dppf) and CsF base, resulting into the nitro derivative. Utilizing Raney-Ni and H_2 gas yields the removal of the benzyl protecting group and reduces the nitro-group to the aniline derivative. The addition of excess nitrosobenzene yields the azobenzene and through saponification, yielding the dicarboxylic acid derivative. These azobenzene units can reversibly switch between *cis* and *trans*

conformation through excitation at 408 nm. If the units are in the *cis* conformation the resulting MOF have a pore size of 10.3 Å and in the *trans* conformation a pore size of 8.3 Å. Thus for the *trans* conformation, the pores of the resultant MOF are "closed" and upon excitation of the linker, the *cis* conformation is formed resulting in an "open" pore. These results yield the selective opening and closing of the MOF pores.

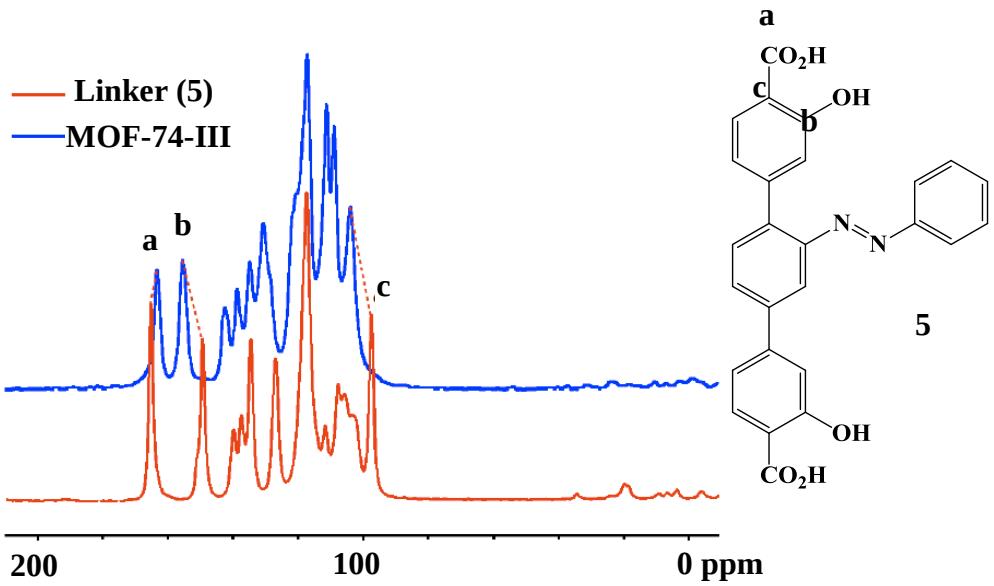

Figure 2.6: ^{13}C solid state NMR spectra of the azobenzene-linker and the resultant MOF-74-III-derivative. Reprinted (adapted) with permission from Jonathan W. Brown, Bryana L. Henderson, Matthew D. Kiesz, Adam C. Whalley, William Morris, Sergio Grunder, Hexiang Deng, Hiroyasu Furukawa, Jeffrey I. Zink, J. Fraser Stoddart and Omar M. Yaghi; Chem. Sci., 2013, 4, 2858–2864. *Science* 25 May **2012**: Vol. 336, Issue 6084, pp. 1018-1023. Copyright 2016, Royal Society of Chemistry.

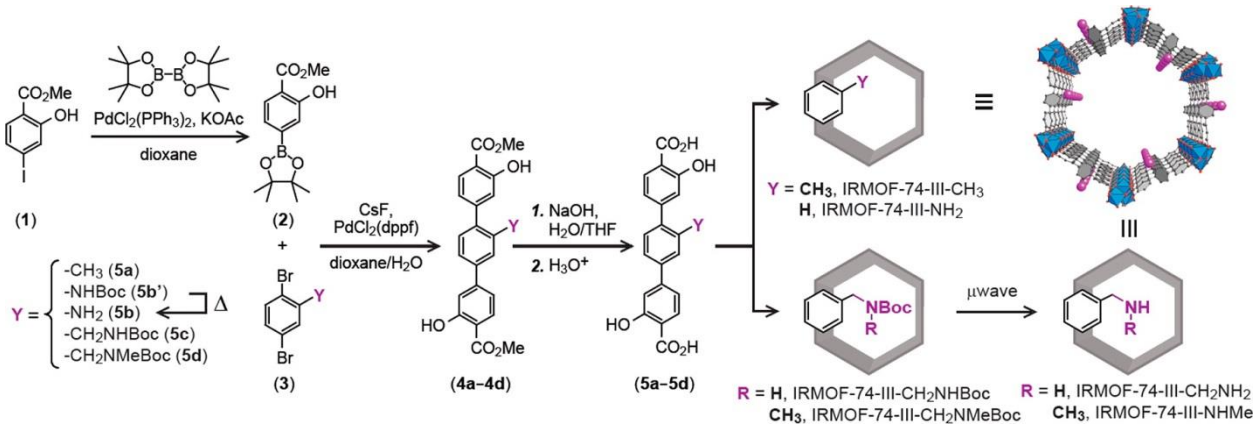

Scheme 2.3: Synthesis of linkers for MOF-74-III with functional groups on the central phenyl ring, resulting in added functionality in the pores of the MOF structure. Reprinted (adapted) with permission from Alejandro M. Fracaroli; Hiroyasu Furukawa; Mitsuharu Suzuki; Matthew Dodd; Satoshi Okajima; Felipe Gándara; Jeffrey A. Reimer; Omar M. Yaghi; *J. Am. Chem. Soc.* **2014**, 136, 8863-8866. Copyright 2014, American Chemical Society.

Scheme 2.3, p. 16, shows the synthesis of IRMOF-74 starting with the commercially available methyl-2-hydroxy-4-iodobenzoate (1), through the utilization of the Suzuki-Miyuara coupling reaction of boronic acid pinacol ester (2) and the functionalized 1,4-dibromobenzenes (3). This is followed by a saponification reaction of the resultant ester (4) to remove the methyl protecting groups on the linker. The Boc-functional group was employed to add $–CH_2NH_2$ and $–CH_2NHMe$ functionality to the linker after the synthesis of the IRMOF-74 (Boc = Tertbutyloxycarbonyl). This is to ensure that the unprotected amines of the $-CH_2NH_2$ and $–CH_2NHMe$ does not react with the metal ions during the synthesis of the IRMOF-74. The IRMOF containing-CH_2NH_2 and $–CH_2NHMe$ functionalities showed high uptake and strong binding of CO_2 gas under dry and wet conditions.[40]

2.2.1.4 Deprotection

The addition of protecting groups is important for the preservation of certain functional groups on a functionalized molecule, so is their deprotection, during the final synthesis steps. Deprotection should be conducted under mild reaction conditions, to prevent decomposition of the functionalized molecule, side-reactions destroying functionality and destruction of stereocentres.[9] Hydroxyl groups protected by an ester or ether can be easily deprotected, but protection by alkyl and benzyl ethers, however, seems to be more permanent due to the difficulty in deprotection of these groups.[22] Slight acidic conditions are the only requirement for the deprotection of acetyl-protection groups.[9]

2.2.2 MOF formation

The formation of MOFs is controlled by intermolecular forces that limit predictability. With some effort to recognize and modify synthetic conditions, the joining of the building units in the desired fashion can be achieved. Solvothermal techniques are mostly used for the formation of MOFs and often the precursors are fused in polar solvents like water, alcohols, acetone or acetonitrile, in a heated sealed vessel (Teflon-lined stainless steel bombs or glass tubes) which is heated, under “self-created” pressure. Crystal growth is enhanced by using mixed solvent systems adapting the polarity and kinetics of solvent ligand exchange.[7]

M-MOF-74s have been previously synthesised for M = Mg, Mn, Fe, Co, Ni, Cu, and Zn. All M-MOF-74s thus far are isostructural, sharing the same topology,[2] a 3D hexagonal packing of

O_5M chains (M= Mg^{2+}, Mn^{2+}, Fe^{2+}, Co^{2+}, Ni^{2+}, Cu^{2+} and Zn^{2+}) connected by 2,5-dihydroxyterephthalate linkers resulting in a honeycomb-type structure. The metal centres inhabit the apexes of the hexagons formed by the organic linkers. All the oxygen atoms of the carboxylate and hydroxyl groups, on the ligands, coordinate to the metal cation. Five oxygen atoms occupy in the coordination sphere of each metal cation, with a sixth coordination position occupied by a water and/or solvent molecule, Figure 2.7, p. 18.[4, 23]

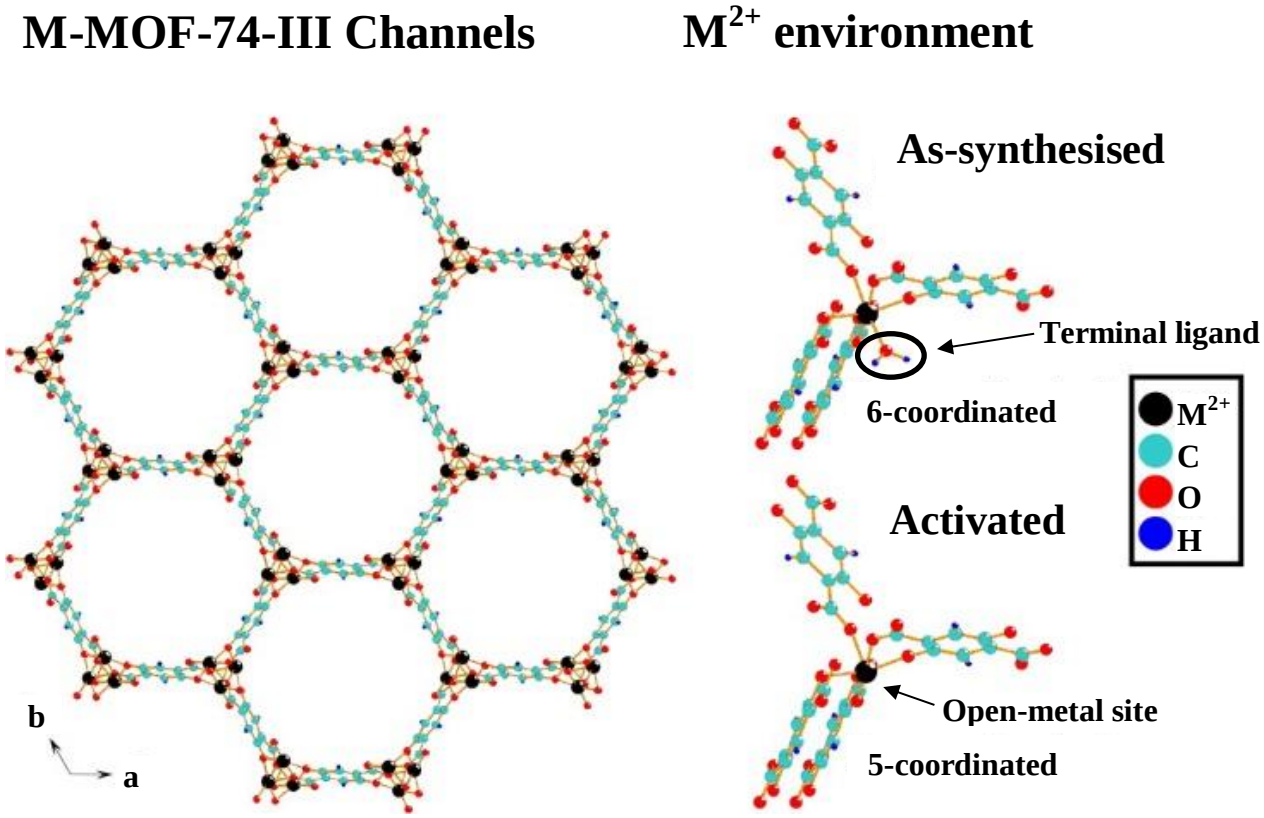

Figure 2.7: Structure of M-MOF-74-III, showing a water molecule as a terminal ligand bound to the M^{2+}-metal centre. The activated form, without the terminal ligand, is also shown. Reprinted (adapted) with permission from J. Xu, R. Sinelnikov, and Y. Huang, *J. Am. Chem. Soc.* ***2016***, 136, *8863* Copyright 2016, American Chemical Society.

Solvent molecules bound to the square-pyramidal coordination metal centres of the as-synthesised M-MOF-74, are evacuated during thermal treatment, creating the open-metal sites.[2] These solvent molecules act as terminal ligands for the metal cations of the porous framework.[4]

2.3 Infrared Spectroscopy of MOF-74 (IR)

In Figure 2.8 a, p. 19, the stretching vibrational frequency at 1630 cm^{-1} (i) is due to the C=O and the frequencies at around 1560 and 1518 cm^{-1} (ii) are for the COO- stretching asymmetric vibration of the 3-(pyridine-3-yloxy)benzene-1,2-dicarboxylic acid) of the linker.[32] The pyridine functional group on the linker, Figure 2.8 b, p. 19, is relatively electron deficient, due to the nitrogen being electronegative. This IR spectrum will be compared totheCo-MOF-74 derivatives in this study, containing electron withdrawing, electron donating and bulky substituents on the linkers.

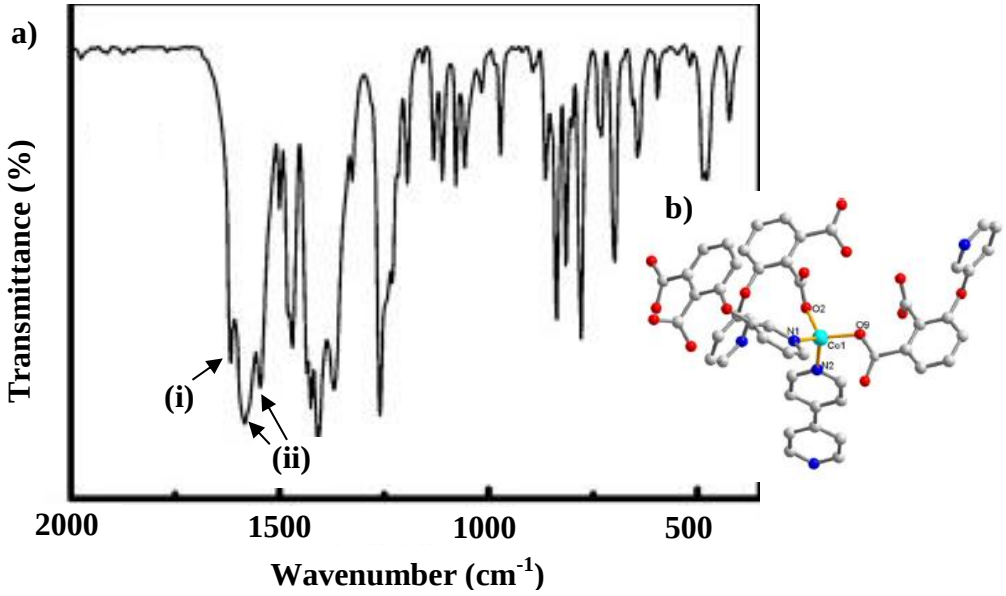

Figure 2.8: a) Infrared spectrum of Co-MOF-74. b) The structure of linker used in the synthesis of this Co-MOF-74. Reprinted (adapted) with permission from Lizi Yang, Cailing Xu, Weichun Ye, Weisheng Liu; Sensors and Actuators B: Chemical, Volume 215, **2015**, 489. Copyright 2016, Elsevier.

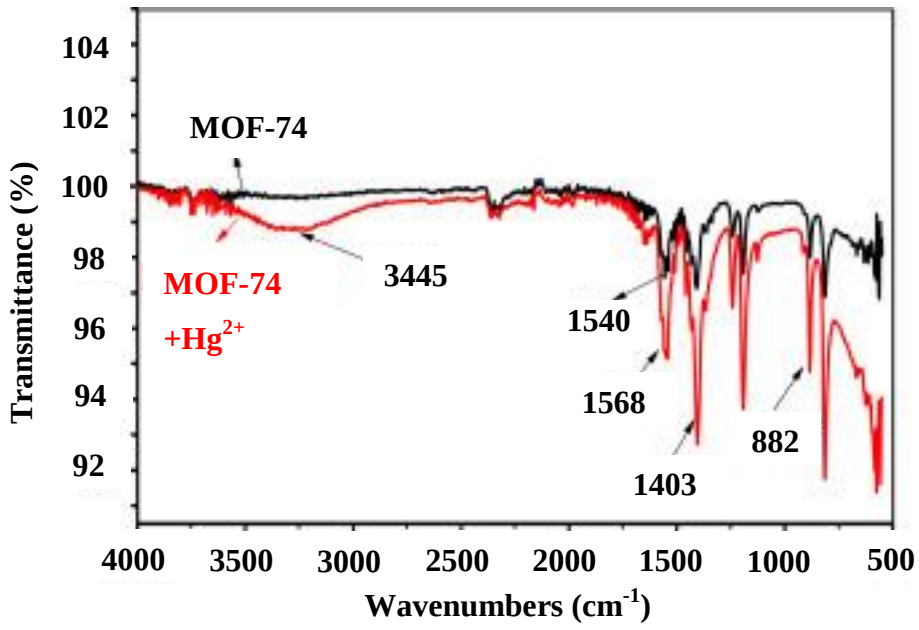

Figure 2.9: Infrared spectrum of Zn-MOF-74 (black) and the spectrum of Zn-MOF-74 after adsorption of Hg^{2+}. Reprinted (adapted) with permission from Y. Y. Xiong, J. Q. Li, L. L. Gong, X. F. Feng, L. N. Meng, L. Zhang, Pan Pan Meng, Ming Biao Luo, Feng Luo; Journal of Solid State Chemistry, Volume 246, **2017**, 16–22; Copyright 2016, Elsevier.

When certain molecules are adsorbed in MOF-74 it has an effect on its IR spectrum. Figure 2.9, p. 20, shows a peak at 1403 cm^{-1} which is for the stretching vibration of carboxylic acid, the broad peak at 3445 cm^{-1} is due to water molecules that remained inside the pores of Zn-MOF-74 after the adsorption of Hg^{2+}. The benzene skeleton of the linker of the Zn-MOF-74 shows a vibrational peak between 1600 cm^{-1} to 1500 cm^{-1}.[33]

2.4 Accelerated Surface Area and Porosity Analysis (ASAP)

In order to determine the porosity of a material, free gas flow into its pores is measured. Type I isotherms are typical of a microporous material.[7] Type IV isotherms are typical of a mesoporous material.[49]

These isotherms provide information about the strength of the physisorptive interaction between the adsorptive molecules and the MOF structure. Through the measurement of nitrogen or argon adsorbed, assuming Langmuir-type monolayer coverage, the pore size, and surface area are determined. In determining the pore size and surface area of MOF frameworks, organic vapours like chloroform, benzene and cyclohexane have also been used.[7]

Data from isotherms provide information about the binding energy of the molecules on the framework but does not provide information about the binding mechanism.[52] Measurements of the adsorption of toxic gasses, like hydrogen cyanide, phosgene and carbondioxide can also be conducted to determine the adsorption abilities of frameworks with these gasses.[6] Analysis the physisorptive properties of the MOF framework, can be done at low or high pressure.[53]

At the metal centre chemi-adsorption of CO_2 can take place, which causes an increase in the adsorption energy, and prevents the re-use of the MOF since the adsorbed molecules are fully fused in the MOF framework.[54] Mesoporous materials display a much higher N_2 uptake due to the large pore size.[55] If the adsorbed gas (N_2 or CO_2) is less at a second analysis this is an indication of the deterioration of the sample.[56]

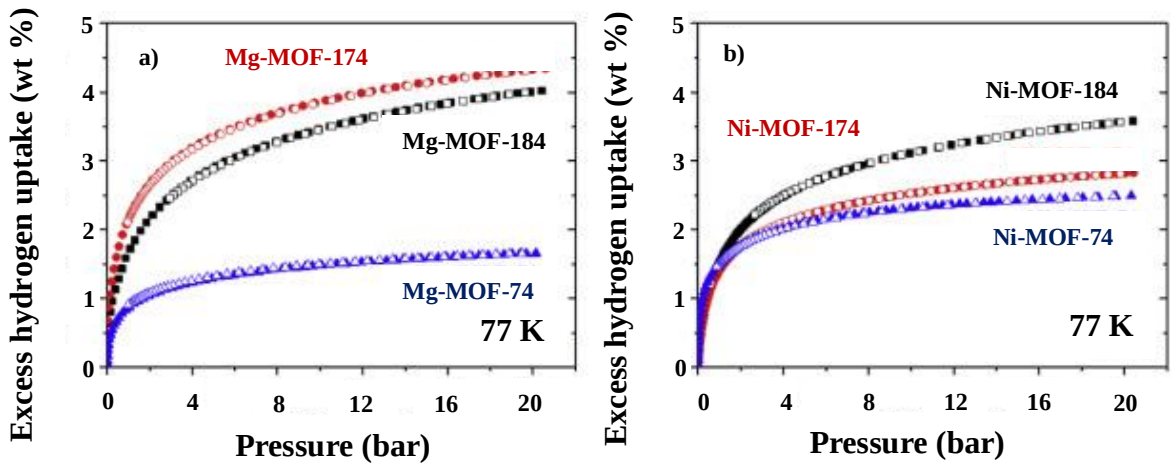

Figure 2.10: ASAP isotherms for Mg-MOF-74, 184, 174 (a) and Ni-MOF-74, 184, 174 (b) showing excess hydrogen uptake at 77K. Reprinted (adapted) with permission from Hyunchul Oh, Stefan Maurer, Rafael Balderas-Xicohtencatl, Lena Arnold, Oxana V. Magdysyuk, Gisela Schűtz, Ulrich Műller, Michael Hirscher; International Journal of Hydrogen Energy, **2016**, http://dx.doi.org/10.1016/j.ijhydene.2016.08.153

From the adsorption/desorption isotherms for Mg-MOF-74 (Figure 2.10 a, p. 21) and Ni-MOF-74 (Figure 2.10 b), the maximum amount of excess hydrogen adsorbed at 77 K was determined as 1.66 wt % and 2.49 wt % for Mg-MOF-74 and Ni-MOF-74 respectively. The adsoption below 2 bars, shows a steep increase in hydrogen uptake, a good indication of the interaction of the hydrogen molecules with the open-metal sites of the MOF-74. MOF-174 and MOF-184 have longer linkers than MOF-74, and thus larger pores, resulting in much larger hydrogen uptake capacity. This confirms that longer linkers do not only increase the pore size, but also result in an increase of surface area.[41]

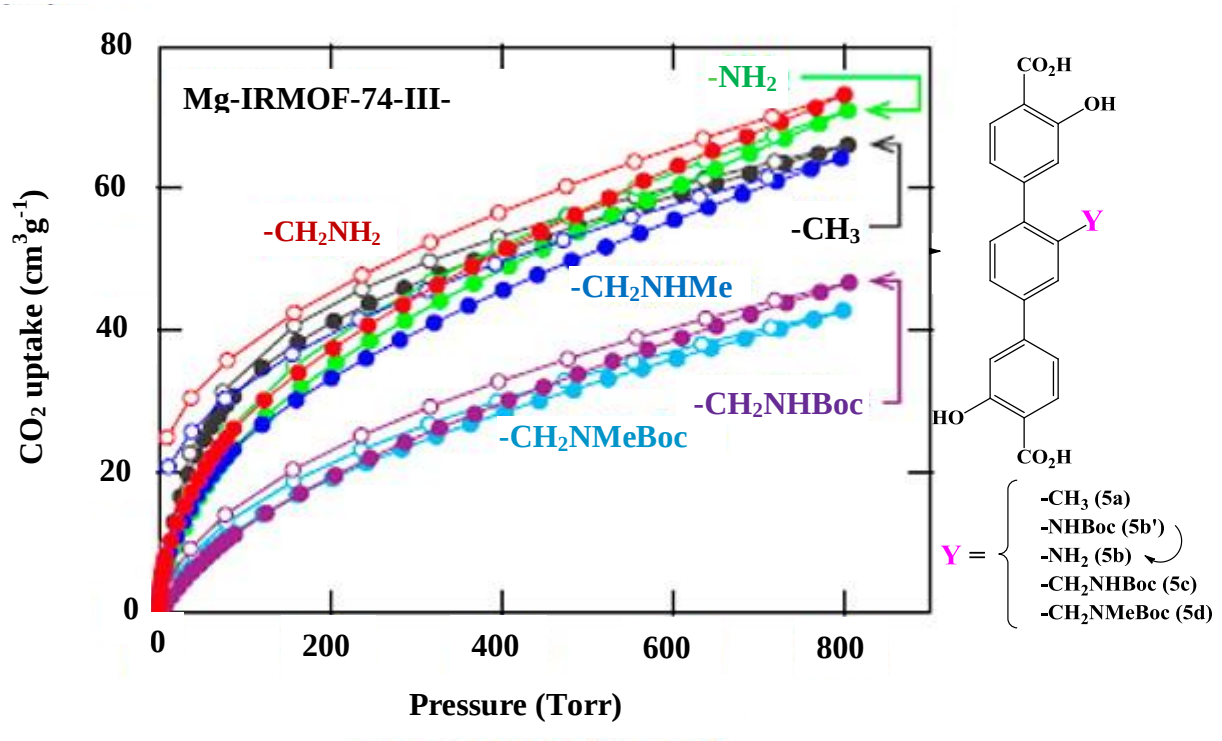

Figure 2.11: Carbon dioxide uptake for Mg-IRMOF-74-III derivatives with different functionalities on the central phenyl ring. (Boc = tertbutyloxycarbonyl). Reprinted (adapted) with permission from Alejandro M. Fracaroli; Hiroyasu Furukawa; Mitsuharu Suzuki; Matthew Dodd; Satoshi Okajima; Felipe Gándara; Jeffrey A. Reimer; Omar M. Yaghi; *J. Am. Chem. Soc.* **2014**, 136, 8863-8866. Copyright 2014, American Chemical Society.

Due to the sterically bulky Boc groups, the CO_2 uptake of the Boc-protected IRMOF-74-III derivatives is less than that of IRMOF-74-III-CH_3, -NH_2, CH_2NH_2 and –CH_2NHMe, Figure 2.11 a, p. 22. IRMOF-74-III derivatives with the amine functionalities showed the highest CO_2 uptake, due to the strong interactions between CO_2 and amines.[41]

The argon adsorption and desorption curves, Figure 2.12, p. 23, for Mg-IRMOF-74-III are type IV isotherms, typical of mesoporous materials. The second step (at P/P_o = 0.21) is due to the higher pressures (P/P_o) required to fill the larger pores. The BET surface area for Mg-IRMOF-74-III is 2440 $m^2.g^{-1}$ which is much larger than that of mesoporous silica, porous carbon and zeolites with similar pore sizes. The use of Mg, a light metal, in the synthesis of Mg-IRMOF-74-III, which is a light metal, added to the increased open space, results in the low density (0.531 $g.cm^{-3}$) observed for Mg-IRMOF-74-III.[26]

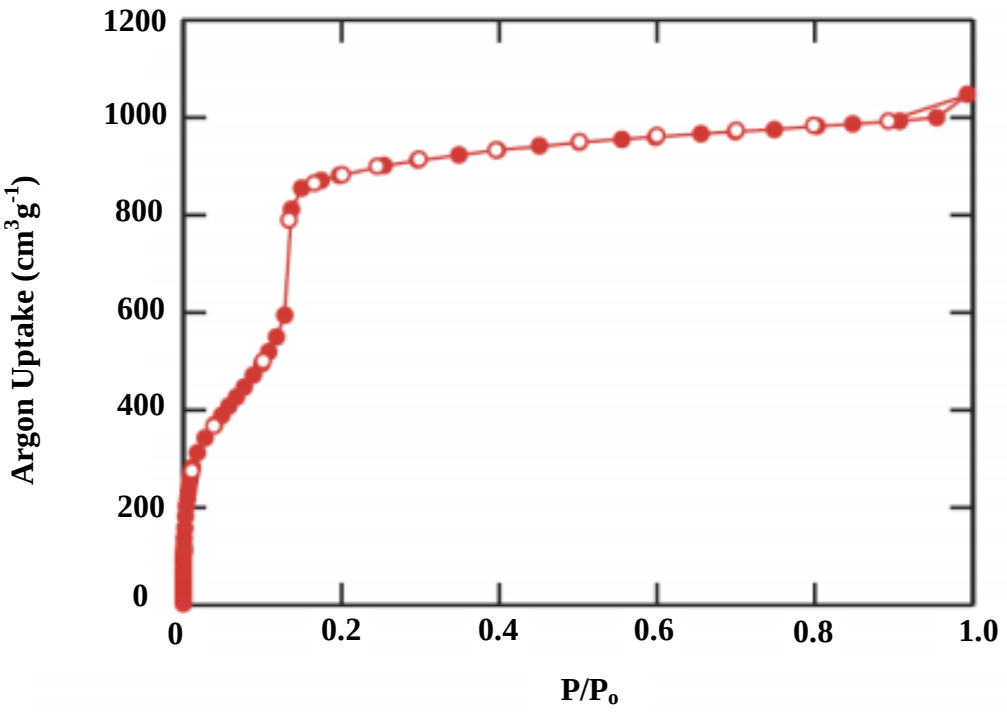

Figure 2.12: Argon adsorption (filled symbols) and desorption (open symbols) isotherms for Mg-IRMOF-74-III at 87 K. Reprinted (adapted) with permission from Hexiang Deng, Sergio Grunder, Kyle E. Cordova, Cory Valente, Hiroyasu Furukawa, Mohamad Hmadeh, Felipe Gándara, Adam C. Whalley, Zheng Liu, Shunsuke Asahina, Hiroyoshi Kazumori, Michael O'Keeffe, Osamu Terasaki, J. Fraser Stoddart, Omar M. Yaghi; *Science* 25 May **2012**: Vol. 336, Issue 6084, pp. 1018. Copyright 2016, The American Association for the Advancement of Science.

2.5 Thermal Gravimetric Analysis (TGA)

Figure 2.13, p. 24, shows a loss of 79.49 % between 200 ^{o}C and 300 ^{o}C, a good indication of the high thermal stability of Mg-IRMOF-74-II. It also indicates that the IRMOF-74-III is free from any solvents or lattice water molecules in the pores.

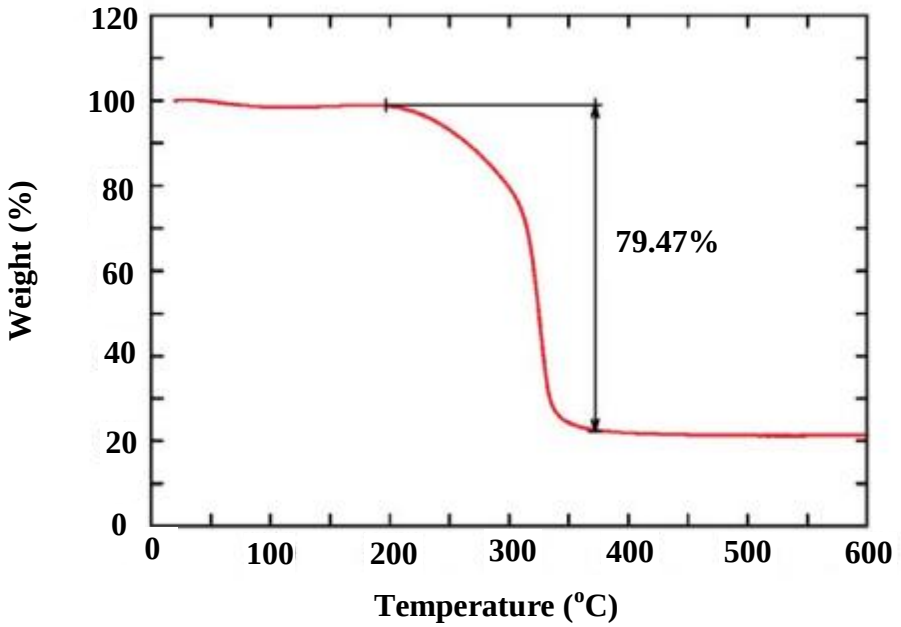

Figure 2.13: TGA for activated IRMOF-74-III. Reprinted (adapted) with permission from Hexiang Deng, Sergio Grunder, Kyle E. Cordova, Cory Valente, Hiroyasu Furukawa, Mohamad Hmadeh, Felipe Gándara, Adam C. Whalley, Zheng Liu, Shunsuke Asahina, Hiroyoshi Kazumori, Michael O'Keeffe, Osamu Terasaki, J. Fraser Stoddart, Omar M. Yaghi; *Science* 25 May **2012**: Vol. 336, Issue 6084, pp. 1018. Copyright 2016, The American Association for the Advancement of Science.

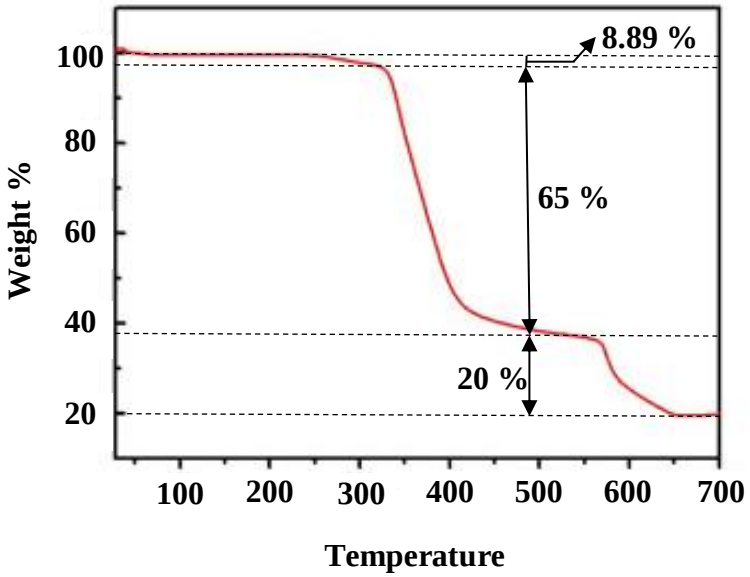

Figure 2.14: TGA thermogram of Co-MOF-74 under N_2. Reprinted (adapted) with permission from Lizi Yang, Cailing Xu, Weichun Ye, Weisheng Liu; Sensors and Actuators B: Chemical, Volume 215, **2015**, 489–496. Copyright 2016, Elsevier.

The TGA curve of Co-MOF-74, synthesised from $Co(Ac)_2 \cdot 4H_2O$ and 3-(pyridine-3-yloxy)benzene-1,2-dicarboxylic acid, (Figure 2.14, p. 24) shows a weight loss of

8.89 % from room temperature till 350 °C, corresponding to the removal of lattice water molecules and solvent. Between 380 °C and 700 °C Co-MOF-74 loses 85 % in two weight loss steps, an indication that the Co-MOF-74 is stable up to 380 °C.[32]

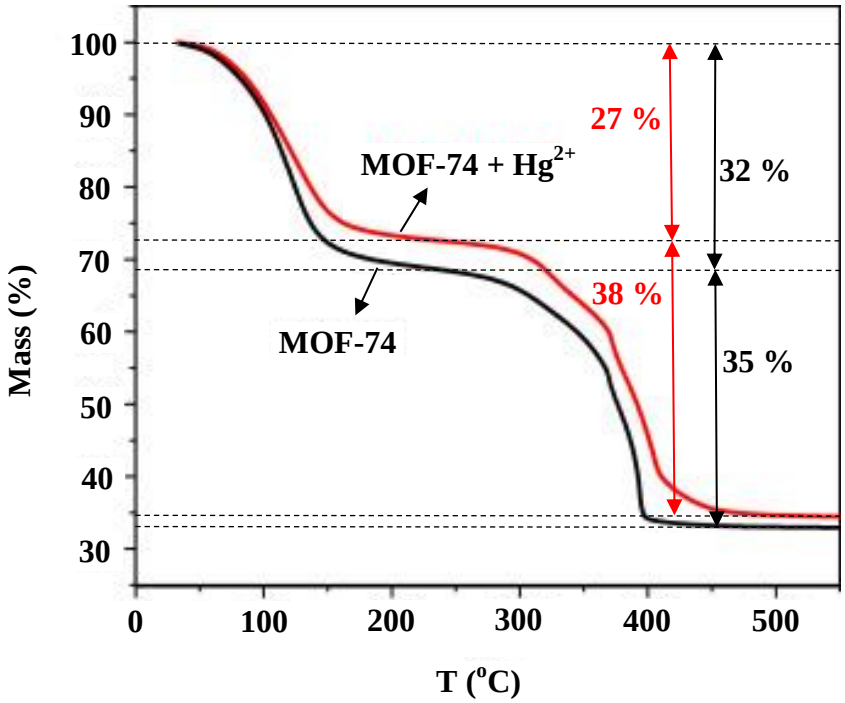

Figure 2.15: TGA thermogram of Zn-MOF-74 and Zn-MOF-74 after the adsorption of Hg^{2+} taken under N_2. Reprinted (adapted) with permission from Yang Yang Xiong, Jian Qiang Li, Le Le Gong, Xue Feng Feng, Li Na Meng, Le Zhang, Pan Pan Meng, Ming Biao Luo, Feng Luo; Journal of Solid State Chemistry, Volume 246, **2017**, 16–22. Copyright 2016, Elsevier.

Figure 2.15, p. 25, shows that Zn-MOF-74 contains 5 % more solvent and guest molecules than Zn-MOF-74 with Hg^{2+} adsorbed in the pores. This is an effect of the adsorbed Hg^{2+} in the Zn-MOF-74 pores.[33]

In this study, TGA will mainly be used to establish the thermal stability and purity of the activated MOF-74-III derivatives.

2.6 Scanning Electron Microscopy (SEM)

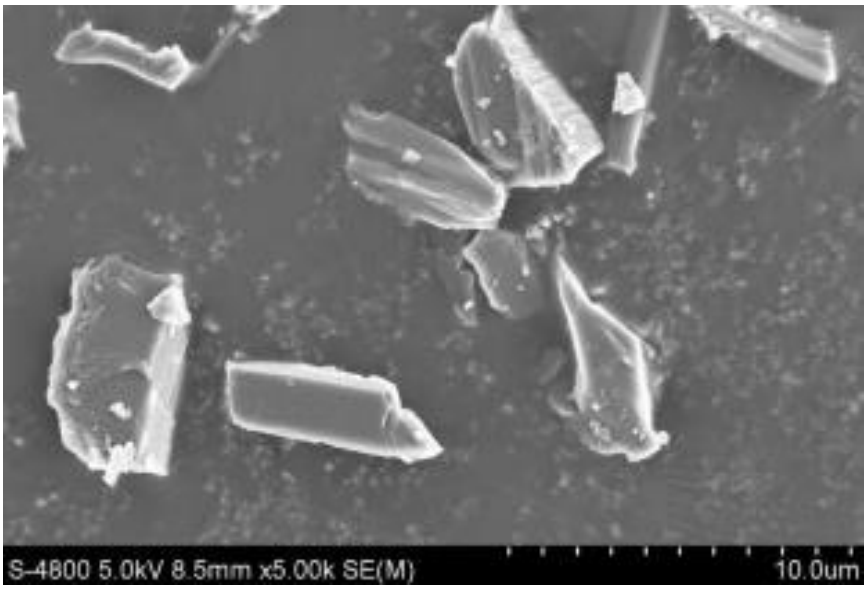

Figure 2.16: SEM image of Co-MOF-74. Reprinted (adapted) with permission from Lizi Yang, Cailing Xu, Weichun Ye, Weisheng Liu; Sensors and Actuators B: Chemical, Volume 215, **2015**, 489. Copyright 2016, Elsevier.

Figure 2.16, p. 26, shows that the particles of Co-MOF-74, synthesised from $Co(Ac)_2{\cdot}4H_2O$ and 3-(pyridine-3-yloxy)benzene-1,2-dicarboxylic acid), have an irregular shape with an average size of 45.0 μm.[32]

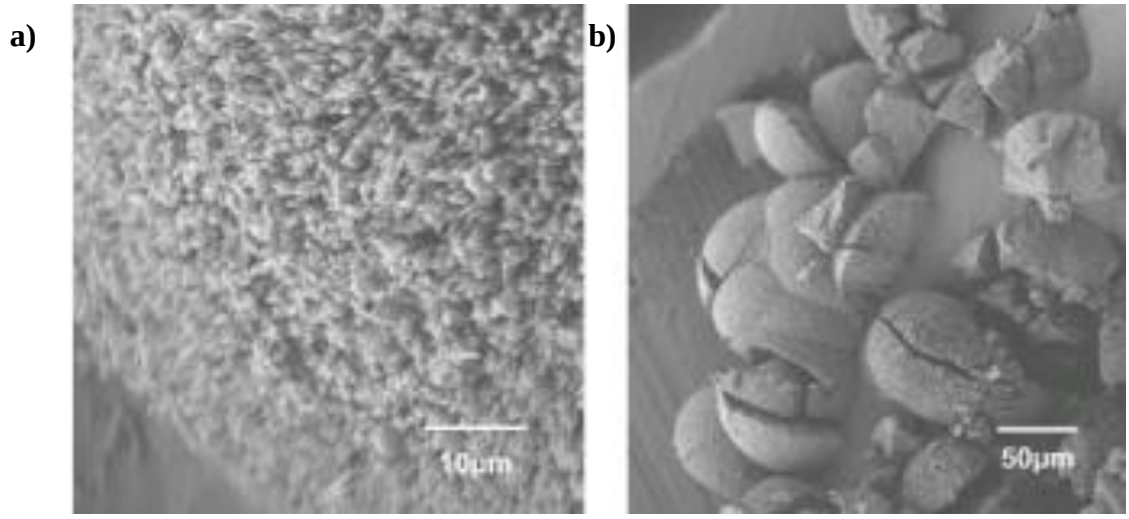

Figure 2.17: SEM images of Mg-IRMOF-74-III. Reprinted (adapted) with permission from Hexiang Deng, Sergio Grunder, Kyle E. Cordova, Cory Valente, Hiroyasu Furukawa, Mohamad Hmadeh, Felipe Gándara, Adam C. Whalley, Zheng Liu, Shunsuke Asahina, Hiroyoshi Kazumori, Michael O'Keeffe, Osamu Terasaki, J. Fraser Stoddart, Omar M. Yaghi; *Science* 25 May **2012**: Vol. 336, Issue 6084, pp. 1018. Copyright 2016, The American Association for the Advancement of Science.

The SEM image (Figure 2.17 a, p. 26) of the Mg-MOF-74-III, synthesised from $Mg(NO_3)_2 \cdot 6H_2O$ and 3,3”-di[hydroxy]-2’,5’-dimethyl-[1,1’:4’,1”-terphenyl]-4,4”-dicarboxylic acid shows a needle-like crystal morphology. Figure 2.17 b, p. 26, shows a SEM image of the same sample at a larger scale, indicating a single-phase morphology.[26]

In this study, detail of the morphology, topology and structural features will be verified using SEM. SEM imaging will also be used to detect impurities[55,] mean crystal diameter and crystal dis-formaties throughout the sample. SEM will be used to compare the morphology of the different functionalized MOF-74-III with that of MOF-74-III in Figure 2.17, p. 26.

2.7 Electrochemistry

2.7.1 Voltammetry

Cyclic voltammetry (CV) is an electroanalytical technique utilized to study electroactive species, through rapidly observing their redox behaviour,[27] while cycling the potential of the working electrode, in an unstirred solution. The current measured depends on the movement of electroactive material to and from the surface and the electron transfer process on the surface of the working electrode.[30] Anodic peak current (i_{pa}), cathodic peak current (i_{pc}), anodic peak potential (E_{pa}) and cathodic peak potential (E_{pc}) are the most important values obtained from a CV, Figure 2.18, p. 28.[27] The measured current depends on time and not on the applied potential.[30] Electrochemically reversible couples are redox couples having rapid electron exchange with the working electrode, maintaining the concentration of the oxidized and reduced forms at the electrode surface.[27, 30] For a reversible couple the formal reduction potential ($E^{0\prime}$) is centered between E_{pa} and E_{pc}:

$$E^{0\prime} = \frac{E_{pa} - E_{pc}}{2} \quad (1)$$

For a reversible couple the number of electrons (n) transferred, can be determined from the separation between the peak potentials:

$$\Delta E_p = E_{pa} - E_{pc} \cong \frac{0.059\,V}{n} \quad (2)$$

Electrochemical irreversibility is due to electron transfer taking place at a slow rate and this causes the peak separation to increase ($> \frac{0.059}{n}$). For reversibility the electron transfer should be

fast enough, so that the values for the peak currents, i_{pc} and $i_{pa,}$ can be identical. This reversibility is usually expressed in terms of the peak current ratio:

$$\frac{i_{pa}}{i_{pc}} = 1 \quad (3)$$

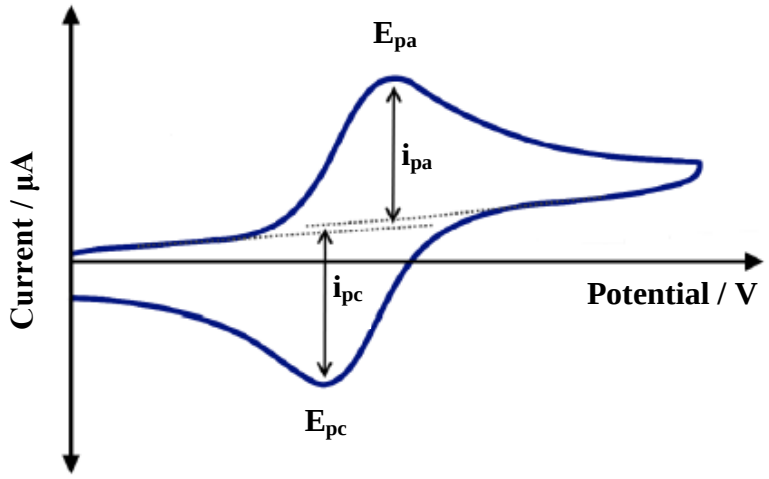

Figure 2.18: A typical cyclic voltammogram. Reprinted (adapted) with permission from H. J. Gericke, N. I. Barnard, E. Erasmus, J. C. Swarts, M. J. Cook and M. A. S. Aquino, *Inorganica Chim. Acta*, **2010**, 363, 2222.

Linear-sweep voltammetry is similar to cyclic voltammetry, but it only makes use of one forward scan, at a scan rate of 1 or 2 mV/s, usually much slower than those used for cyclic voltammetry.[28, 29] This method is often used for systems where the number of electrons in a transfer process is uncertain. The relative number of electrons transferred in electrochemical processes for the entire system can be determined (by comparison with an internal standard) using a linear-sweep voltammogram.[28]

2.7.2 Solid-State electrochemistry

Solid-State electrochemistry consists of a solid material deposited on (or forming) the electrode, immersed in a liquid or, eventually a solid electrolyte. Several methods were developed for the deposition of the material on the electrode surface: Direct deposition from suspension, fixation into a polymer coating, mechanical transference and adsorptive and covalent linkage to electrolyte surfaces.[38]

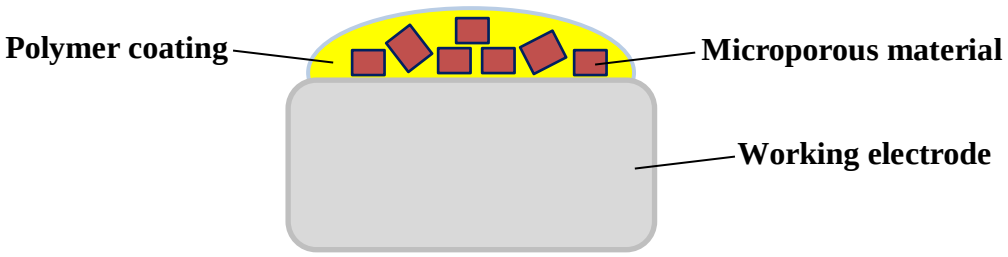

Figure 2.19: A working electrode surface covered with microparticles in a discontinued layer, fixed with a polymer coating.

2.7.3 MOF electrochemistry

The incorporation of redox-active ligands in multi-functional materials is capable of changing the properties of these materials, as a function of the redox state.[36]

The catalytic performance of an MOF is determined by the metal centres as the active sites. Guest molecules, like metals, can be diffused into the bulk MOF structure limited by the pore shape and size. The electrochemical activity of selected MOFs allowed them to be applied in fields like fuel cells, lithium-ion rechargeable batteries, supercapacitors, solar cells and lithium-sulphur batteries.[32]

Both non-Faradaic and Faradaic processes are present in supercapacitors, working together or independently, depending on the electrode material. Materials combining both processes can provide the best energy storage and power density. MOFs synthesised with a combination of different metal centres and tunable organic ligands can participate in electron exchange processes and can be utilized for energy storage purposes. Reports indicate that MOF-5, containing cobalt in the MOF pores achieved a storage capacity of 2 $F.g^{-1}$, this is due to the added cobalt not participating in any Faradaic process.[33]

A general property of MOFs with regard to electrochemistry is its ionic conductivity which can be more or less restricted depending on the type and concentration of defects in the structure of the MOF and temperature at which the electrochemistry is conducted.[38] Electron and ion transport in porous materials are facilitated through a combination of electron hopping between redox-active sites and ion diffusion across the micropores of the porous materials.[38]

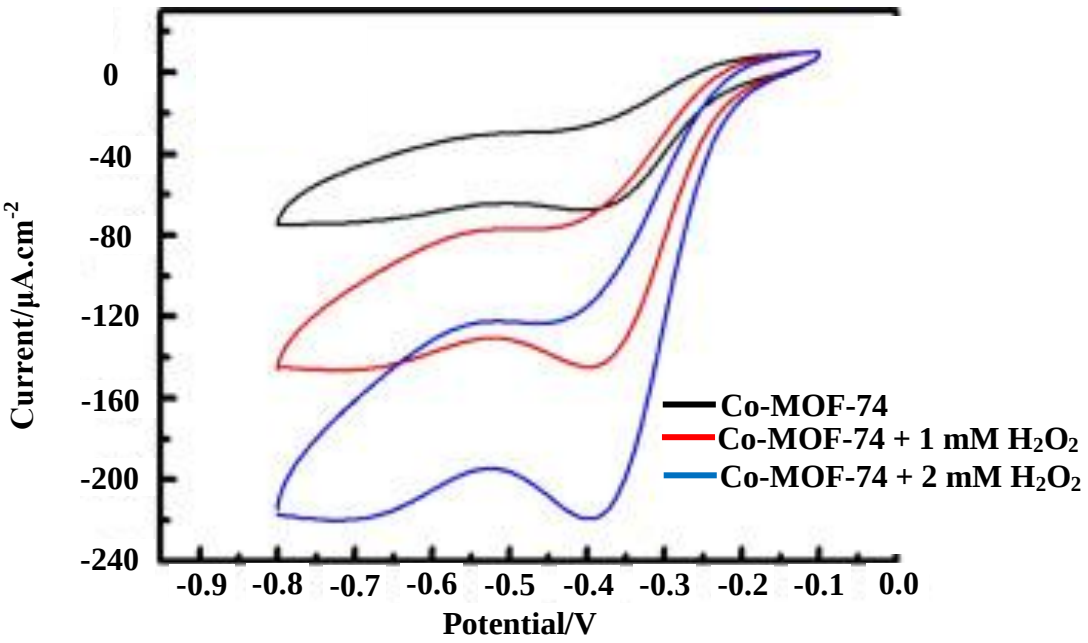

Figure 2.20: CV of Co-MOF-74, synthesised from $Co(Ac)_2 \cdot 4H_2O$ and 3-(pyridine-3-yloxy)benzene-1,2-dicarboxylic acid**,** without H_2O_2 (black), with 1 mM (red) and 2 mM (blue) H_2O_2 in 0.1 NaOH solutions, recorded at scan rate of 20 $mV.s^{-1}$. Reprinted (adapted) with permission from Lizi Yang, Cailing Xu, Weichun Ye, Weisheng Liu; Sensors and Actuators B: Chemical, Volume 215, **2015**, 489–496. Copyright 2016, Elsevier.

The reduction process at -0.4 V are for Co^{III} to Co^{II}. The solutions containing 0.1 M NaOH with 1 and 2 mM H_2O_2 shows a significant increase in the reduction current due to the catalytic reduction of H_2O_2 by the central metal of Co-MOF-74.[32]

Very little electrochemistry was published on MOF-74 derivatives. This study aims to contribute to the knowledge in this regard.

2.7.4 Ferrocene in MOFs: Electrochemistry

Ferrocene and ferrocene-containing derivatives are used for electron-transfer in electrochemical biosensors and can be linked to the backbone of MOFs through post-synthetic modification and used as redox active materials. In addition to all the advantages of MOFs, the organic linker can provide chemical versatility. MOFs in general have a hopping mechanism of electrons between redox centres, which may be localized on the organic linkers or the metal centres of the MOF. Literature reported a quasi-reversible electrochemical response after immobilizing a ferrocene derivative inside the channels of an Al-MOF.[58] MOFs with their high surface area, tunable pore sizes and a high density of redox active centres, can be used as electrochemical capacitors.[58]

2.8 Possible Applications of MOF-74

Applications of MOFs include gas storage, catalysis, luminescent sensing and drug delivery. Many MOFs show excellent biodegradability, biocompatibility, and excellent drug loading capabilities, proving its potential as a drug delivery host.[24] MOF-74 with its open Lewis acidic metal sites and its hygroscopic properties promotes its use as a drying agent, even better than alumina.[25]

Li-O_2 battery performance can be improved by using MOF-74, with well-defined pores and open-metal sites. This is due to O_2 adsorption onto the open-metal sites of an MOF-74 cathode. The O_2 enriched electrode acts as an O_2 store, promoting the cathode reaction. MOF-74 has a more polarized surface resulting in enhanced interaction with small molecules and ions. MOF-74's pores are large enough to contain the O_2 molecules, allowing its transportation during operation of the battery, improving the overall performance of these batteries.[45]

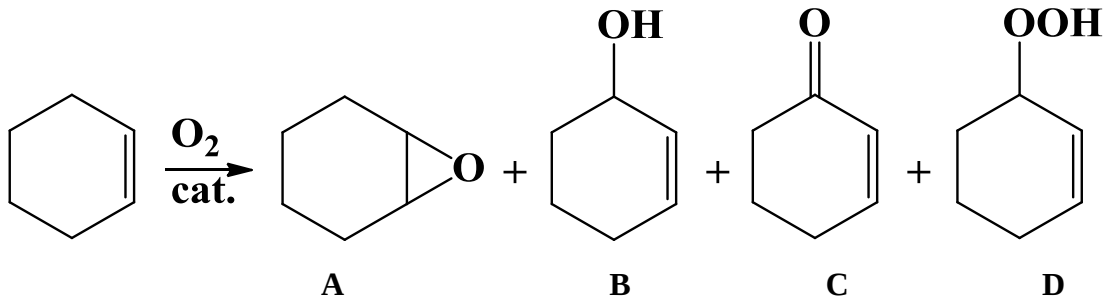

Scheme 2.4: Oxidation of cyclohexene.[48]

A possible catalytic application of Co-MOF-74 is the oxidation of cyclohexene, Scheme 2.4, p. 31. Although Ni-MOF-74 was shown to be inactive towards the oxidation of cyclohexene, the combination of Ni^{2+} and the Co-MOF-74, a mixed metal MOF, showed the most promising results for the oxidation of cyclohexene with product C (Scheme 2.4) as the most favourable product and minor amounts of the other products in Scheme 2.4.[47]

2.9 References

1. Q. Zhang, B. Li, L. Chen, *Inorg. Chem*., **2013**, 52, 9356.
2. K. Lee, J.D. Howe, L.C. Lin, B. Smit, J.B. Neaton, *Chem. Mater*., **2015**, 27, 668.
3. P.C. Banerjee, D.E. Lobo, R. Middag, W.K. Ng, M.E. Shaibani, M. Majumder, *Appl. Mater. Interfaces,* **2015**, 7, 3655.
4. C.O. Are, S. Chavan, C.P. Cabello, E. Garrone, G.T. Palomino, *Chem PhysChem*, **2010**, 11, 3237.
5. T. Pham, K. A. Forrest, K. McLaughlin, J. Eckert, B. Space, *J. Phys. Chem. C,* **2014,** 118, 22683.
6. T.G. Glover, G.W. Peterson, B.J. Schindler, D. Britt, O.M. Yaghi, *Chemical Engineering Science*, **2011**, 66, 163.
7. J.L.C. Rowsell, O.M. Yaghi, *Microporous and Mesoporous Materials*, **2004**, 73, 3.
8. T.W. Greene, P.G.M. Wuts, *Protective Groups in Organic Synthesis*, 4th ed., Wiley & Sons, New York, **1999**.
9. E. Saniger, M. Diaz-Gavilan, B. Delgado, D. Choquesillo, J.M. Gonzalez-Perez, S. Aiello, M.A. Gallo, A. Espinosa, J.M. Campos, *Tetrahedron*, **2004**, 60, 11453.
10. H. Fujioka, Y. Minamitsuji, O. Kubo, K. Senami, T. Maegawa, *Tetrahedron*, **2011**, 67, 2949.
11. G. Sabitha, R.S. Babu, M. Rajkumar, R. Srividya, J.S. Yadav, *Org. Lett.*, **2001**, 3, 8.
12. S. Makhseed, A. Cook, N.B. McKeown, *Chemical Comm*., **1999**, 419.
13. N. Miyaura, A. Suzuki, *Chem. Rev.*, **1995**, 95, 2457.
14. S. R. Chemler, D. Trauner, S. J. Danishefsky, *Angew. Chem. Int. Ed.*, **2001**, 40, 4544.
15. M. R. Netherton, G. C. Fub, *Adv. Synth. Catal.*, **2004**, 346, 1525.
16. K. C. Nicolaou, P. G. Bulger, D. Sarlah, *Angew. Chem. Int. Ed*., **2005**, 44, 4442.
17. M. Miura, *Angew. Chem. Int. Ed*., **2004**, 43, 2201.
18. J. P. Wolfe, R. A. Singer, B. H. Yang, S. L. Buchwald, *J. Am. Chem. Soc*., **1999**, 121(41), 9550.
19. A. Gillie, J. K. Stille, *J. Am. Chem. Soc*., **1980**, 15, 102.
20. T. Hayashi, M. Konishi, Y. Kobori, M. Kumada, T. Higuchi, K. Hirotsuf, *J. Am. Chem. Soc*, **1984**, 106(1), 158.
21. J. Suzuki, *Organometallic Chemistry*, **1999**, 576, 147.

22. G.V.M. Sharma, K.L. Reddy, P.S. Lakshmi, P.R. Kirshna, *Tetrahedron Letters*, **2004**, 45, 9229.
23. D.L. Chen, H. Shang, W. Zhu, R. Krishna, *Chemical Engineering Science*, **2014**, 117, 407.
24. Q. Hu, J. Yu, M. Liu, A. Liu, Z. Dou, Y. Yang, *J. Med. Chem*., **2014**, 57, 5679.
25. S. Dasgupta, S. Divekar, A.I. Spjelkavik, T. Didriksen, A. Nanoti, R. Blom, *Chemical Engineering Science*, **2015**, 137, 525.
26. H. Deng, S. Grunder, K. E. Cordova, C. Valente, H. Furukawa, M. Hmadeh, F. Gándara, A. C. Whalley, Z. Liu, S. Asahina, H. Kazumori, M. O'Keeffe, O. Terasaki, J. F. Stoddart, O. M. Yaghi, *Science*, **2012**, 336, 6084, pp. 1018.
27. W. R. Heineman, P. T. Kissinger, *J. Chem. Educ*., **1983**, 60, 702.
28. D. A. Skoog, D. M. West, F. J. Holler, S. R. Crouch, *Fundamentals of Analytical Chemistry*, Thomson-Brooks/Cole, 8th ed, **2004**.
29. H. J. Gericke, N. I. Barnard, E. Erasmus, J. C. Swarts, M. J. Cook, M. A. S. Aquino, *Inorganica Chim. Acta*, **2010**, 363, 2222.
30. G. A. Mabbott, *J. Chem. Educ*., **1983**, 60, 697.
31. E. Jakobsche, A. Choudhary, S. J. Miller, R. T. Raines, *J Am Chem Soc*., **2010**, 132(19), 6651.
32. L. Yang, C. Xu, W. Ye, W. Liu, *Sensors and Actuators B: Chemical*, **2015**, 215, 489.
33. Y. Y. Xiong, J. Q. Li, L. L. Gong, X. F. Feng, L. N. Meng, L. Zhang, P. P. Meng, M. B. Luo, F. Luo, *Journal of Solid State Chemistry*, **2017**, 246, 16.
34. H. Gholipour-Ranjbar, M. Soleimania, H. R. Naderi, *New J. Chem*., **2016**, 40, 9187.
35. S. Dou, X. Li, L. Tao, J. Huo, S. Wang, *Chem. Commun*., **2016**, 52, 9727.
36. C. Hua, B. F. Abrahams, D. M. D'Alessandro, *Cryst. Growth*, **2016**, 16, 1149.
37. A. Kong, C. Mao, Q. Lin, X. Wei, X. Bu, P. Feng, *Dalton Trans*., **2015**, 44, 6748.
38. A. Doménech-Carbó, *Electrochemistry of Porous Materials*, CRC Press, **2010**.
39. J. W. Brown, B. L. Henderson, M. D. Kiesz, A. C. Whalley, W. Morris, S. Grunder, H. Deng, H. Furukawa, J. I. Zink, J. F. Stoddart, O. M. Yaghi, *Chem. Sci*., **2013**, 4, 2858.
40. A. M. Fracaroli, H. Furukawa, M. Suzuki, M. Dodd, S. Okajima, F. Gándara, J. A. Reimer, O. M. Yaghi, *J. Am. Chem. Soc*., **2014**, 136, 8863.
41. H. Oh, S. Maurer, R. Balderas-Xicohtencat, L. Arnold, O. V. Magdysyuk, G. Schűtz, U. Műller, M. Hirscher, *International Journal of Hydrogen Energy*, **2016**, http://dx.doi.org/10.1016/j.ijhydene.2016.08.153.

42. X. Hu, H. Hu, C. Li, T. Li, X. Lou, Q. Chen, B. Hu, *Journal of Solid State Chemistry*, **2016**, 242, 71.
43. J. Hu, V. A. Blatov, B. Yu, K. Van Hecke, G. Cui, *Dalton Trans*., **2016**, 45, 2426.
44. C. Hua, B. F. Abrahams, D. M. D'Alessandro, *Cryst. Growth*, **2016**, 16, 1149.
45. D. Wu, Z. Guo, X. Yin, Q. Pang, B. Tu, L. Zhang, Y.G. Wang, Q. Li, *Adv. Mater*., **2014**, 26, 3258.
46. A. N. Rudenko, S. Bendt, F. J. Keil, *J. Phys. Chem. C*, **2014,** 118, 16218.
47. D. Sun, F. Sun, X. Deng, Z. Li, *Inorg. Chem*., **2015**, 54(17), 8639.
48. S. A. FitzGerald, J. M. Schloss, C. J. Pierce, B. Thompson, J. L. C. Rowsell, K. Yu, J. R. Schmidt, *J. Phys. Chem. C*, **2015**, 119, 5293.
49. S. Chen, M. Xue, Y. Li, Y. Pan, L. Zhu, S. Qiu, *J. Mater. Chem. A*, **2015**, DOI: 10.1039/c5ta02557e.
50. Wen, H.; Wang, H.; Li, B.; Wang, H.; Qian, G.; Chen, B.; *Inorg. Chem*., **2016**, DOI: 10.1021/acs.inorgchem.6b00748.
51. S. Han, H. Kim, Y. Jung, *Phys. Chem. Chem. Phys*., **2015**, 17, 16977.
52. J. Xu, R. Sinelnikov, Y. Huang, *J. Am. Chem. Soc*., **2016**, 136, 8863.
53. K. Sumida, C.M. Brown, Z.R. Herm, S. Chavan, S. Bordiga, J.R. Long, *Chem. Commun*., **2011**, 47, 1157.
54. P. Canepa, C.A. Arter, E.M. Conwill, D.H. Johnson, B.A. Schocmaker, K.Z. Soliman, T. Thouhauser, *J. Mater. Chem. A*, **2013**, 1, 13597.
55. M. Diaz-Garcia, A. Mayoral, I. Diaz, M. Sánchez- Sánchez, *Cryst. Growth*, **2014**, 2479.
56. K. Tan, S. Zuluaga, Q. Gong, P. Canepa, H. Wang, J. Li, Y.J. Chabal, T. Thonhauser, *Chem. Mater*., **2014**, 26, 6886.
57. Z. Chang, N. Gao, Y. Li, X. He, *Anal. Methods*, **2012**, 4, 4037.
58. F. Jaouen, A Morozan, *Encyclopedia of Inorganic and Bioinorganic Chemistry*, **2014**, John Wiley & Sons, Ltd; DOI: 10.1002/9781119951438.eibc2226.
59. R. Trivedi, S.B. Deepthi, L. Giribabu, B. Sridhar, P. Sujitha, C.G. Kumar, K.V.S. Ramakrishna, *Appl. Organometal. Chem*., **2012**, 26, 369.
60. A. Ghorbani-Choghamarani, M. Norouzi, *New J. Chem.*, **2016**, 40, 6299.
61. M. Eckhardt, G. C. Fu, *J. Am. Chem. Soc.*, **2003**, *125*, 13642.
62. B. Saito, G. C. Fu, *J. Am. Chem. Soc.*, **2007**, *129*, 9602.
63. J. Y. Lee, G. C. Fu, *J. Am. Chem. Soc.*, **2003**, *125*, 5616.

3 Results and Discussions

3.1 Introduction

A series of novel 4,4”-di[methoxyethoxymethoxy]-[1,1’:4’,1”-terphenyl]-3,3”-di[methoxyethoxy-methoxycarbonyl] derivatives, , were synthesised, as shown in Scheme 3.1: 4,4”-di[methoxyethoxymethoxy]-2’,5’-dimethyl-[1,1’:4’,1”-terphenyl]-3,3”-di[methoxyethoxy-methoxycarbonyl], **3**, 4,4”-di[methoxyethoxymethoxy]-2’,5’-dihydroxy-[1,1’:4’,1”-terphenyl]-3,3”-di [methoxyethoxymethoxycarbonyl], **6**, 4,4”-di[methoxyethoxymethoxy]-2’,5’-dibenzyloxy-[1,1’:4’,1”-terphenyl]-3,3”-di[methoxyethoxymethoxycarbonyl], **8** and 4,4”-di[methoxyethoxymethoxy]-3’-[3-ferrocenylpropamide]-[1,1’:4’,1”-terphenyl]-3,3”-di[methoxyethoxymethoxycarbonyl], **14**.

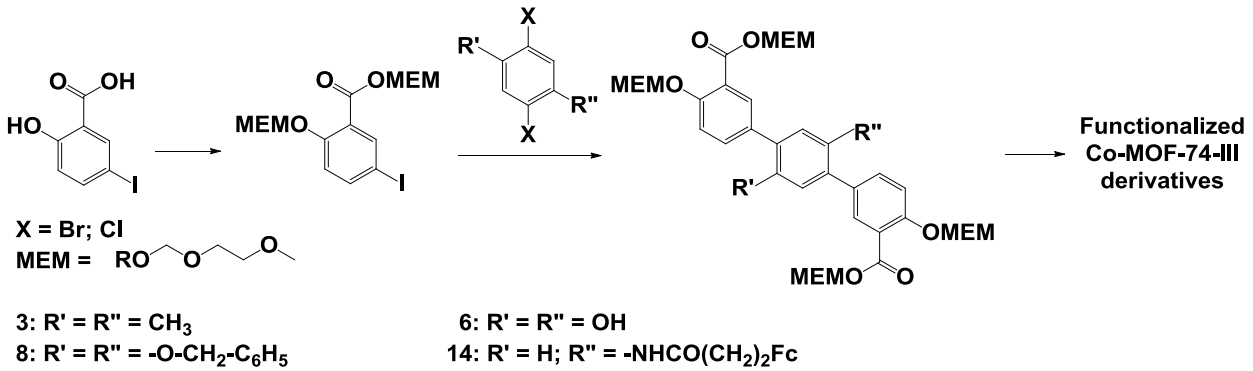

Scheme 3.1: Chemical structure of the 4,4”-di[methoxyethoxymethoxy]-[1,1’:4’,1”-terphenyl]-3,3”-di[methoxyethoxymethoxycarbonyl] derivatives synthesised in this study.

The compounds were characterized using nuclear magnetic resonance spectroscopy (^{1}H and ^{13}C NMR) and infrared spectroscopy (IR). The 4,4”-di[methoxyethoxymethoxy]-[1,1’:4’,1”-terphenyl]-3,3”-di[methoxyethoxymethoxycarbonyl] derivatives were then used as linkers in the synthesis of Co-MOF-74-III derivatives, characterized using Accelerated Surface Area and Porosity (ASAP) and Thermal Gravimetric Analysis (TGA) techniques. Selected compounds were analysed using electrochemical methods (cyclic voltammetry).

From literature, all the linkers to synthesise MOF-74-III, have the same structural layout. The carboxylic acid functionalities are linear with respect to the linker backbone and the hydroxy-

functionalities always in the *ortho*-position with respect to the neighbouring carboxylic acid functionalities (Figure 3.1a, p. 36).

a)

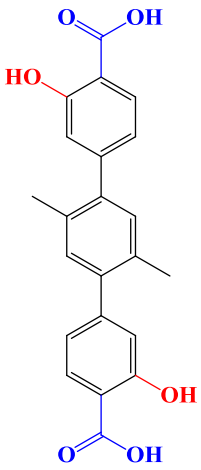

b)

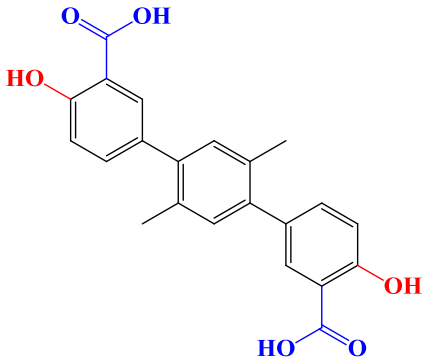

Figure 3.1: **a)** Linkers found in literature[1, 10]; **b)** linkers synthesised in this study.

The linkers synthesised in this study have a different structural layout with the hydroxy-functionalities now linear with respect to the linker backbone and the carboxylic acid functionalities in the *ortho*-position with respect to the hydroxyl-functionality (Figure 3.1b, p. 36). This was done to lower the cost of the starting material, as well as to investigate whether the switching of positions of the carboxylic acid and hydroxyl-functional groups will have an influence on the MOFs formation.[1, 10]

3.2 Synthesis

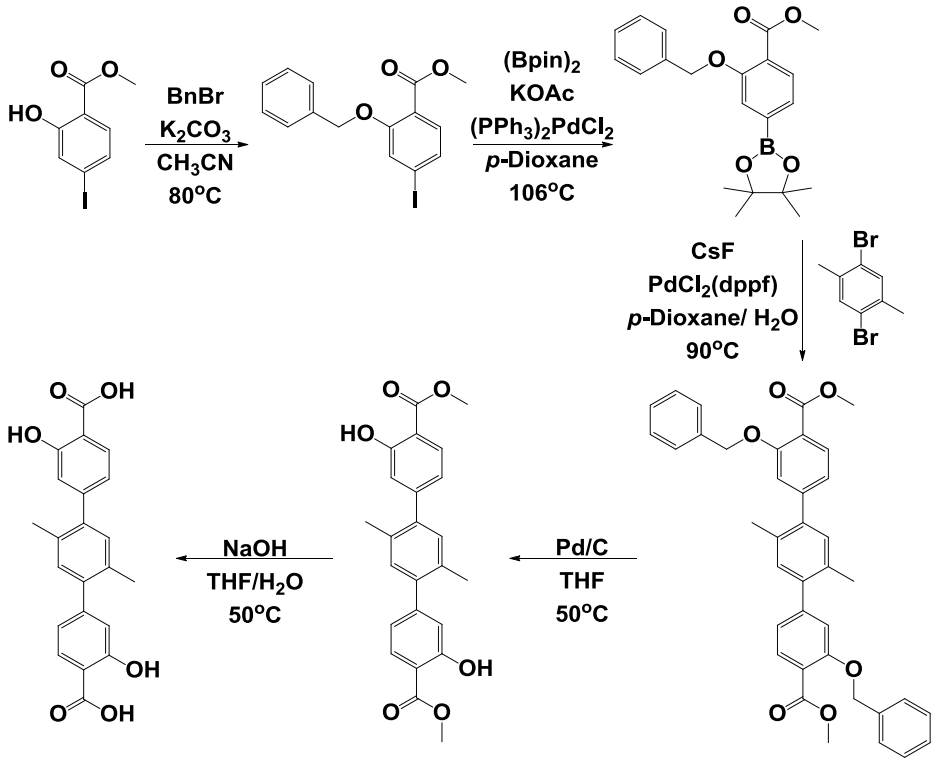

Scheme 3.2: Current (literature) linker synthesis route.[1]

Scheme 3.2 shows the tried and trusted synthesis route for 4,4”-di[hydroxy]- 2’,5’-dimethyl-[1,1’:4’,1”-terphenyl]- 3,3”-di[caboxylic acid]. These reaction conditions are harsh and proved to be problematic with protecting and de-protecting. This synthesis route consists out of 5 steps, lowering the overall yield of the reaction. In this study, the reaction conditions and reagents will be changed with the aim to reduce the number of reaction steps and improve yields.

3.2.1 Adding protecting groups

Protecting the carboxylic acid and alcohol functionality of the iodosalicylic acid, was the first step in the synthesis process, according to Scheme 3.2, p. 37.

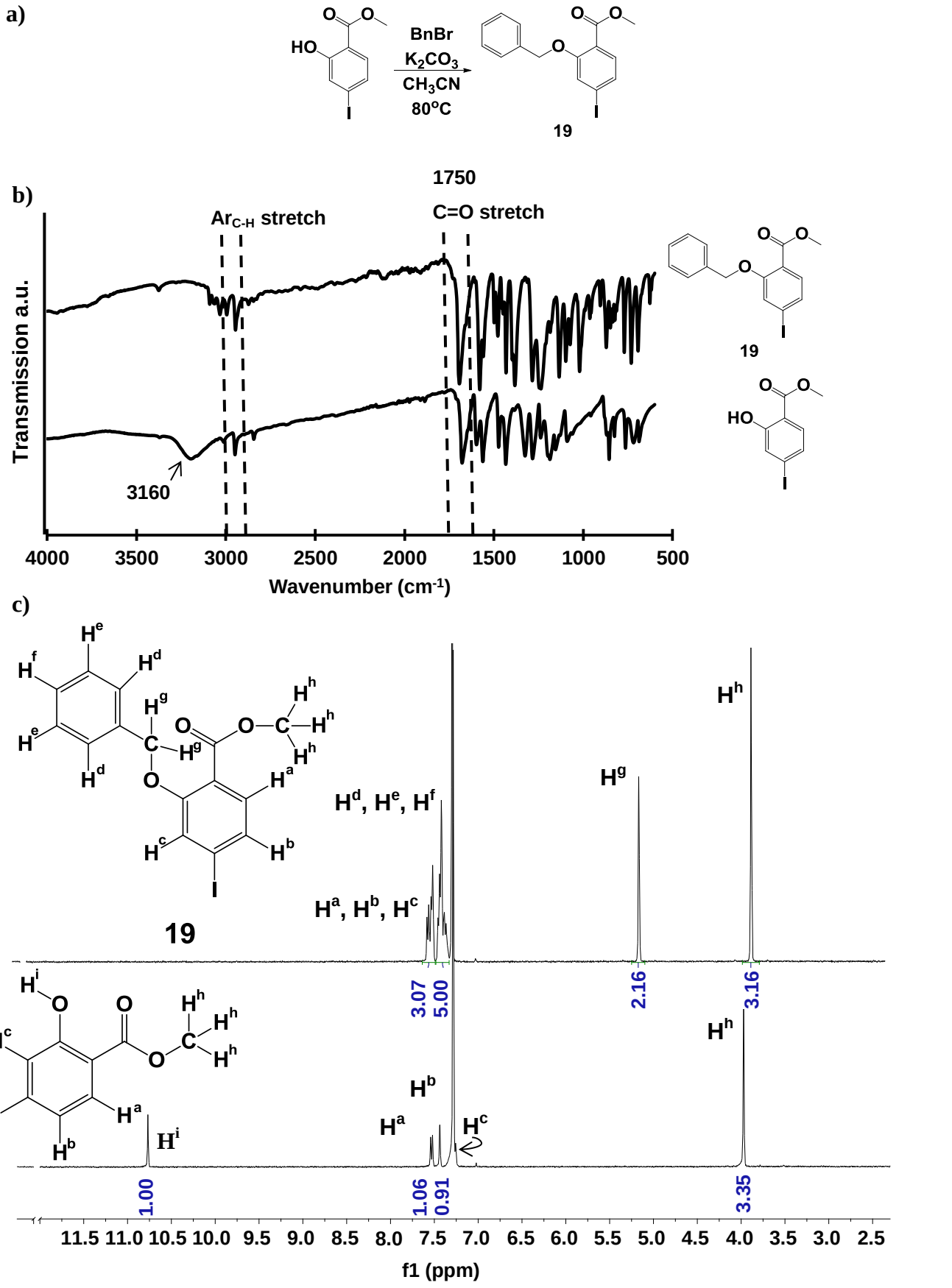

Figure 3.2: a) Synthesis **b)** Transmission FTIR spectra and **c)** ^{1}H NMR spectra of methyl-2-benzyloxy-4-iodobenzoate, **19.**

Protecting the alcohol functionality with a benzyl-group, Figure 3.2a, p. 38, proved to be a success with a high yield of 80 % of methyl-2-benzyloxy-4-iodobenzoate, **19**. The results of this synthesis will be compared to the synthesis of 5-iodo-2-methoxyethoxymethoxy-1-methoxyethoxymethoxycarbonylphenyl, **1** (Figure 3.3a, p. 40). Methyl-2-hydroxy-4-iodobenzoate was treated with benzyl bromide in the presence of a base, potassium carbonate, in acetonitrile. The transmission FTIR spectra (Figure 3.2b, p. 38) of methyl-2-hydroxy-4-iodobenzoate and methyl-2-benzyloxy-4-iodobenzoate, **19** shows a C=O stretching at 1750 cm^{-1} and aromatic C-H stretching frequencies around 3000 cm^{-1}. Compound **19**, however, gave an extra set of peaks at around 3010 cm^{-1} due to the benzyloxy-protecting group. The FTIR transmission spectrum of compound **19** shows no O-H stretching at 3160 cm^{-1}, which is a good indication that the hydroxyl-group of methyl-2-hydroxy-4-iodobenzoate was completely protected with the benzyloxy-protecting group. Compound **19** shows a strong peak at 1018 cm^{-1} which is absent in the starting material (methyl-2-hydroxy-4-iodobenzoate) which is also an indication of product formation.

The ^{1}H NMR spectrum (Figure 3.2c, p. 38) for the methyl-2-hydroxy-4-iodobenzoate starting material shows a singlet at 10.50 ppm for the hydroxy-functionality of the, three singlets between 7 and 6.9 ppm representing the protons of the phenyl ring and a singlet at 4.0 ppm for three methyl protons. In comparison, the proton spectrum of methyl-2-benzyloxy-4-iodobenzoate, **19** shows an extra singlet at 5.2 ppm for two protons of the $–CH_2$ linker, a multiplet at 7.25 ppm for the five protons of the extra phenyl ring and no peak at 10.50 ppm, indicating the absence of the –OH functionality. Deprotection of the carboxylic acid functionality (last step in Scheme 3.2, p. 38) proved to be less successful since the removal of the methyl-group resulted in a yield of less than 20 %.

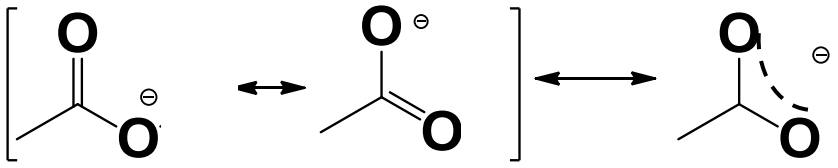

Scheme 3.3: Electron-releasing inductive effect of methylesters

In methylesters, the electron-releasing inductive effect, illustrated in Scheme 3.3, of the alkyl group increases the electron density on the oxygen and thus hinders the breaking of the $O-CH_3$ bond. In benzoic acid, the carbon atoms in the ring are sp_2-hybridised as well as the carbon atom of the carboxylic functionality. As a result, benzoic acid is a stronger acid than cyclohexane

carboxylic acids. Electron withdrawing groups substituted in the ortho and para positions can enhance the acid strength. The electron withdrawing group in the para position of methyl-2-benzyloxy-4-iodobenzoate, **19** as well as the stabilizing effect of the ring and carbonyl carbon, causes difficulty in the deprotection of the methyl-protecting group.

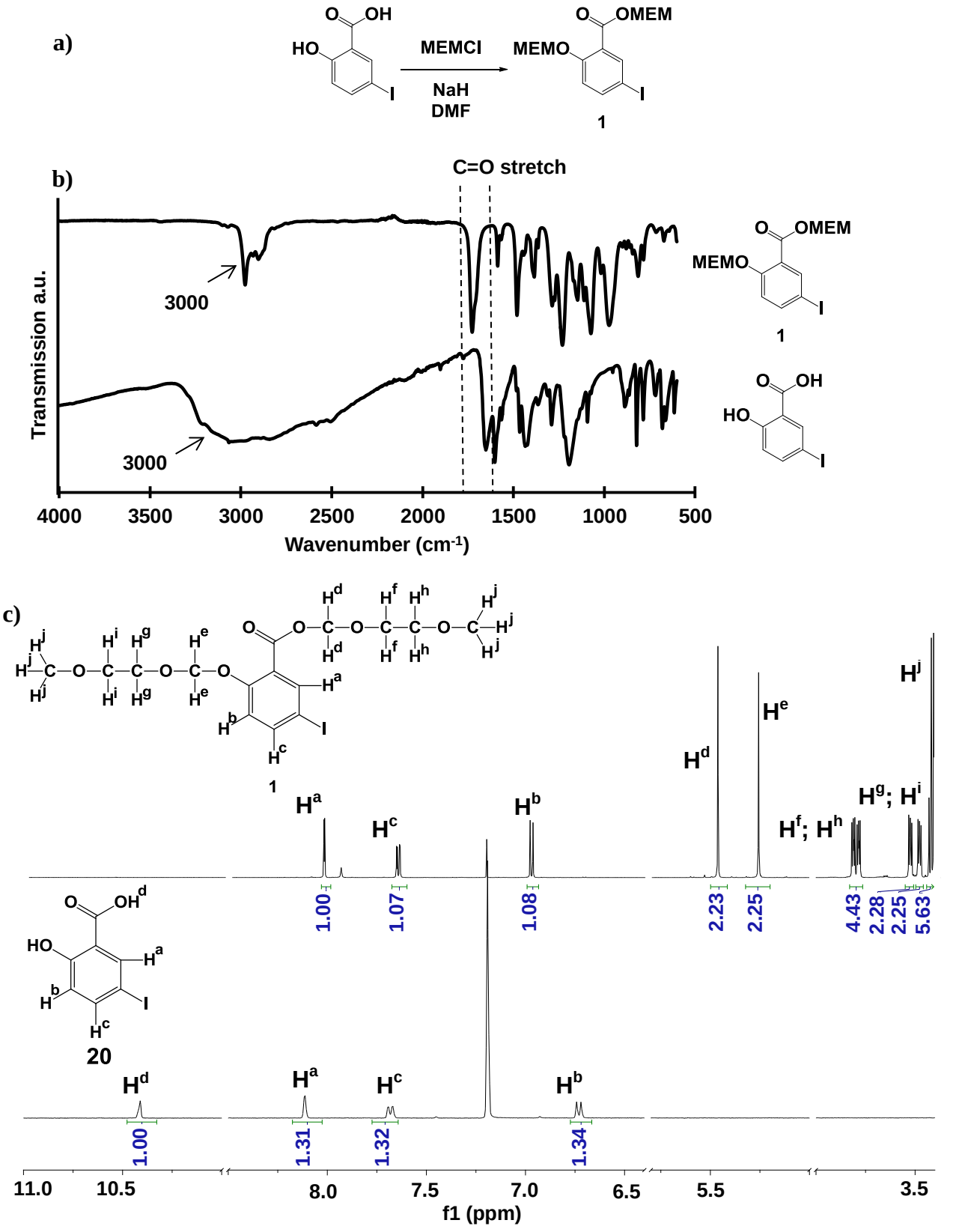

Figure 3.3: a) Synthesis, **b)** Transmission FTIR spectra and **c)** ^{1}H NMR spectra of 5-iodo-2-methoxyethoxymethoxy-1-methoxyethoxymethoxy-carbonyl-phenyl**, 1** and 5-iodosalicylic acid, **20**.

In an attempt to solve this problem the alcohol and carboxylic acid functionality of 5-iodosalicylic acid were both protected with methoxyethoxymethoxy chloride (MEMCl). The original synthesis process (Figure 3.3 a, p. 40) is reduced with two steps since both the protecting groups can be added in a single step and removed with another. The electron withdrawing iodo-group on 5-iodosalicylic acid, **20**, in the meta-position with respect to the carbonyl functionality, doesn't enhance the acid strength. Sodium hydride and 5-iodosalicylic acid were separately dissolved in DMF before adding the two solutions together dropwise. MEMCl was then added, yielding 72% of 5-iodo-2-methoxyethoxymethoxy-1-methoxyethoxymethoxycarbonyl-phenyl, **1**.

The transmission FTIR spectra (Figure 3.3b, p. 40) of 5-iodosalicylic acid and 5-iodo-2-methoxyethoxymethoxy-1-methoxyethoxymethoxycarbonyl-phenyl, **1** both show a C=O stretching frequency at 1750 cm^{-1}. Compound **1**, shows an aromatic C-H stretching frequency at 3000 cm^{-1} while 5-iodosalicylic acid shows a broad peak at around 3000 cm^{-1} which is due to the OH- and carboxylic acid functionalities of the 5-iodosalicylic acid.

The NMR spectrum (Figure 3.3c, p. 40) for 5-iodo-methoxyethoxymethoxy-2-methoxyethoxy-methoxycarbonyl-phenyl, **1** shows a singlet at 8.03 ppm, doublet at 7.66 ppm and a doublet at 6.98 ppm which are for the protons of the phenyl ring. The singlet at 5.46 ppm is for the MEM $–CH_2$ group bound to the ester functionality. The singlet at 5.26 ppm is for the MEM $–CH_2$ group bound to the ether functionality. The multiplet at 3.4 ppm is for the MEM $–CH_3$ groups of the ester and ether functionality. The peak at 10.5 ppm of the starting material (5-iodosalicylic acid), is absent in the NMR spectrum of 5-iodo-methoxyethoxymethoxy-2-methoxyethoxy-methoxycarbonyl-phenyl, **1**, which is an indication that the carboxylic acid functionality is protected with an MEM-group.

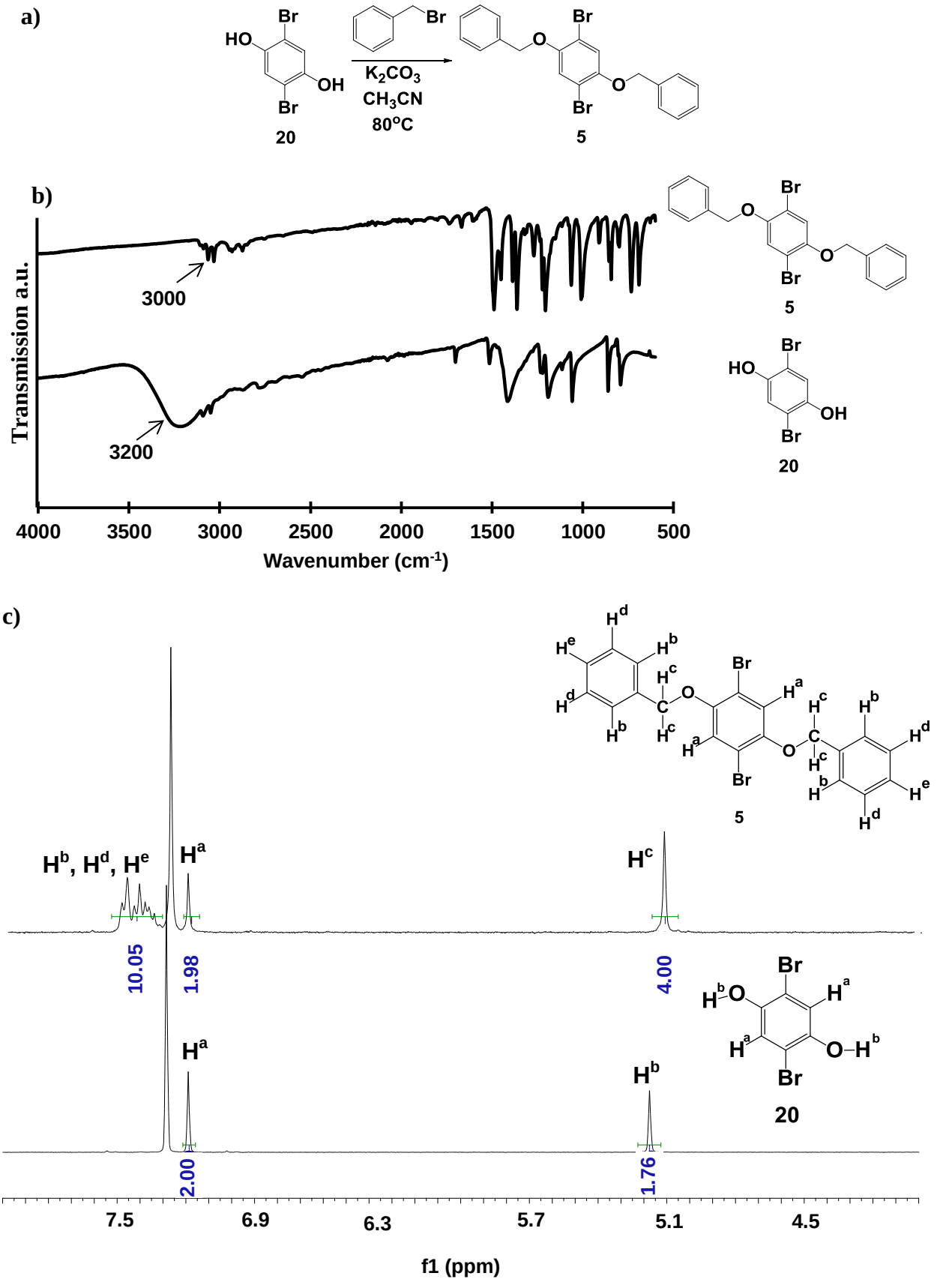

Figure 3.4: a) Synthesis of 1,4-bisbenzyloxy-2,5-dibromophenyl, **5**, **b)** Transmission FTIR spectra and **c)** ^{1}H NMR spectra of 2,5-dibromohydroquinone, **20** and 1,4-bisbenzyloxy-2,5-dibromophenyl, **5**.

The hydroxy-groups on 2,5-dibromohydroquinone, **20**, were protected by a benzyl protecting group, different from that of 5-iodo-2-methoxyethoxymethoxy-1-methoxyethoxymethoxy-carbonyl-phenyl, **1**. This would allow the deprotection to take place separately, when both types of protecting groups (benzyl and MEM) are on the same molecule as in 4,4”-di[methoxyethoxy-methoxy]-2’,5’-bis-benzyloxy-[1,1’:4’,1”-terphenyl]-3,3”-di[methoxyethoxymethoxycarbonyl], **8** (Scheme 3.1, p. 35). During the synthesis of 1,4-bisbenzyloxy-2,5-dibromophenyl, **5** the crude product was washed with ethyl acetate which forms a low-boiling azeotrope with acetonitrile making it easier to remove the solvent.

The FTIR transmission spectrum (Figure 3.4b, p. 42) of 2,5-dibromohydroquinone, **20**, shows a broad O-H stretching frequency at 3200 cm^{-1}, which is absent in the spectrum of 1,4-bisbenzyloxy-2,5-dibromophenyl, **5**, a good indication that the protection of 2,5-dibromohydroquinone, **20** was successful.

The NMR spectrum (Figure 3.4c, p. 42) of 1,4-bisbenzyloxy-2,5-dibromophenyl, **5** shows a multiplet between 7.42 and 7.35 ppm representing the 10 protons on the two equivalent phenyl rings of the benzyloxy-functional groups, which is not present in the NMR spectrum of 2,5-dibromohydroquinone, **20**. It also shows a singlet at 7.21 ppm for the two protons on the central phenyl ring and a singlet at 5.10 ppm for the four protons of the two equivalent $–CH_2$ groups of the benzyloxy-groups.

3.2.2 Cross-coupling reactions

The second step in the synthesis process, according to Scheme 3.1, was the carbon-carbon bond formation through a relevant cross-coupling reaction between 5-iodo-2-methoxyethoxy-methoxy-1-methoxyethoxymethoxycarbonyl-phenyl, **1** and the functionalized aryl halide derivatives. There are several cross-coupling reactions, as mentioned in Chapter 2. In this study, the Suzuki-Miyuara cross-coupling reaction was used since it allows easy synthesis of the boron intermediate. There are several different reaction conditions for Suzuki-Miyuara cross-coupling. For the formation of the 4,4”-di[methoxyethoxymethoxy]-[1,1’:4’,1”-terphenyl]-3,3”-di[methoxyethoxymethoxycarbonyl] derivatives (Scheme 3.1, p. 35), several reaction conditions were investigated. The synthesis of 4,4”-di[methoxyethoxymethoxy]-2’,5’-dimethyl-[1,1’:4’,1”-terphenyl]-3,3”-di[methoxyethoxymethoxycarbonyl], **3** (Scheme 3.4, p. 45) was used to optimized the different reaction conditions, tabulated in Table 3.1., p. 44, The optimal conditions

(entry #6) were then also utilized in the synthesis of the other 4,4”-di[methoxyethoxymethoxy]-[1,1’:4’,1”-terphenyl]-3,3”-di[methoxyethoxymethoxycarbonyl] derivatives, Scheme 3.1, p. 35.

Table 3.1: Suzuki-Miyuara cross-coupling reaction conditions employed during the synthesis of 4,4”-di[methoxyethoxymethoxy]-2’,5’-dimethyl-[1,1’:4’,1”-terphenyl]-3,3”-di[methoxyethoxymethoxycarbonyl], **3**

#	Boron Source	Reaction Conditions	Product yield (%)
1	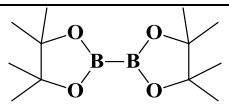	NaOH, $(PPh_3)_4Pd$, Benzene, 80^oC, 16h	0
2	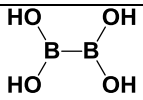	NaOH, (dppf)PdCl, THF, 65^oC, 16h	6
3	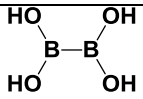	*p*-dioxane, KOAc, $(PPh_3)_2PdCl_2$, 90^oC, 16h	20
4	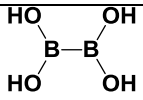	*p*-dioxane, KOAc, $(PPh_3)_2PdCl_2$, 60^oC, 60h	47
5	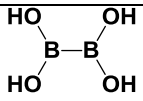	*p*-dioxane, KOAc, Excess $(PPh_3)_2PdCl_2$, 60^oC, 16h	52
6	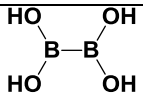	*p*-dioxane, Excess KOAc, Excess $(PPh_3)_2PdCl_2$, 60^oC, 16h	90

From entry #1, #2 and #3 (Table 3.1), it was concluded that *p*-dioxane is a better solvent than benzene and THF and a lower temperature (60 ^oC) prevents decomposition of the catalyst. Together with a longer reaction time, it resulted in a higher product yield of 47 %, entry #4, Table 3.1. In order to reduce reaction time, the amount of catalyst, $(PPh_3)_2PdCl_2$, was increased from 0.017 mmol to 0.17 mmol, giving 52 % after 16h, entry #5 (Table 3.1). In the last attempt (entry #6) the amount of base, KOAc, was increased from 1.77 mmol to 3.33 mmol, to give a 90 % yield of the desired 4,4”-di[methoxyethoxymethoxy]-2’,5’-dimethyl-[1,1’:4’,1”-terphenyl]-3,3”-di[methoxyethoxymethoxycarbonyl], **3**.

The base plays an important role in the coordination sphere of the palladium and in the acceleration of the transmetallation step[2]. Excess base accelerates the transmetallation step, in forming the desired product. The palladium catalyst often leads to the formation of self-coupled products and phosphine-bound aryl coupled products. To prevent the formation of these by-products, a catalyst with bulky phosphine ligands was employed. An increased amount of catalyst also sped up the desired reaction.

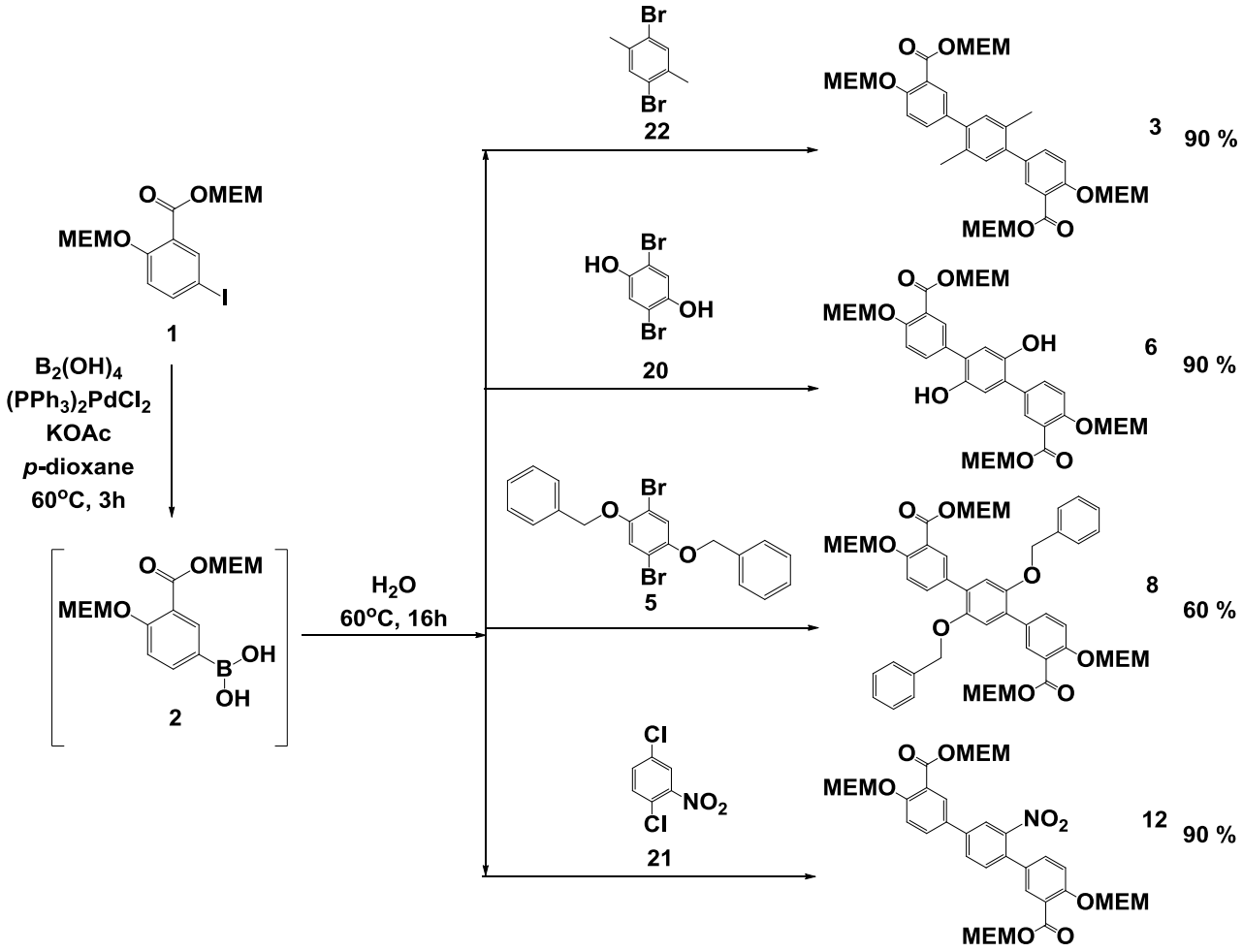

Scheme 3.4: Suzuki-Miyuara cross-coupling of 5-iodo-2-methoxyethoxymethoxy-1-methoxyethoxymethoxy-carbonyl-phenyl, **1** with functionalized aryl halide derivatives (**22, 20, 5, 21**) to give 4,4”-di[methoxyethoxy-methoxy]-[1,1’:4’,1”-terphenyl]-3,3”-di[methoxyethoxymethoxycarbonyl] derivatives.

A crucial step in the synthesis of the 4,4”-di[methoxyethoxymethoxy]-[1,1’:4’,1”-terphenyl]-3,3”-di[methoxyethoxymethoxycarbonyl] derivatives, is the *in situ* formation of the intermediate, 5-[dihydroxy]-boron-methoxyethoxymethoxy-2-methoxyethoxymethoxy-carbonyl-phenyl, **2** after 3 hours at 60 ^{o}C (Scheme 3.4). After the addition of H_2O and the differently functionalized aryl halide derivatives (**22**, **20**, **5**, **21**), the different 4,4”-di[methoxyethoxymethoxy]-[1,1’:4’,1”-terphenyl]-3,3”-di[methoxyethoxymethoxycarbonyl] derivatives were obtained in good yields.

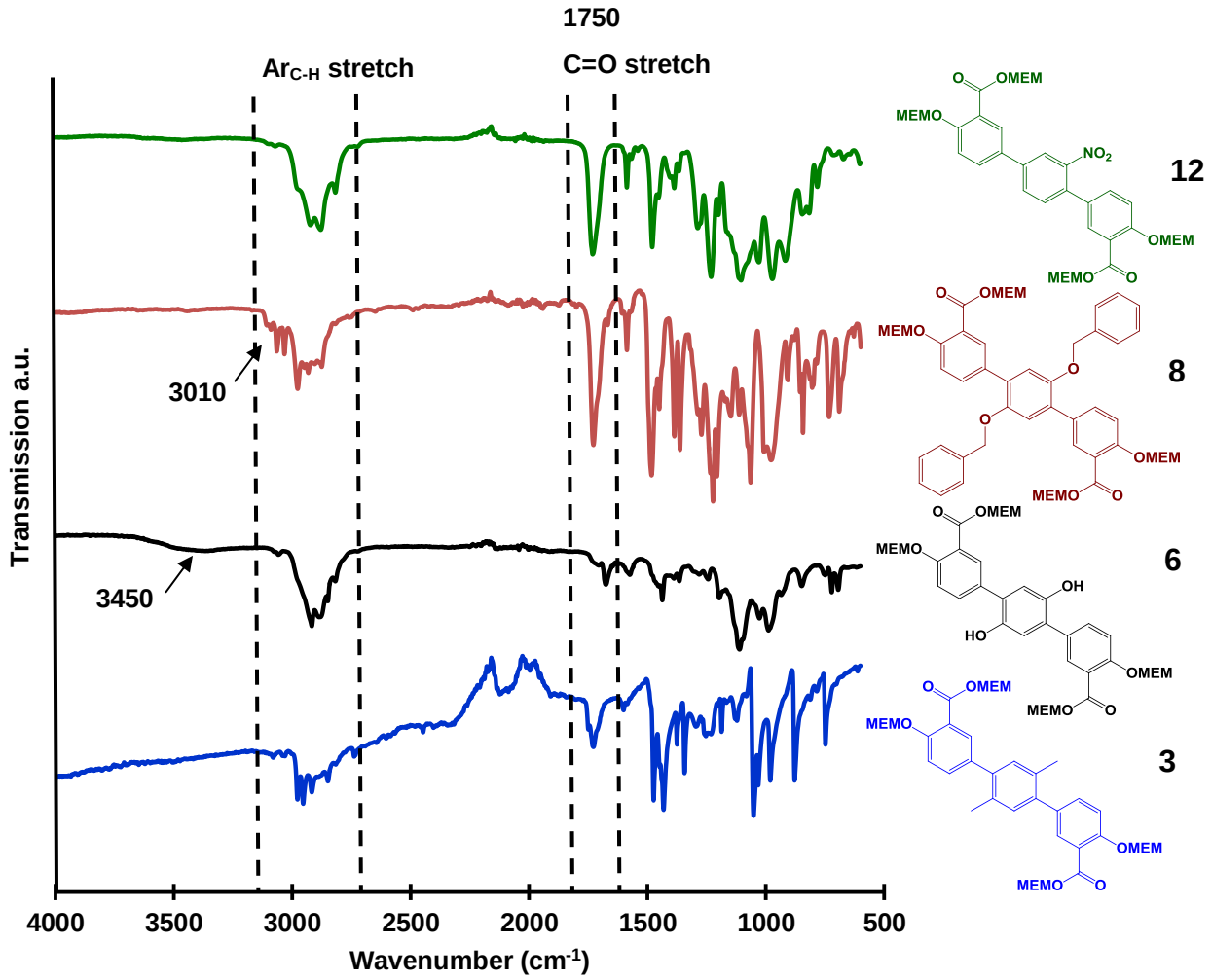

Figure 3.5: Transmission FTIR spectra of 4,4”-di[methoxyethoxymethoxy]-2’,5’-dimethyl-[1,1’:4’,1”-terphenyl]-3,3”-di[methoxyethoxymethoxycarbonyl], **3;** 4,4”-di[methoxyethoxymethoxy]-2’,5’-dihydroxy-[1,1’:4’,1”-terphenyl]-3,3”-di[methoxyethoxymethoxycarbonyl]**, 6;** 4,4”-di[methoxyethoxymethoxy]-2’,5’-bis-benzyloxy-[1,1’:4’,1”-terphenyl]-3,3”-di[methoxyethoxymethoxycarbonyl**], 8** and 4,4”-di[methoxyethoxymethoxy]-3’-nitro-[1,1’:4’,1”-terphenyl]-3,3”-di[methoxyethoxymethoxycarbonyl]**, 12**

All the 4,4”-di[methoxyethoxymethoxy]-[1,1’:4’,1”-terphenyl]-3,3”-di[methoxyethoxy-methoxycarbonyl] derivatives showed a C=O stretching frequency at 1750 cm^{-1} and aromatic C-H stretching frequencies around 3000 cm^{-1}. Compound **8** gave an extra aromatic C-H stretching frequency at 3010 cm^{-1}, due to the two benzyloxy-protecting groups on the central phenylene ring. A broad peak at around 3450 cm^{-1} for compound **6**, originates from the stretching of the two O-H groups. (Figure 3.5, p. 46)

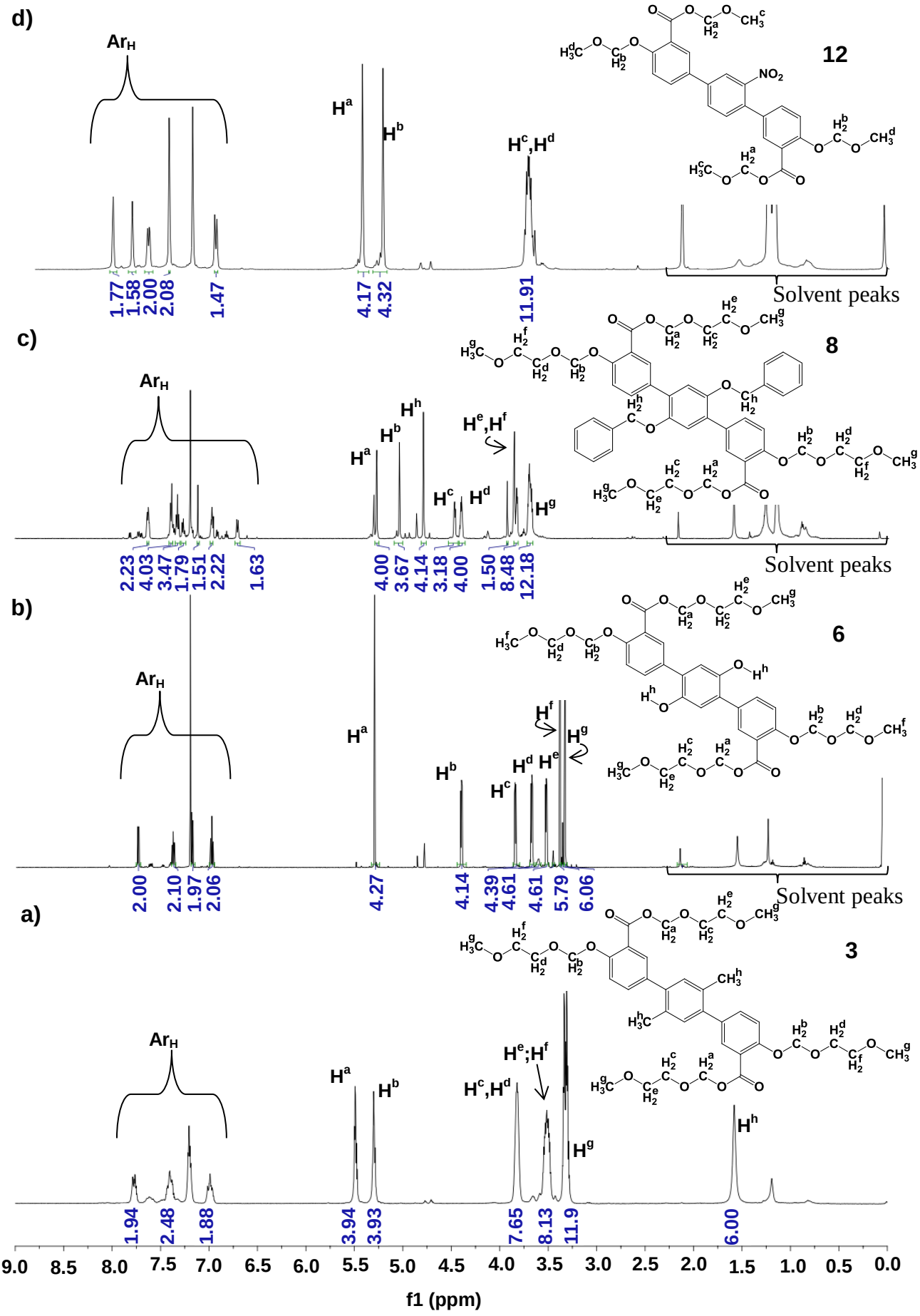

Figure 3.6: ^{1}H NMR spectra in $CDCl_3$ of the 4,4”-di[methoxyethoxymethoxy]-[1,1’:4’,1”-terphenyl]-3,3”-di[methoxyethoxymethoxycarbonyl] derivatives, **3**, **6**, **8** and **12**.

The ^{1}H NMR spectra of the 4,4”-di[methoxyethoxymethoxy]-[1,1’:4’,1”-terphenyl]-3,3”-di[methoxyethoxymethoxycarbonyl] derivatives in Figure 3.6 (p. 47) show the resonance of the aromatic protons between 8.0 and 6.5 ppm, which are accounted for collectively (marked Ar_H), due to overlapping of peaks in this region. For all four compounds the $–CH_2$ and $-CH_3$ protons of the methyl ethyl methyl (MEM) protecting groups resonate between 6 and 3 ppm (marked H^a-H^g). The spectrum of compound 3 also shows a singlet at 1.62 ppm (marked H^h) for the $–CH_3$ groups on the central phenyl-ring.

The protons of the –OH group on the central phenyl ring of compound 6 (marked H^h) did not resonate in the measurement window (Spectrum b).

Spectrum c (Figure 3.6, p. 47) shows an extra peak for the $–CH_2$ group of the benzyloxy functionality at 4.75 ppm (marked H^h). This compound was particularly difficult to separate during column chromatography due to the bulky bis-benzyloxy functionalities and long MEM chains.

The reaction to form compound **12**, was more exothermic than the reactions for compound **3**, **6** and **8**. This could result in thermal degradation of the MEM chains protecting the hydroxy- and carbonyl-functionality. In addition, the added hydrochloric acid could assist in shortening the MEM protecting chains. The reaction time was thus restricted to minimize the shortening of the MEM chains. Figure 3.6d (p. 47) shows peaks for the $–CH_2$ and $-CH_3$ protons of the MEM-remnants between 6 and 3 ppm.

3.2.3 Binding a ferrocenyl-derivative to 4,4”-di[methoxyethoxy-methoxy]-3’-nitro-[1,1’:4’,1”-terphenyl]-3,3”-di[methoxy-ethoxymethoxycarbonyl], 12

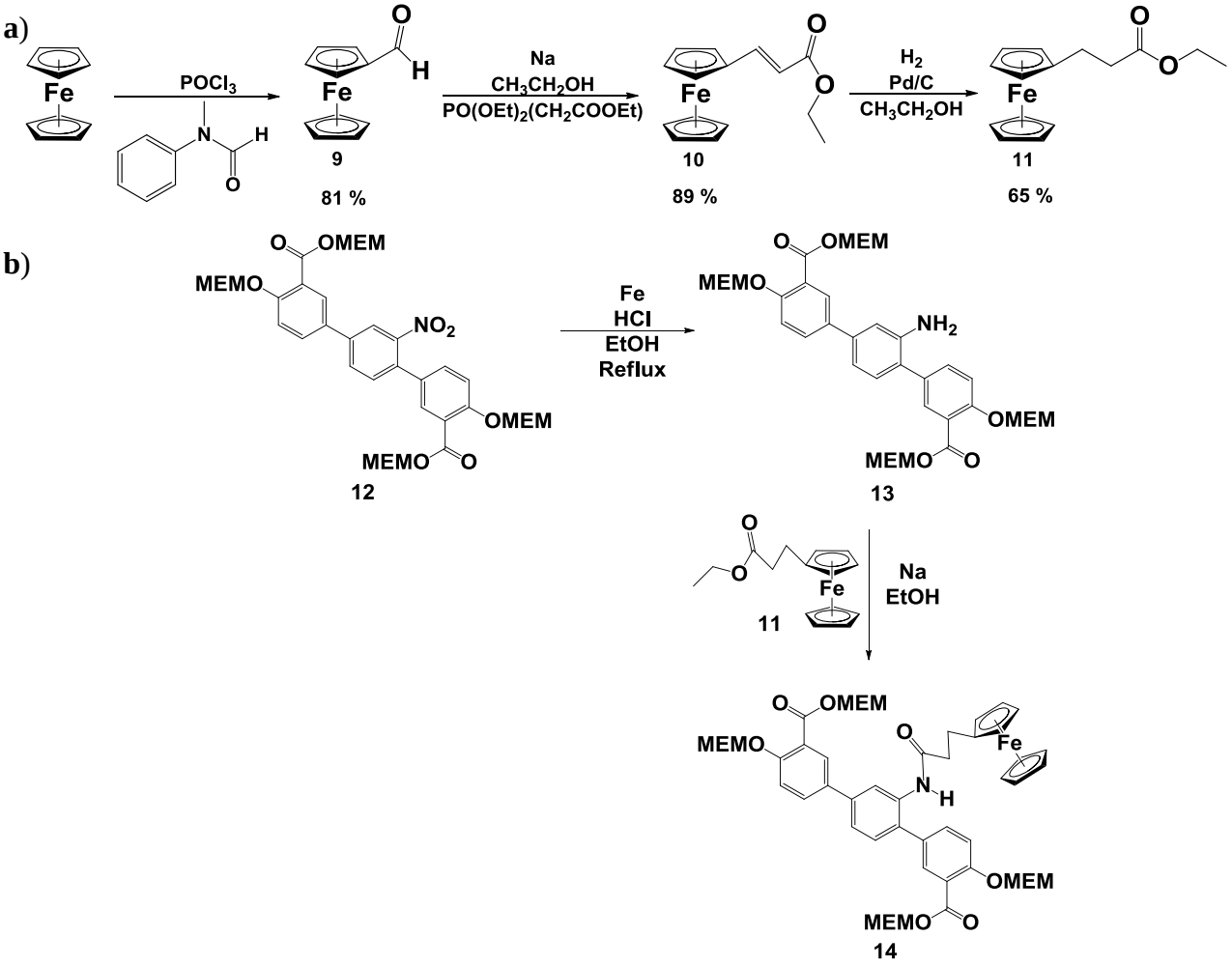

Scheme 3.5: a) Synthesis of ethyl -3-ferrocenylpropanoate, **b)** Binding of ethyl-3-ferrocenylpropanoate, **11** to 4,4”-di[methoxyethoxymethoxy]-3’-nitro-[1,1’:4’,1”-terphenyl]-3,3”-di[methoxyethoxymethoxycarbonyl] , **12**.

The synthesis of ethyl-3-ferrocenylpropanoate is a known reaction and was followed exactly as in literature[8]. The first step is a Vilsmeier formylation of ferrocene to form ferrocene carboxaldehyde, **9**, secondly reacting with triethylphosphonoacetate forming ethyl-3-ferrocenylethenoate, **10**, and lastly reducing the double bond, forming ethyl-3-ferrocenylethanoate, **11**.

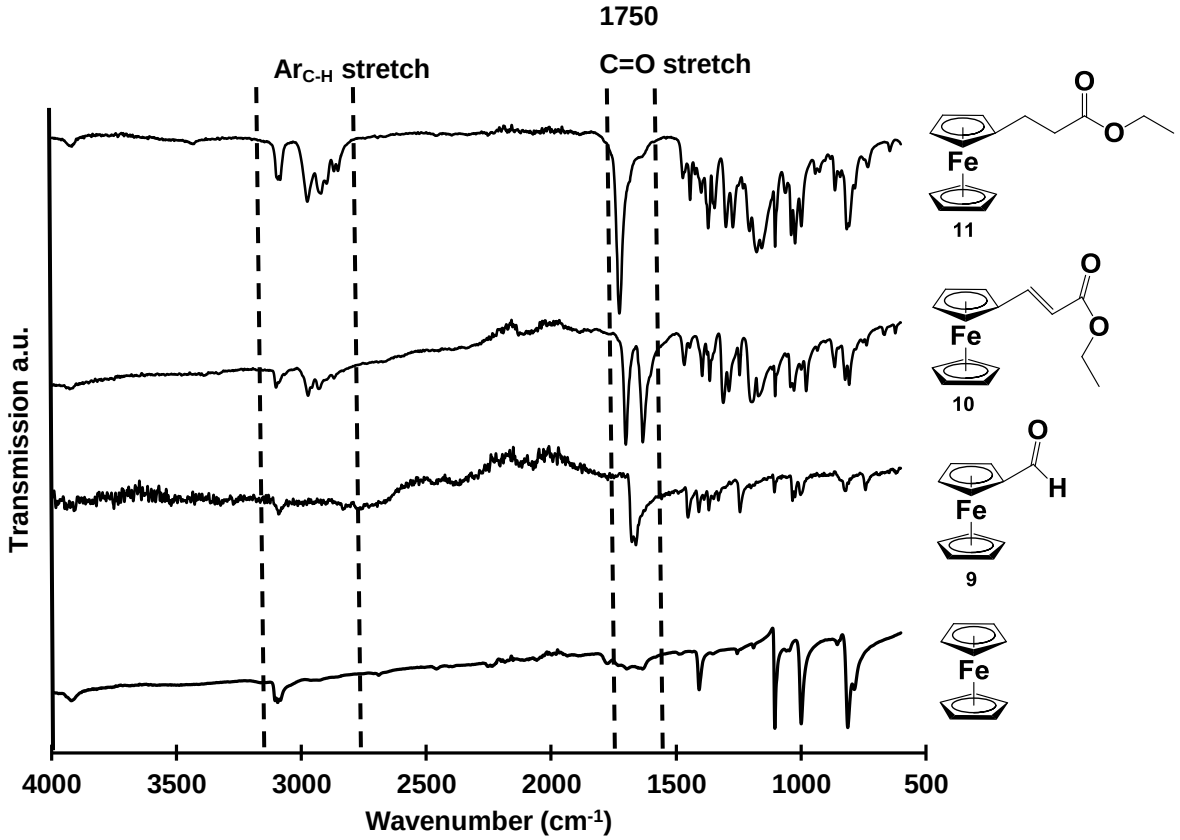

Figure 3.7: Transmission FTIR spectra of ferrocene; ferrocene carboxaldehyde, **9**; ethyl-3-ferrocenylethenoate, **10** and ethyl-3-ferrocenylethanoate, **11**.

In comparing the FTIR spectra (Figure 3.7, p. 50) of ferrocene, ferrocene carboxaldehyde, **9**; ethyl-3-ferrocenylethtenoate, **10** and ethyl-3-ferrocenylethanoate, **11** it is clear that the C=O stretching frequency at 1750 cm^{-1} is present in the spectra of all the functionalized ferrocene compounds. The peaks at around 3000 cm^{-1} represent the aromatic C-H stretching frequencies of the ferrocene moiety.

The nitro functionality on 4,4”-di[methoxyethoxymethoxy]-3’-nitro-[1,1’:4’,1”-terphenyl]-3,3”-di[methoxyethoxymethoxycarbonyl], **12**, is a poor leaving group, and was replaced with an amine group. This was done using the Bechamp reduction method. 4,4”-Di[methoxyethoxy-methoxy]-3’-nitro-[1,1’:4’,1”-terphenyl]-3,3”-di[methoxyethoxymethoxycarbonyl], **12**, was added to a mixture of iron powder, HCl and ethanol, and refluxed until all the iron powder was dissolved (Scheme 3.5, p. 49). 4,4”-Di[methoxyethoxymethoxy]-3’-amino-[1,1’:4’,1”-terphenyl]-3,3”-di[methoxyethoxymethoxycarbonyl], **13** was employed in the next reaction without isolation or purification.

The amino-functionality of compound **13** will easily leave to form an amide. Ethyl-3-ferrocenylpropanoate, **11** was slowly added to a mixture of sodium and ethanol. The crude 4,4”-di[methoxyethoxymethoxy]-3’-amino-[1,1’:4’,1”-terphenyl]-3,3”-di[methoxy-ethoxymethoxycarbonyl], **13,** was added dropwise to the reaction mixture, and allowed to react for 16 hours, yielding 70% of 4,4”-di[methoxyethoxymethoxy]-3’-[3-ferrocenylpropamide]-[1,1’:4’,1”-terphenyl]-3,3”-di[methoxyethoxymethoxycarbonyl], **14**.

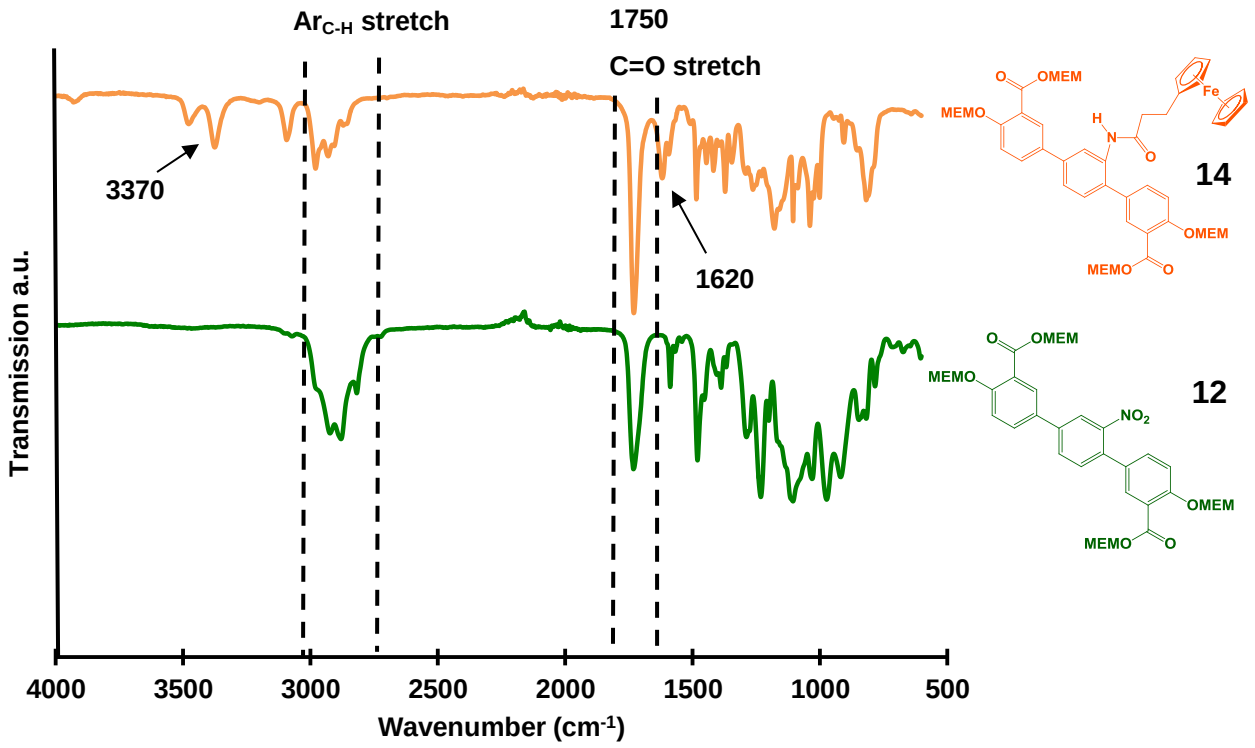

Figure 3.8: Transmission FTIR spectra of 4,4”-di[methoxyethoxymethoxy]-3’-nitro-[1,1’:4’,1”-terphenyl]-3,3”-di[methoxyethoxymethoxycarbonyl]**,** 12 and 4,4”-di[methoxyethoxymethoxy]- 3’-[3-ferrocenylpropamide]-[1,1’:4’,1”-terphenyl]-3,3”-di[methoxyethoxymethoxycarbonyl]**, 14.**

The FTIR spectra of compound **12** and **14** both show a C=O and aromatic C-H stretching frequency at 1750 cm^{-1} and 3000 cm^{-1}, respectively. This is in accordance with the spectra of similar derivatives in Figure 3.5 (p. 46). Compound **14** has an N-H and a C=O stretching frequency at 3370 cm^{-1} and 1620 cm^{-1} respectively, due to the amide-functionality.

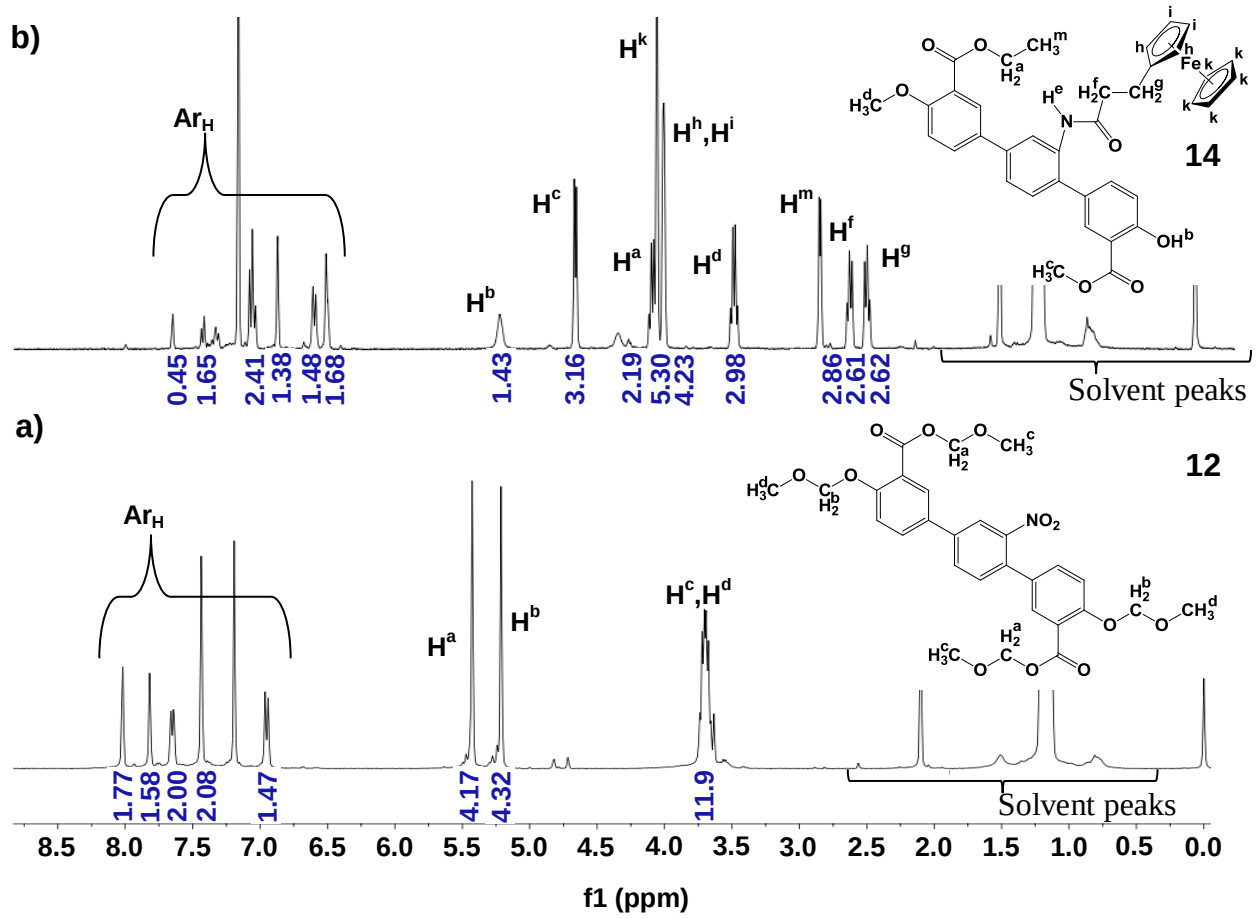

Figure 3.9: ^{1}H NMR spectra in $CDCl_3$ of compound **12** and **14**.

In Figure 3.9 (p. 52) the ^{1}H NMR spectra of the starting material, **12** and product, **14**, of the two step reaction, Scheme 3.5b (p. 52), are compared. Both spectra show the aromatic protons between 8.0 and 6.5 ppm. The $–CH_2$ and $-CH_3$ protons of the protective groups of both compounds resonate between 6 and 2.5 ppm. For compound **14**, the ferrocenyl-fragment shows the following proton resonance: a singlet at 4.0 ppm (marked H^k) for the five protons of the unsubstituted cyclopentadienyl ring; singlet at 4.1 ppm (marked H^h, H^i) for the two sets of protons on the monosubstituted cyclopentadienyl ring; two peaks between 2.75 and 2.25 ppm (marked H^f and H^g) for the four methylene protons of the alkyl chain between the amide bond and ferrocene.

3.2.4 Removal of the MEM-protecting groups

Deprotection is the final step in the linker synthesis before the synthesis of the Co-MOF-74-III derivatives. MEM-protecting groups are easily removed in the presence of acid.

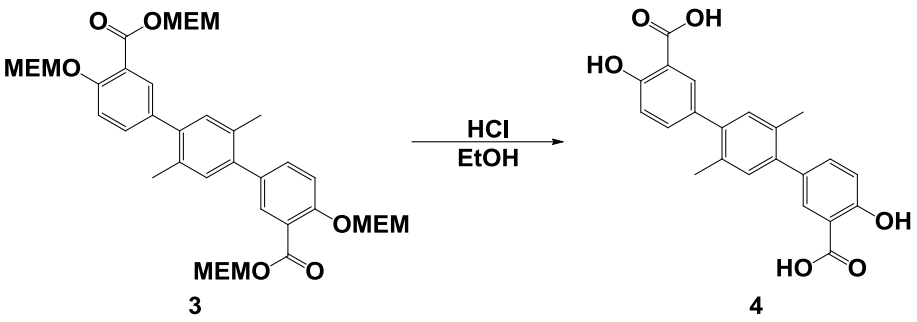

Scheme 3.6: Deprotection of the hydroxyl-functionalities of 4,4”-di[hydroxy]-2’,5’-dimethyl-[1,1’:4’,1”-terphenyl]-3,3”-dicarboxylic acid , **4**

4,4”-Di[methoxyethoxymethoxy]-2’,5’-dimethyl-[1,1’:4’,1”-terphenyl]-3,3”-di[methoxy-ethoxymethoxycarbonyl] , **3**, was added to a mixture of HCl and ethanol, and refluxed to give 60% of 4,4”-di[hydroxy]-2’,5’-dimethyl-[1,1’:4’,1”-terphenyl]-3,3”-dicarboxylic acid , **4**.

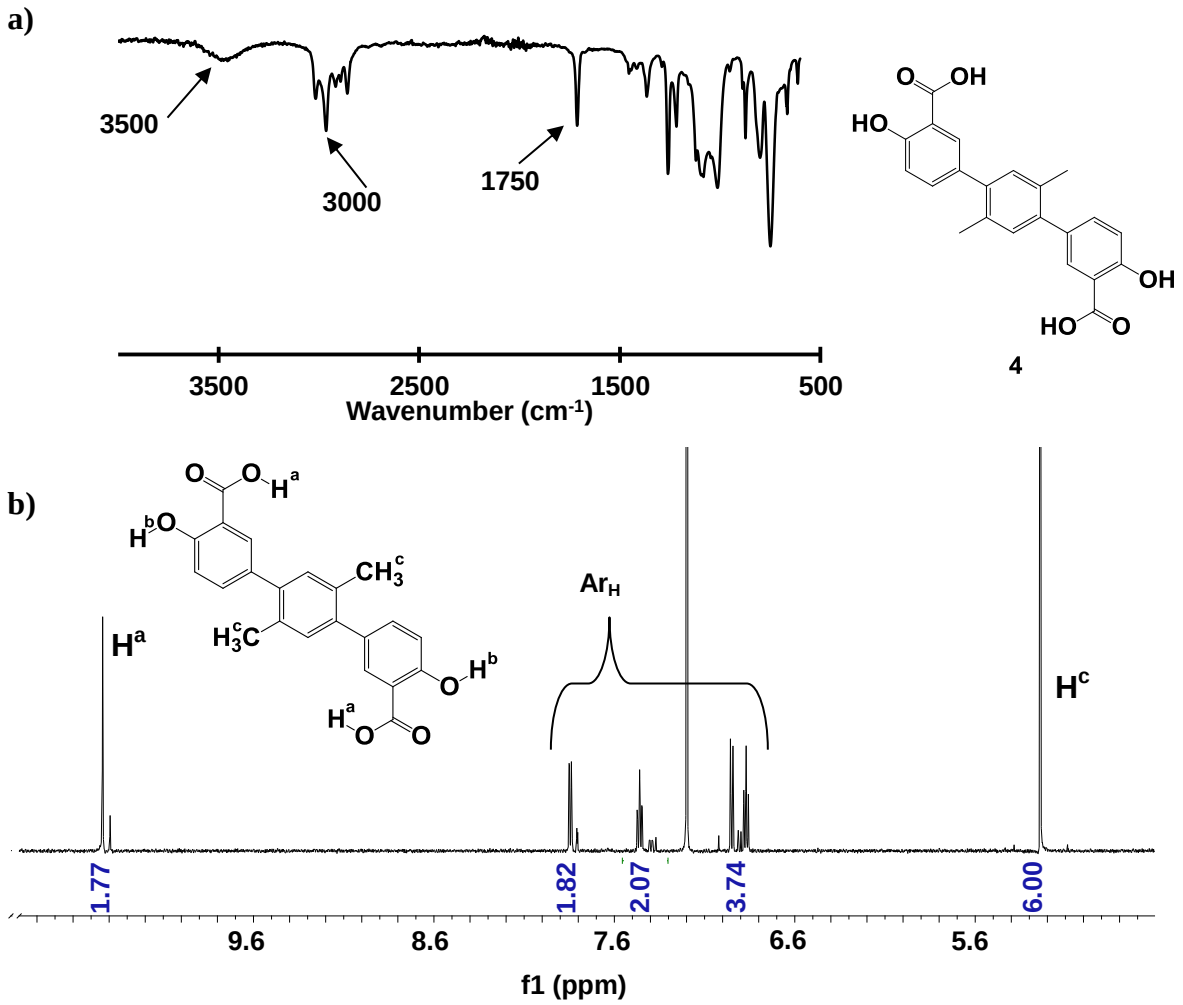

Figure 3.10: a) Transmission FTIR and **b)** ^{1}H NMR spectra of 4,4”-di[hydroxy]-2’,5’-dimethyl-[1,1’:4’,1”-terphenyl]-3,3”-dicarboxylic acid**, 4.**

When comparing the FTIR spectrum (Figure 3.10a, p. 53) of compound **4** with that of compound **3** (Figure 3.5, p. 46), the C=O stretching frequency at 1750 cm^{-1} and the aromatic C-H stretching frequency at 3000 cm^{-1} is still present, and now accompanied by the O-H stretching frequency at 3500 cm^{-1}.

The ^{1}H NMR spectrum of compound **4** (Figure 3.10b, p. 53) shows a peak at 10.45 ppm typical for the carboxylic acid functionalities. All the aromatic protons are accounted for. No peaks were detected below 5.2 ppm, an indication that the protecting groups were completely removed from the 4,4”-di[hydroxy]-2’,5’-dimethyl-[1,1’:4’,1”-terphenyl]-3,3”-dicarboxylic acid, **4**, linker (compare with Figure 3.3c, p. 40, compound **1**).

It was, however, possible to use the 4,4”-di[methoxyethoxymethoxy]-[1,1’:4’,1”-terphenyl]-3,3”-di[methoxyethoxymethoxycarbonyl] derivatives (Scheme 3.1, p. 35) as is, without deprotection, to form the Co-MOF-74-III derivatives. Thus, the protected 4,4”-di[methoxyethoxymethoxy]-[1,1’:4’,1”-terphenyl]-3,3”-di[methoxyethoxymethoxycarbonyl] derivatives were not deprotected for the synthesis of Co-MOF-74-III derivatives.

DMF, the solvent commonly used in the formation of MOFs, slowly hydrolyse in the presence of water, to give formic acid and dimethylamine. These impurities are weakly acidic and weakly basic respectively.[3] Thus; the formic acid will easily cleave the MEM-protecting groups on the ligands during the hydrolysing process of DMF, leading to *in situ* deprotection during MOF synthesis.

3.2.5 Co-MOF-74-III derivatives using Solvothermal techniques

After the synthesis of the 4,4”-di[methoxyethoxymethoxy]-[1,1’:4’,1”-terphenyl]-3,3”-di[methoxyethoxymethoxycarbonyl] derivatives, they were used as linkers in the synthesis of Co-MOF-74-III derivatives (Scheme 3.11, p. 55).

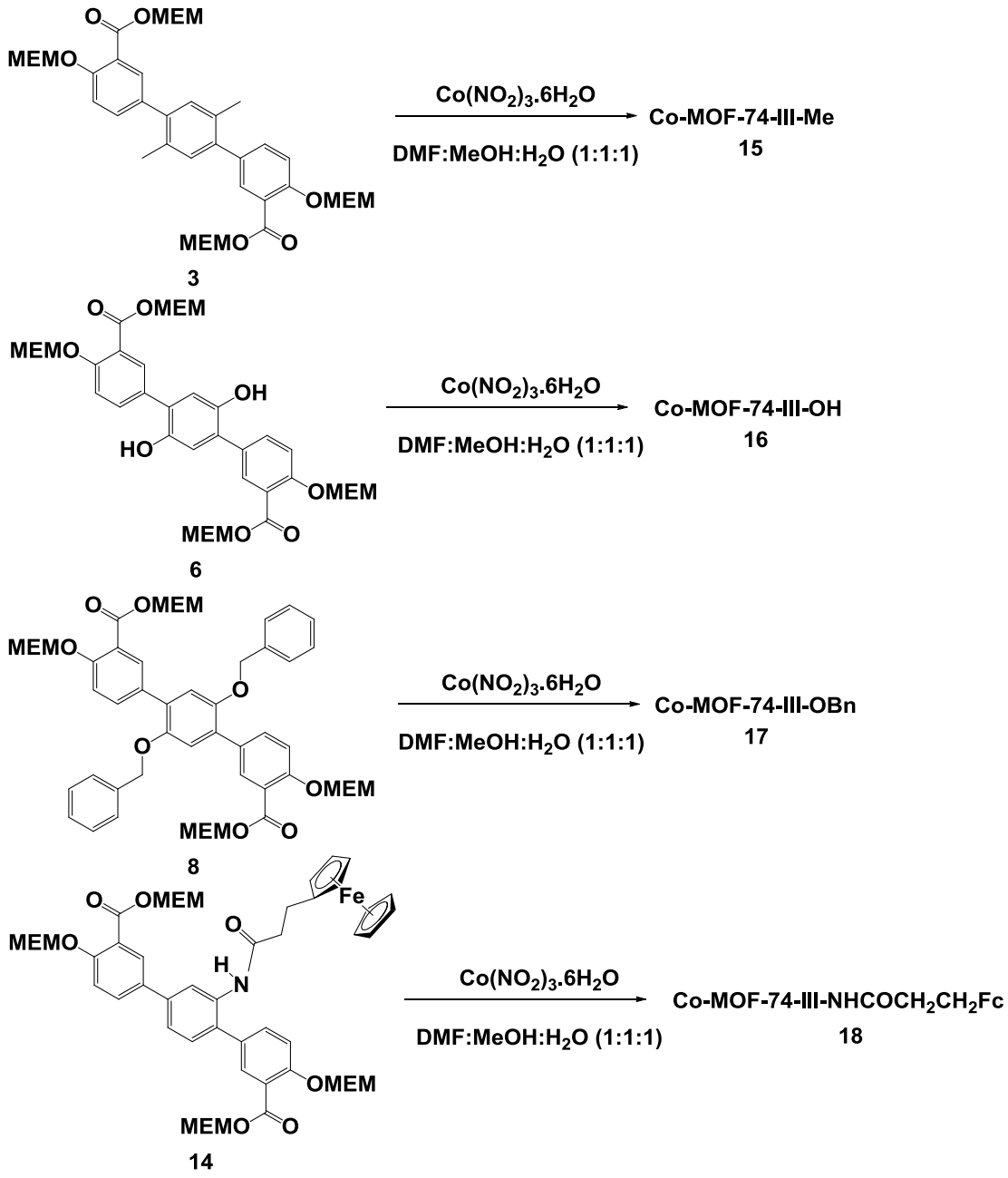

Scheme 3.7: Synthesis of Co-MOF-74-III derivatives

As an example of a typical synthesis, compound **3** and $Co(NO_2)_3.6H_2O$ was sonicated in a solvent mixture of DMF: MeOH: H_2O (1:1:1), before sealing it in a solvothermal vessel and keeping it at 100^oC for 66 hours, to produce Co-MOF-74-III-Me, **15**. The other linkers **6**, **8** and **14** were subjected to the same reaction conditions to yield the Co-MOF-74-III derivatives **16**, **17** and **18** respectively.

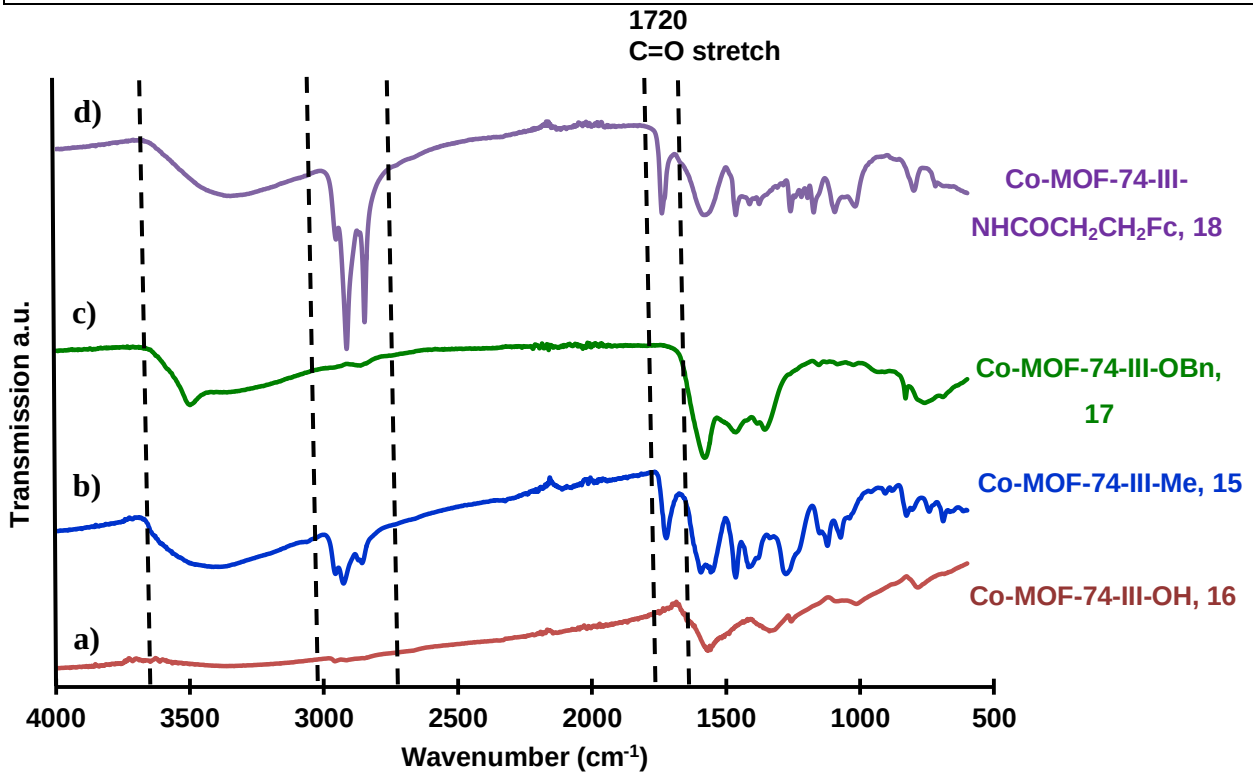

Figure 3.11: Transmission FTIR spectra of **a)** Co-MOF-74-III-OH**, 16; b)** Co-MOF-74-III-Me**, 15**; **c)** Co-MOF-74-III-OBn**, 17** and **d)** Co-MOF-74-III-NHCOCH$_2$CH$_2$Fc**, 18.**

The stretching vibrations of the alkyl chain in Co-MOF-74-III-NHCOCH$_2$CH$_2$Fc, **18**, and the methyl groups of the Co-MOF-74-III-Me, 15, are found between 2700 and 3000 cm-1, (Figure 3.11 d and b, p. 56). The C=O stretching vibration at 1720 cm^{-1} observed for Co-MOF-74-III-NHCOCH$_2$CH$_2$Fc, **18**, was shifted by 30 cm^{-1} when compared with the C=O peaks of the respective linkers, compound **3** (1750 cm^{-1}) and **14** (1750 cm^{-1}), prior to MOF formation. This is an indication of MOF formation. This C=O stretching frequency is absent in the FTIR spectra for Co-MOF-74-III-OH, **16** and Co-MOF-74-III-OBn, **17**, an indication that MOF formation was not achieved. The broad O-H stretching frequency at 3500 cm^{-1} is associated with atmospheric water in the pores or on the surface of the materials.

3.3 Accelerated Surface Area and Porosity Analysis (ASAP)

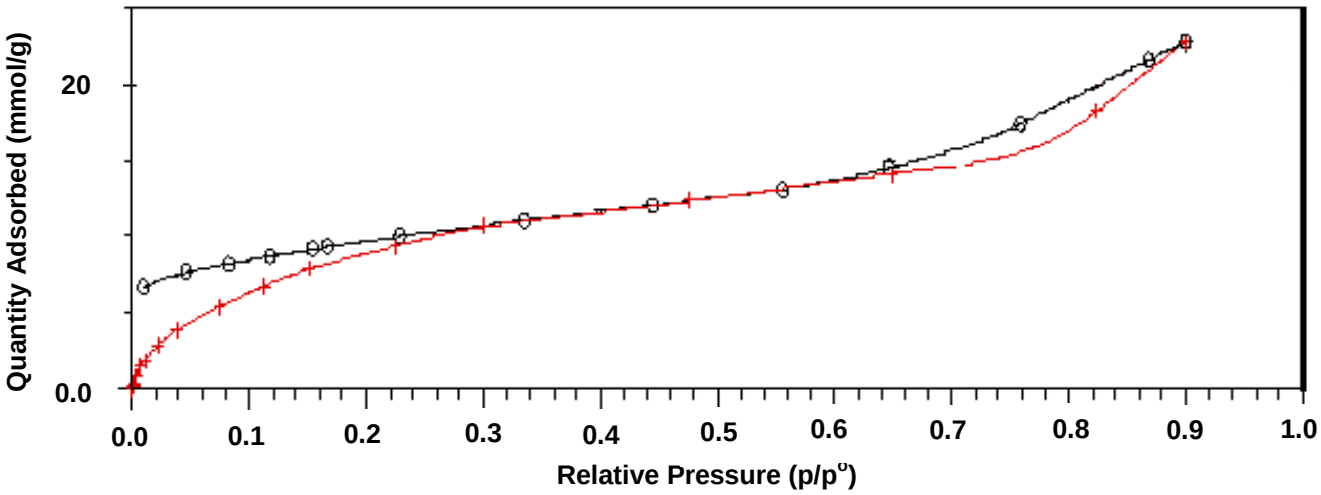

Figure 3.12: N_2 adsorption (red crosses) and desorption (black circles) isotherms at 77 K for Co-MOF-74-III-Me, **15**

The adsorption and desorption isotherms of Co-MOF-74-III-Me, **15**, Figure 3.12, p. 57, are of type IV and compare well to those found in literature[1], showing that the compound is mesoporous with a BET surface area of 169 ± 34 m^2g^{-1}; Langmuir Surface area of 1811 ± 81 m^2g^{-1} and a pore width of 32.6 Å. The steep adsorption in the initial phase could be due to the interaction of the nitrogen absorbent with the open-metal sites.

The large difference between the observed BET and Langmuir Surface Area of Co-MOF-74-III-Me, **15** is an indication of small amounts of unreacted linkers still trapped in the pores of the MOF. This correlates with the results from FTIR transmission spectroscopy (Figure 3.10, p. 53) and TGA thermograms (Figure 3.13, p. 58). Conclusive results, with regards to ASAP, TGA and PXRD could not be obtained for Co-MOF-74-III-OH, **16**, Co-MOF-74-III-OBn, **17** and Co-MOF-74-III-$NHCOCH_2CH_2Fc$, **18** due to an insufficient amount of sample.

3.4 Thermal Gravimetric Analysis (TGA)

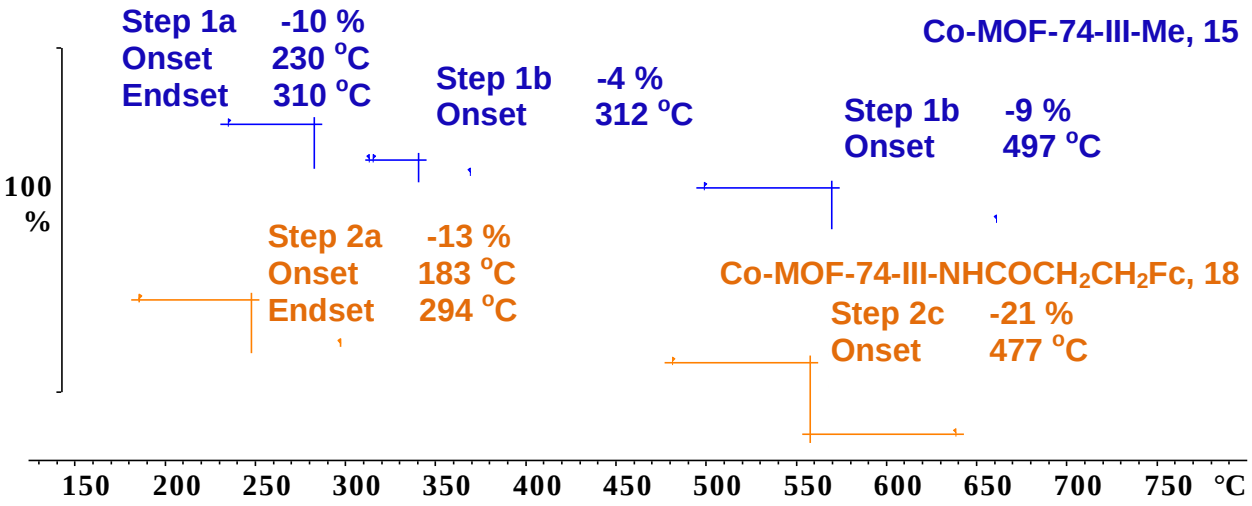

Figure 3.13: TGA thermograms for Co-MOF-74-III-Me**, 15** and Co-MOF-74-III-NHCOCH$_2$CH$_2$Fc**, 18**, obtained under an argon atmosphere.

The TGA thermograms of the two different Co-MOF-74 derivatives, synthesised in this study, show that there are no solvents present in the pores since all the solvents used have boiling points below 150 °C.

The TGA thermogram for Co-MOF-74-III-Me, **15** shows a three step mass loss (Figure 3.13, p. 58): the first between 230 °C and 310 °C (step 1a) is due to decomposition of the unreacted linker still inside the Co-MOF-74-III-Me pores; the second and third step starting after 312 °C (steps 1b and 1c), represents the structural breakdown of compound **15**.

The TGA thermogram for Co-MOF-74-III-NHCOCH$_2$CH$_2$Fc, **18** shows only two weight loss steps: the first step between 183 °C and 294 °C (step 2a) could be due to decomposition of unreacted ferrocene-containing linker, 4,4”-di[methoxyethoxymethoxy]-3’-[3-ferrocenylpropamide]-[1,1’:4’,1”-terphenyl]-3,3”-di[methoxyethoxymethoxycarbonyl], **14**. The second weight loss step after 477 °C (step 2c) is due to the structural breakdown of the Co-MOF-74-III- NHCOCH$_2$CH$_2$Fc, **18**.

3.5 Scanning Electron Microscopy (SEM)

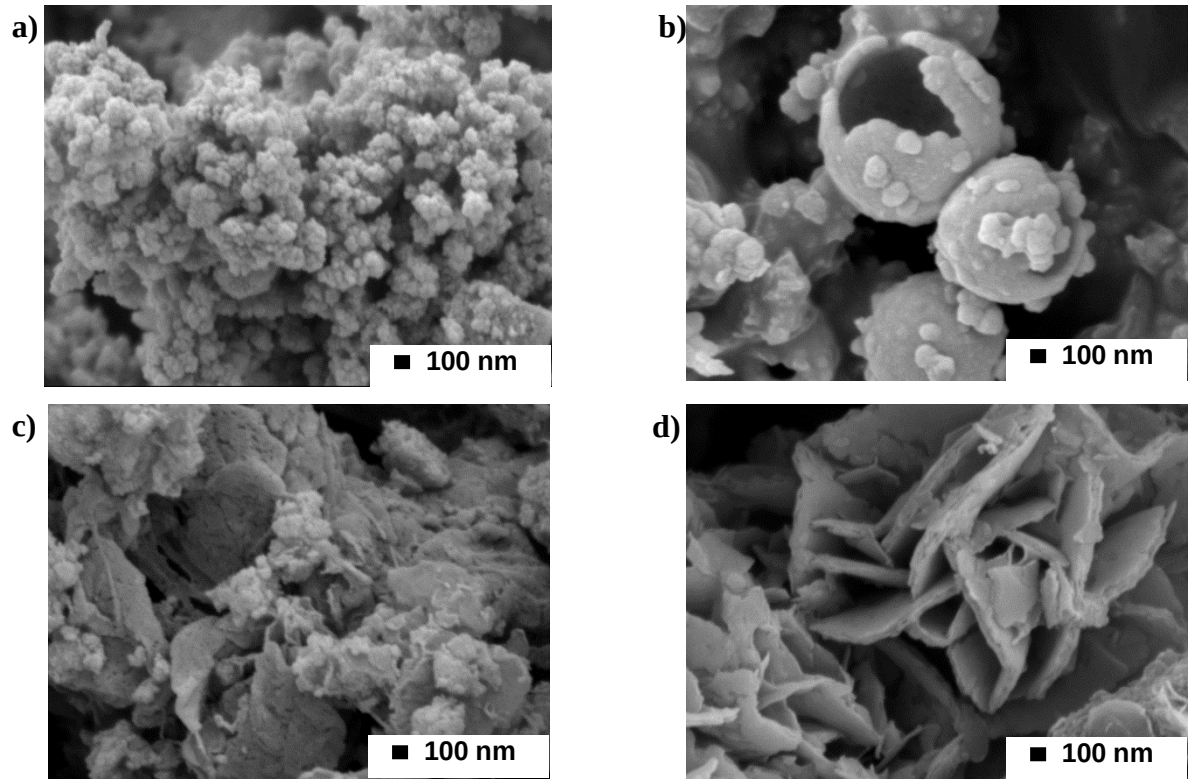

Figure 3.14: SEM images of **a**) Co-MOF-74-III-Me, **15**; **b**) Co-MOF-74-III-OH, **16**; **c**) Co-MOF-74-III-OBn, **17**; **d**) Co-MOF-74-III-NHCOCH$_2$CH$_2$Fc, **18** at a magnification of 40 000, 5.0 kV.

The SEM image of Co-MOF-74-III-Me, **15**, (Figure 3.14a, p. 59), shows that Co-MOF-74-III-Me particles form clusters with an average size of 100 nm distributed uniformly over the bulk of the sample. This morphology corresponds to that of Mg-MOF-74-III reported in literature[5] (Figure 2.17, in Chapter 2).

Co-MOF-74-III-OH, **16**, a non-porous MOF, (Figure 3.14b, p. 59) displays a round morphology with an average size of 100 nm for the smaller granules. Co-MOF-74-III-OBn, **17**, (Figure 3.14c, p. 59) has circular granules clustered together, with an uneven distribution of the sheet segments. The morphologies of compounds **16** and **17** are completely different to the morphology of compound **15.** Co-MOF-74-III-NHCOCH$_2$CH$_2$Fc, **18**, (Figure 3.14d, p. 59) have flat sheets in an irregular arrangement, unlike the round granules of the other compounds. These sheets or flakes are uniformly distributed throughout the sample.

Changes to the orientation of the functional groups of the linkers can thus result in different morphologies for these MOFs, while some minimal changes to the linkers do not affect the morphology of these MOFs at all.[6]

3.6 Electrochemistry

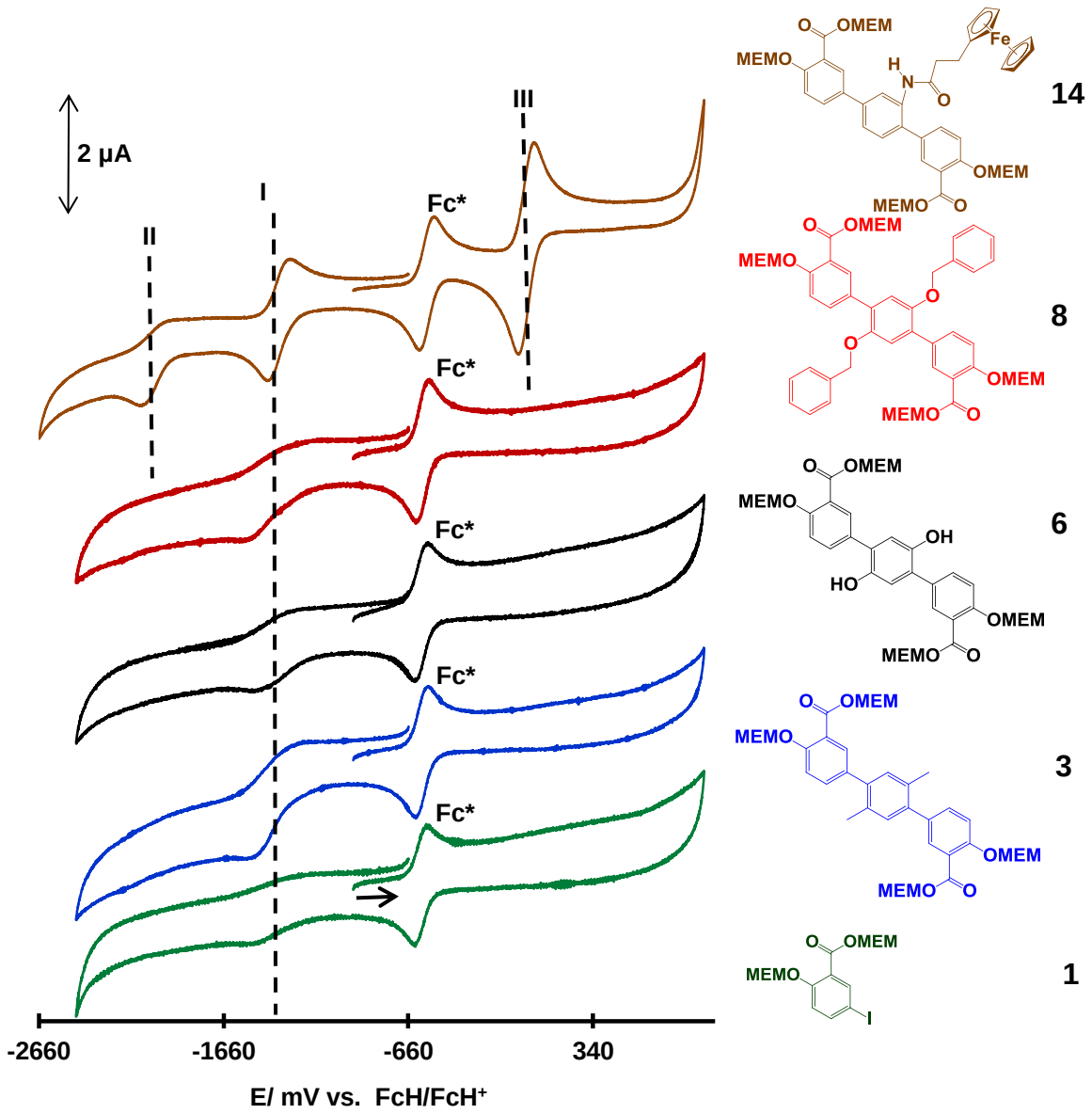

Figure 3.15: Cyclic voltammograms of 0.2 mmol.dm^{-3} DCM solutions of the different functionalized 4,4"-di[methoxyethoxymethoxy]-[1,1':4',1"-terphenyl]-3,3"-di[methoxyethoxymethoxycarbonyl] derivatives in the presence of $[NBu_4][PF_6]$ at a scan rate of 100 mV.s^{-1}, with internal reference decamethylferrocene, under argon, at room temperature.

The redox couple at -1500 mV (marked I) in the CV spectra, of compound **1**, **3**, **6**, **8** and **14** (Figure 3.15) could be due to reduction at the carbonyl groups protected by MEM, present in all these compounds. The redox couple (marked II) close to -2160 mV could be due to a reduction in the amide functionality of compound **14**. In this compound, the two oxidation-reduction processes associated with the MEM-protected carbonyl (marked I) and the amide bond (marked II) are electrochemically quasi-reversible, with ΔE = 118 mV and 97 mV, respectively; and

chemically irreversible, with i_{pc}/i_{pa} = 1.3 and 3.4, respectively (Table 3.2, p. 63). The redox couple (marked III) for compound **14** is electrochemically and chemically reversible with ΔE = 90 mV and i_{pc}/i_{pa} = 1.0, respectively. $E^{o\prime}$= 17 mV for the oxidation of Fe^{2+} to Fe^{3+} of the ferrocenyl-functionality, a positive shift compared to the redox couple of unbound ferrocene (0 mV). This is caused by the electron withdrawing amide functionality separated from the ferrocenyl-group by only a short alkyl chain.

Previous studies have shown that electron-withdrawing groups attached to a π-conjugated system will extract electronegativity from the system, causing a positive shift in the formal reduction potential. Electron-donating groups, however, donate electronegativity to the π-conjugated system, causing a negative shift in the formal reduction potential[11]. Such a positive shift of ± 35 mV was observed for couple I of compound **8**, (at -1403 mV) when compared to compounds **1**, **3** and **6 (**couple I around -1370 mV). This is due to the oxygen atoms of the benzyloxy groups withdrawing electrons from the π-conjugated system, resulting in a higher oxidation potential.

For compound **14**, a greater positive shift of couple I was observed, with a $E^{o\prime}$ at about -1315 mV, a difference of ± 55 mV, when compared to compounds **1**, **3** and **6**. This greater shift is due to the strong electron withdrawing amide-functionality extracting much more electron density from the π-conjugated system than in the case of compound **8**.

The electron-rich ferrocene moiety of compound **14** is effectively isolated from the rest of the molecule by the two carbon-alkane chain and cannot influence the redox potential of couple I.

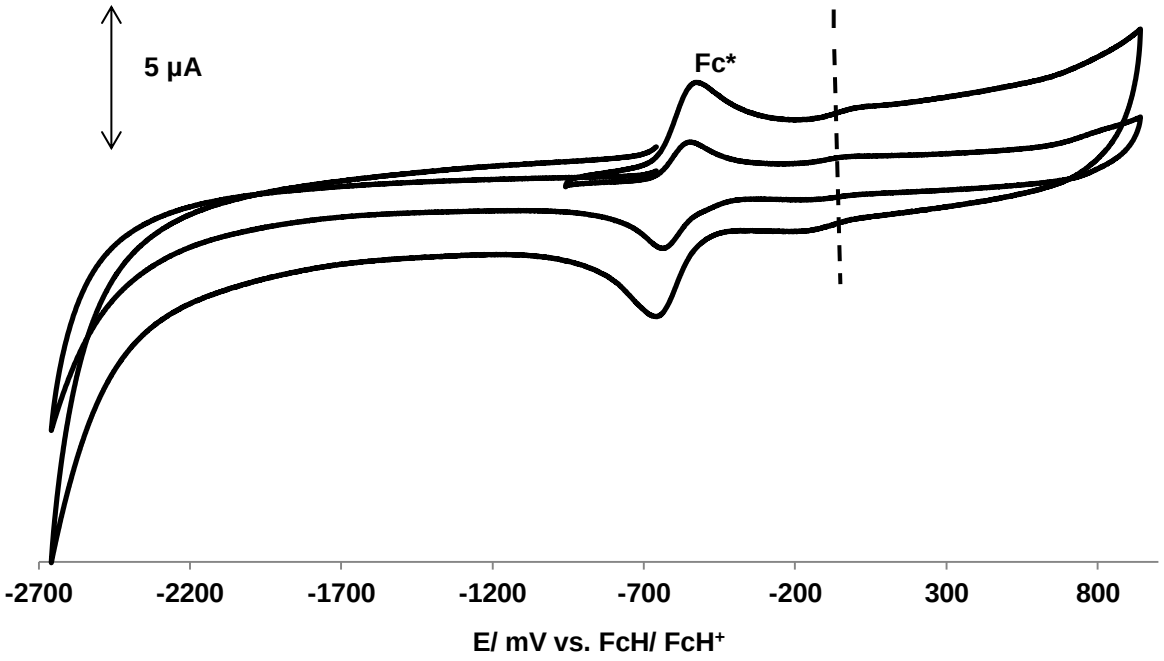

Figure 3.16: Solid state cyclic voltammograms of Co-MOF-74-III-$NHCOCH_2CH_2Fc$, **18** in 0.2 $mmol.dm^{-3}$ DCM with $[NBu_4][PF_6]$ at a scan rate of 500 $mV.s^{-1}$ and 2000 $mV.s^{-1}$, with internal reference decamethylferrocene, under argon, at room temperature.

With most MOFs, it is difficult to detect the oxidation-reduction processes of the linker-functionality due to the electrons that are not fast enough to escape the pores. However, with Co-MOF-74-III-$NHCOCH_2CH_2Fc$, the oxidation-reduction couple of the bound ferrocene at 64 mV has a ΔE_p value of 128 mV (Figure 3.16, p. 62), with $\frac{i_{pc}}{i_{pa}} = 0.67$ (Table 3.2, p. 63). This is a good indication that this couple is electrochemically quasi-reversible and partially chemically reversible. The MOF-bound ferrocene is oxidized at about 40 mV more positive than the ferrocene in compound **14** (couple III at 21 mV), due to the fact that it is tightly bound in a crystal lattice.

Table 3.2: E_{pc}, ΔE_p, $E^{o\prime}$, i_{pc} and i_{pc}/i_{pa} of the values from cyclic voltammetry (CV) of 0.2 mmol.dm^{-3} DCM solutions of the 4,4"-di[methoxyethoxymethoxy]-[1,1':4',1"-terphenyl]-3,3"-di[methoxyethoxymethoxycarbonyl] derivatives (structure below) in the presence of $[NBu_4][PF_6]$, with internal reference decamethylferrocene, under argon, at room temperature. The CV results for Co-MOF-74-III-NHCOCH$_2$CH$_2$Fc, **18**, are included. Solid state CV of Co-MOF-74-III-NHCOCH$_2$CH$_2$Fc, **18** in 0.2 mmol.dm^{-3} DCM with $[NBu_4][PF_6]$ with internal reference decamethylferrocene, under argon, at room temperature.

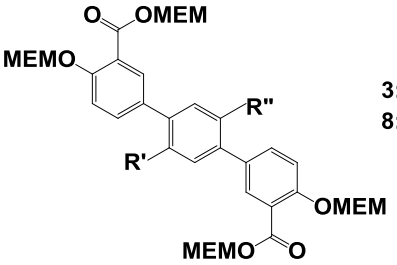

3: R' = R" = CH_3
8: R' = R" = -O-CH_2-C_6H_5

6: R' = R" = OH
14: R' = H; R" = -NHCO$(CH_2)_2$Fc

Compound	Scan rate (mV/s)	E_{pc} (mV)	ΔE_p (mV)	$E^{o\prime}$ (mV)	i_{pc} (µA)	i_{pc}/i_{pa}
1 (couple I)	100	-1493	228	-1379	8.5	2.1
	200	-1500	243	-1379	9.0	3.0
	300	-1500	250	-1375	10.0	2.5
	400	-1500	279	-1360	3.0	3.0
	500	-1500	279	-1360	3.0	3.0
3 (couple I)	100	-1519	250	-1394	20.0	1.7
	200	-1519	324	-1356	23.0	1.5
	300	-1519	324	-1356	18.0	1.6
	400	-1519	296	-1370	5.5	2.2
	500	-1519	296	-1370	3.5	1.8
6 (couple I)	100	-1481	231	-1366	11.0	1.2
	200	-1481	231	-1366	13.0	1.6
	300	-1481	231	-1366	14.5	1.8
	400	-1481	241	-1361	5.0	2.5
	500	-1481	241	-1361	3.0	3.0
8 (couple I)	100	-1537	269	-1403	17.0	1.7
	200	-1537	407	-1333	13.0	1.6
	300	-1537	417	-1329	13.0	2.2
	400	-1519	361	-1338	3.5	1.8
	500	-1519	361	-1338	3.0	1.5
14 (couple III)	100	-28	90	17	31.0	1.0
	200	-28	97	21	45.0	1.0
	300	-35	111	21	58.0	1.0
	400	-35	111	21	27.0	1.0
	500	-35	111	21	29.0	1.0
14 (couple II)	100	-2028	97	-1979	13.5	3.4
	200	-2056	125	-1993	18.0	2.6
	300	-2069	153	-1993	21.0	2.3
	400	-2083	132	-2017	11.0	2.8

	500	-2083	125	-2021	12.0	3.0
14 (couple I)	100	-1375	118	-1316	19.0	1.3
	200	-1375	118	-1316	23.0	1.2
	300	-1382	132	-1316	28.0	1.3
	400	-1375	132	-1309	13.0	1.3
	500	-1382	146	-1309	14.0	1.4
Co-MOF-74-III-$NHCOCH_2CH_2Fc$, **18**	500	43	128	64	1.0	0.7
	2000	43	128	64	1.0	0.7

The cyclic voltammograms for the different 4,4”-di[methoxyethoxymethoxy]-[1,1’:4’,1”-terphenyl]-3,3”-di[methoxyethoxymethoxycarbonyl] derivatives at different scan rates are in the appendix (Spectrum 1.7.1 – Spectrum 1.7.5, p. A9 – A11).

3.7 References

1. H. Deng, S. Grunder, K. E. Cordova, C. Valente, H. Furukawa, M. Hmadeh, F. Gándara, A.C. Whalley, Z. Liu, S. Asahina, H. Kazumori, M. O’Keeffe, O. Terasaki, J. F. Stoddart, O. M. Yaghi, *Science*, **2012**, 336, 6084, pp. 1018.
2. S. Kotha, K. Lahiri, D. Kashinath, *Tetrahedron*, **2002**, 58, 9633.
3. J. Juillard, *Pure & Appl. Chem*., **1977**, 49, 885.
4. D.R. Lide, *CRC Handbook of Chemistry and Physics*., 75th ed. Boca Raton, Fl: CRC Press Inc., **1994**.
5. L. Yang, C. Xu, W. Ye, W. Liu, *Sensors and Actuators B: Chemical*, **2015,** 215, 489.
6. J. L. C. Rowsell, O. M. Yaghi, *Microporous and Mesoporous Materials*, **2004**, 73, 3.
7. L. Sun, C. H. Hendon, M. A. Minier, A. Walsh, M. Dincă, *J. Am. Chem. Soc*., **2015**, 137, 6164.
8. M.A. Sierra, M.J. Mancheño, R. Vicente, M. Gómez-Gallego, *J. Org. Chem.*, **2001**, 66 (26), 8920.
9. J. Coates, *Encyclopedia of Analytical Chemistry*, John Wiley & Sons Ltd.
10. A. M. Fracaroli, H. Furukawa, M. Suzuki, M. Dodd, S. Okajima, F. Gándara, J. A. Reimer, O. M. Yaghi, *J. Am. Chem. Soc*., **2014**, 136, 8863.
11. K. Hernández-Burgos, S. E. Burkhardt, G. G. Rodrígues-Calero, R. G. Henning, H. D. Abruña, *J. Phys. Chem. C*, **2014**, 118, 6046.

4 Experimental

4.1 Introduction

This section provides a description of the materials, equipment, techniques and experimental procedures used during synthesis, analysis and characterization. All relevant spectra can be found in the Appendix.

4.2 Materials

Solid reagents (Merck, Aldrich and Fluka) employed for synthesis were used without further purification. Liquid reagents (Merck and Aldrich) were used without further purification unless otherwise stated. Organic solvents were dried according to published procedures.[1] Column chromatography was performed on Kieselgel 60 (Merck, grain size 0.040-0.063 mm) and ALUMINA (pore size = 58Å, pH = 7.0 ± 0.5 in H_2O). Filtration and vacuum evaporation was performed with the aid of a water aspirator. Melting points onset temperatures were recorded on an Olympus BX51 microscope, using a LINKAM, TMS 600 hot stage, and were uncorrected.

4.3 Spectroscopic measurements

^{1}H and ^{13}C NMR spectra were measured at 298 K on Bruker Advance UltraShield 600MHz NMR, some on the Bruker Advance Ascend 400 MHz NMR and on the Bruker Advance UltraShield 300 MHz spectrometers. All chemical shifts are reported relative to TMS ($Si(CH_3)_4$) at 0.00 ppm. FTIR measurement was performed using a Bruker Tensor 27 IR spectrometer and Pike MIRacle ATR, running OPUS software (Version 1.1).

4.4 Electrochemical studies

Measurements on *ca*. 0.25 mmol dm^{-3} solutions of the complexes in dichloromethane containing 0.1 mol dm^{-3} $[N^{n}Bu_4][B(C_6F_5)_4]$ as supporting electrolyte were conducted under argon at room temperature utilising a PARSTAT 2273 Advanced electrochemical workstation interfaced with a personal computer. A three electrode cell consisting of a Pt auxiliary and reference electrode (Pt) and a glassy carbon working electrode with surface area 7.07 mm^2 polished on a Bueler

microcloth with 1 micron and ¼ micron diamond paste were employed. However, because the ferrocene couple interferes with the ferrocenyl signals of **14**, each experiment was first performed in absence of any internal standard and then repeated in the presence of 0.5 mM decamethylferrocene (Fc*). In a separate experiment, only ferrocene and decamethylferrocene were measured under the same conditions. Data was worked up on a spreadsheet to be referenced against the FcH/FcH^+ couple at 0 V. Under the conditions of this study, the Fc^*/Fc^{*+} couple was shifted to -550 mV versus FcH/FcH^+, $\frac{i_{pc}}{i_{pa}} = 0.98$, ΔE_p = 74 mV.

4.5 Synthesis

4.5.1 Protection of reagents

4.5.1.1 5-Iodo-Methoxyethoxymethoxy-2-methoxyethoxymethoxycarbonyl-phenyl, 1

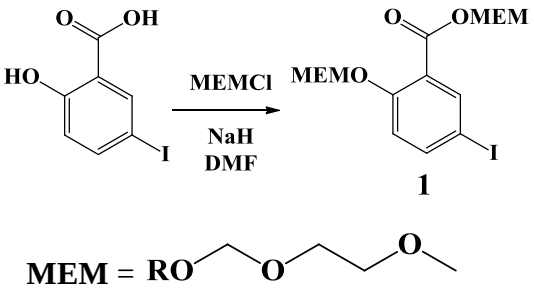

Sodium hydride (1.38 g; 57.5 mmol) was dissolved in anhydrous DMF (40 ml) and cooled to 0°C under an argon atmosphere. A solution of 5-iodosalicylic acid (5.005 g; 18.9569 mmol) in anhydrous DMF (20 ml) was transferred dropwise to the sodium hydride solution. Gas evolved and the reaction mixture turned yellow, after which it was stirred at room temperature for 30 minutes, before being cooled to 0°C. 2-Methoxyethoxymethyl chloride (3.9 ml; 45.006 mmol) was added in one portion to the reaction mixture and stirred at 0°C for 50 minutes, and then at room temperature for 40 minutes. The reaction mixture was diluted with diethyl ether (100 ml) and quenched with water (50 ml). The organic layer was separated and washed with sodium hydroxide (1M, 3 x 30 ml) and brine (3 x 100 ml), dried with $MgSO_4$ and concentrated in vacuo. A light yellow oil (6 g; 72%) was obtained. IR ν/cm^{-1} = 1750 (C=O), 3000 (aromatic C-H). ^1H NMR (600 MHz, $CDCl_3$) δ 8.03 (s, 1H), 7.66 (d, *J* = 8.8Hz, 1H), 6.98 (d, *J* = 8.8 Hz, 1H), 5.46 (s, 2H), 5.26 (s, 2H), 3.83 – 3.76 (m, 4H), 3.55 – 3.50 (m, 2H), 3.48 (m, 2H), 3.41 (m, 6H),

Spectrum 1.2.1a, p. A1. ^{13}C NMR (600 MHz, $CDCl_3$) δ 162.43, 141.54, 139.49, 118.42, 93.63, 64.67, 61.10, 36.39, 31.33, 14.97, 14.20; Spectrum 1.2.1b, p. A1. m/z = 368.9; found m/z = 369.

4.5.1.2 1,4-Bisbenzyloxy-2,5-dibromophenyl, 5

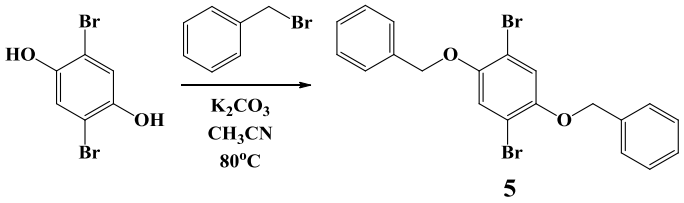

5

Pulverized K_2CO_3 (0.954 g; 6.903 mmol) and 2,5-dibromohydroquinone (0.436 g; 1.627 mmol) were added to acetonitrile (20 ml), whilst stirring under an argon atmosphere. Benzyl bromide (0.4 ml; 3.36 mmol) was added dropwise to the reaction mixture, which turned light yellow upon mixing. The reaction was stirred at 80°C for 16 hours, and then cooled to room temperature and filtered to remove undissolved K_2CO_3. The precipitate was washed with ethyl acetate (20 ml). The filtrate was washed with water (3 x 60 ml) and then concentrated in vacuo. The product was purified by adding ethyl acetate (20 ml) to the product and concentrated in vacuo. This purification step was repeated 3 times, to yield a yellow oil which solidifies upon standing. (0.58 g; 80%) Melting point = 80 °C. IR ν/cm^{-1} = 3000 (aromatic C-H). ^1H NMR (300 MHz, $CDCl_3$) δ 7.54 – 7.32 (m, 10H), 7.21 (s, 2H), 5.10 (s, 4H); Spectrum 1.2.6b, p. A5. ^{13}C NMR (600 MHz, $CDCl_3$) δ 150.09, 139.12, 136.16, 128.63, 128.15, 127.25, 119.27, 111.59, 71.98; Spectrum 1.2.6c, p. A5.

4.5.2 Suzuki-Miyuara cross-coupling reaction

Tetrahydroxydiboron (1.5 equivalents per 5-Iodo-methoxyethoxymethoxy-2-methoxyethoxy-methoxycarbonyl-phenyl, 1), bis(triphenylphosphine)palladium dichloride (catalytic amounts) and potassium acetate (3 equivalents per 5-Iodo-methoxyethoxymethoxy-2-methoxyethoxy-methoxycarbonyl-phenyl, **1**) was dissolved in anhydrous p-dioxane (8 ml) under an argon atmosphere. 5-Iodo-methoxyethoxymethoxy-2-methoxyethoxymethoxycarbonyl-phenyl, **1** (1 equivalent) was added dropwise to the reaction mixture, which was refluxed for 2 to 3 hours following the in situ formation of the intermediate, 5-dihydroxyboron-methoxyethoxymethoxy 2-methoxyethoxymethoxycarbonyl-phenyl, **2**. Aryl dihalide (**19**, **20**, **5**, **21**; 0.5 equivalent) and water (4 ml) was added to the reaction mixture and then refluxed overnight with vigorously stirring. The mixture was allowed to cool to room temperature and extracted with DCM (3 x 60

ml). The combined organic layers were washed with brine (3 x 60 ml), dried with $MgSO_4$ and concentrated in vacuo, yielding the crude product. The workup of each of the four products is described below:

4.5.2.1 4,4”-Di[methoxyethoxymethoxy]-2’,5’-dimethyl-[1,1’:4’,1”-terphenyl]-3,3”-di[methoxyethoxymethoxycarbonyl], 3

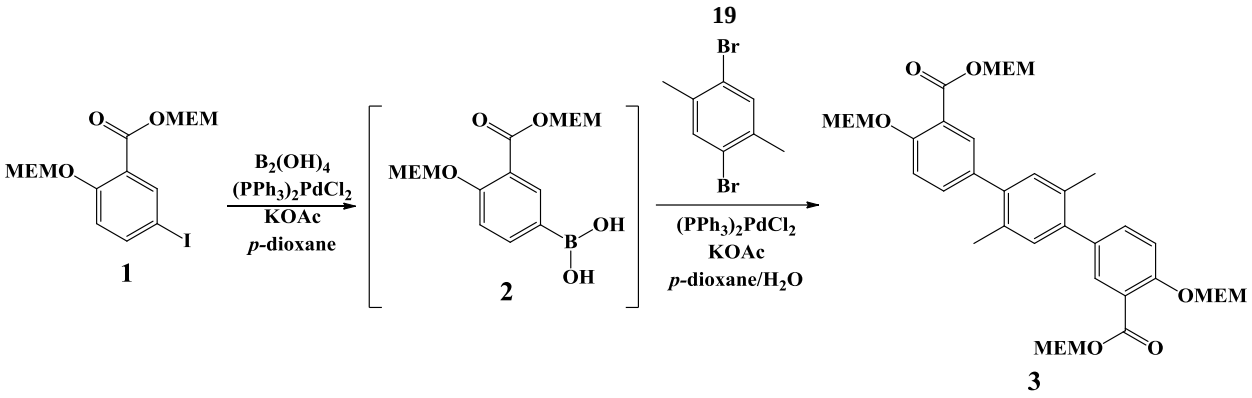

5-Iodo-methoxyethoxymethoxy-2-methoxyethoxymethoxycarbonyl-phenyl, **1** (1.28 g; 2.92 mmol) and 2,5-dibromo-1,4-xylene, **19** (0.388 g; 1.470 mmol) were reacted to form the crude product. Purification was done with column chromatography on neutral alumina by first using DCM to elute impurities and then MeOH for the product. A brown oil (0.970 g; 90%) was obtained. IR ν/cm^{-1} = 1750 (C=O), 3000 (aromatic C-H). ^{1}H NMR (300 MHz, $CDCl_3$): δ 7.75 (m, 2H), 7.32 (m, 2H), 7.0 (m, 2H), 5.65 (s, 4H), 5.29 (s, 4H), 3.76 (s, 8H), 3.57 (m, 8H), 3.38 (m, 12H), 1.58 (s, 6H); Spectrum 1.2.2b, p. A2. ^{13}C NMR δ_C (600MHz, $CDCl_3$)/ppm: 135.02, 133.00, 130.00, 129.00, 128.02, 93.00, 72.00, 68.02, 59.13, 30.00; Spectrum 1.2.2c, p. A2. m/z = 278.18; found m/z = 277.

4.5.2.2 4,4”-Di[methoxyethoxymethoxy]-2’,5’-dihydroxy-[1,1’:4’,1”-terphenyl]-3,3”-di[methoxyethoxymethoxycarbonyl], 6

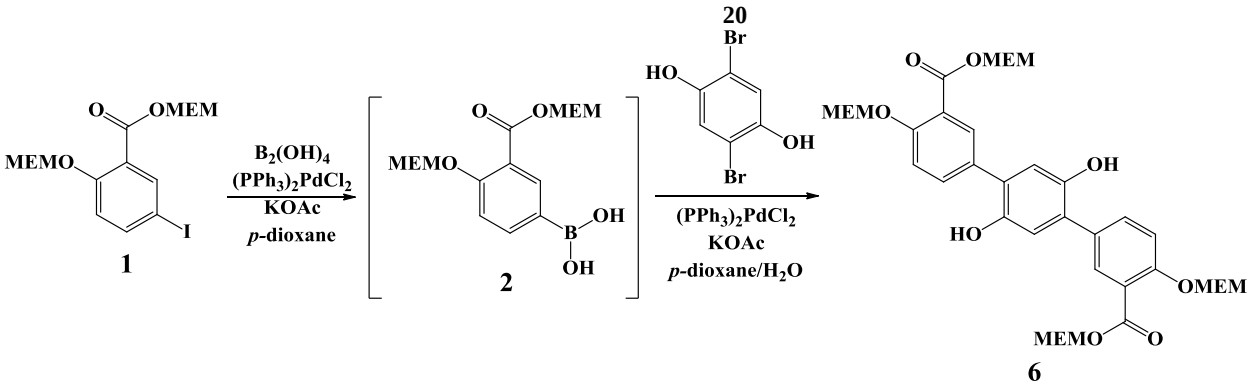

5-Iodo-methoxyethoxymethoxy-2-methoxyethoxymethoxycarbonyl-phenyl, **1** (5.82 g; 13.221 mmol) and 2,5-dibromohydroquinone, **20** (1.772 g; 6.614 mmol) were reacted to form the crude product. Purification was done with column chromatography on neutral alumina by first using DCM to elute impurities and then MeOH for the product. A brown oil (4.36 g; 90%) was obtained. IR ν/cm^{-1} = 1750 (C=O), 3000 (aromatic C-H), 3450 (O-H). ^{1}H NMR (600 MHz, $CDCl_3$) δ 7.73 (m, 2H), 7.37 (m, 2H), 7.17 (m, 2H), 6.97 (m, 2H), 5.28 (s, 4H), 4.37 (m, 4H), 3.84 (m, 4H), 3.66 (m, 4H), 3.57 (m, 4H), 3.47 (m, 6H), 3.42 (m, 6H), Spectrum 1.2.4b, p. A4. ^{13}C NMR (600 MHz, $CDCl_3$) δ 156.76, 133.38, 133.33, 131.47, 131.35, 121.58, 121.30, 116.44, 94.05, 92.37, 71.77, 71.56, 70.55, 67.96, 67.48, 63.87, 59.02; Spectrum 1.2.4c, p. A4. m/z = 514.52; found m/z = 514.278.

4.5.2.3 4,4”-Di[methoxyethoxymethoxy]-2’,5’-bis-benzyloxy-[1,1’:4’,1”-terphenyl]-3,3”-di[methoxyethoxymethoxycarbonyl], 8

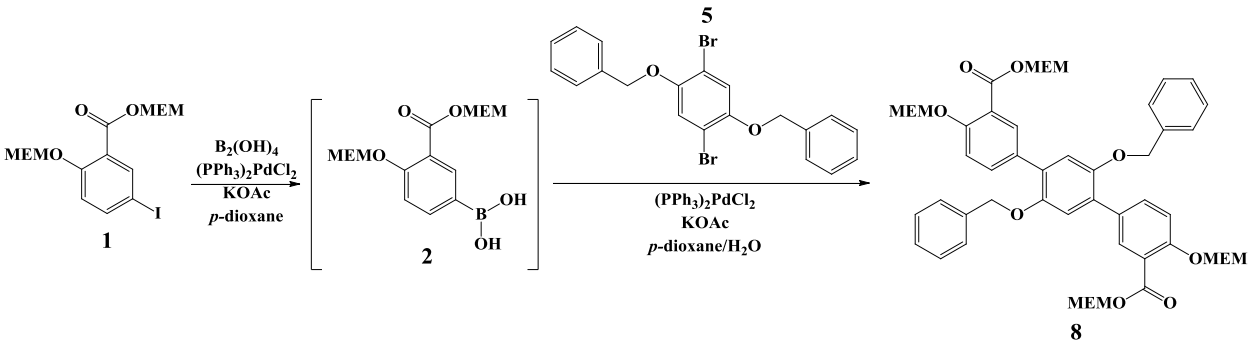

5-Iodo-methoxyethoxymethoxy-2-methoxyethoxymethoxycarbonyl-phenyl, **1** (1.87 g; 4.248 mmol) and 2,5-dibromo-1,4-benzyloxyphenyl, **5** (0.954 g; 2.13 mmol) were reacted to form the crude product. Purification was done with column chromatography on neutral alumina by first

using DCM to elute impurities and then MeOH for the product. A brown oil (1.15 g; 60%) was obtained. IR ν/cm^{-1} = 1750 (C=O), 3000 (aromatic C-H), 3010 (aromatic C-H). ^{1}H NMR (600 MHz, $CDCl_3$) δ 7.64 (d, *J* = 6.6 Hz, 2H), 7.31 – 7.26 (m, *J* = 8.2 Hz,10H), 7.11 (s, 2H), 6.97 (t, *J* = 4.4 Hz, 2H), 6.70 (d, *J* = 8.7 Hz, 2H), 5.25 (d, *J* = 3.2 Hz, 4H), 5.02 (d, *J* = 17.1 Hz, 4H), 4.76 (s, 4H), 4.50 – 4.40 (m, 3H), 4.39 – 4.32 (m, *J* = 9.8, 5.8 Hz, 4H), 3.82 – 3.77 (m, *J* = 11.3, 7.0 Hz, 8H), 3.68 – 3.62 (m, 12H), Spectrum 1.2.7b, p. A6. m/z = 256.2592; found m/z = 259.

4.5.2.4 4,4”-Di[methoxyethoxymethoxy]-3’-nitro-[1,1’:4’,1”-terphenyl]-3,3”-di[methoxyethoxymethoxycarbonyl], 12

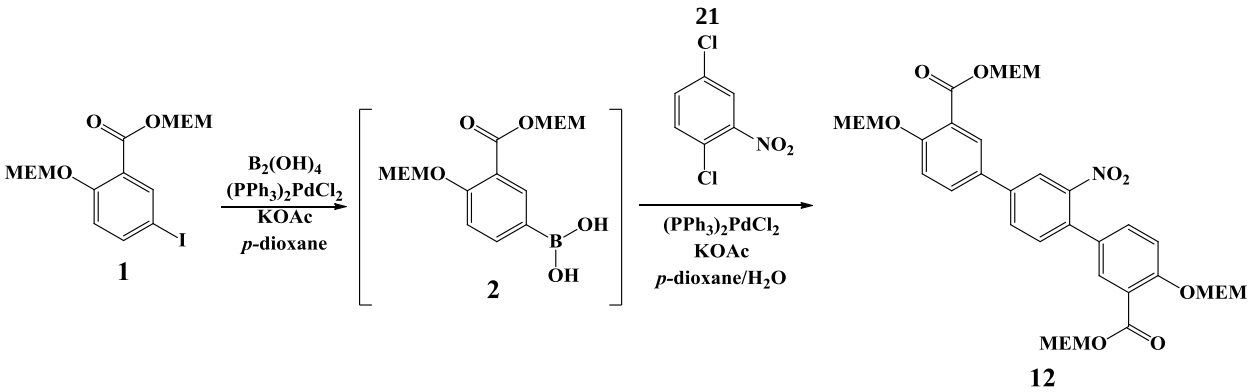

5-Iodo-methoxyethoxymethoxy-2-methoxyethoxymethoxycarbonyl-phenyl, **1** (4.63 g; 10.517 mmol) and 2,5-dichloro-nitrophenyl, **21** (1.01 g; 5.2812 mmol) were reacted to form the crude product. Purification was done with column chromatography on neutral alumina by first using DCM to elute impurities and then MeOH for the product. A brown oil (3.15 g; 80%) was obtained. IR ν/cm^{-1} = 1470 (N-O), 1750 (C=O), 3000 (aromatic C-H). ^{1}H NMR (400 MHz, $CDCl_3$) δ 8.02 (s, 2H), 7.82 (s, 2H), 7.65 (d, *J* = 6.8 Hz, 2H), 7.44 (s, 2H), 6.95 (d, *J* = 8.8 Hz, 1H), 5.43 (s, 4H), 5.32 – 5.17 (m, 4H), 3.70 (m, 8H), Spectrum 1.2.8b, p. A7. ^{13}C NMR (600 MHz, $CDCl_3$) δ 163.91, 156.85, 142.26, 139.87, 122.90, 118.48, 93.99, 90.11, 83.51, 71.58, 69.75, 68.09, 59.05; Spectrum 1.2.8c, p. A7. m/z = 361.28; found m/z = 360.752.

4.5.3 Functionalization

4.5.3.1 Ethyl-3-ferrocenylethanoate, 11

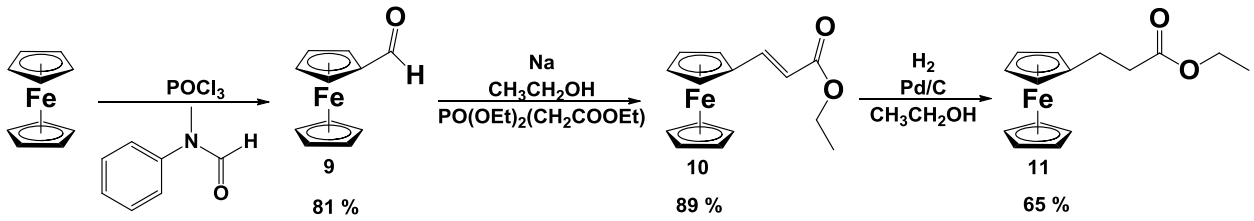

Vilsmeier formylation forming ferrocene carboxaldehyde: A solution of N-methylformanilide (145.8 mmol) and $POCl_3$ (9.01 mmol) was stirred vigorously under an argon atmosphere. Ferrocene (10 g; 54.6 mmol) was added in small portions over 20 minutes while stirring. Stirring was continued for 1 hour at room temperature, then at 65 ^oC for 2 hours and finally at room temperature for 16 hours. The product mixture was extracted with ether (3 x 100 ml), washed first with 1M HCl, then water, and lastly with saturated sodium carbonate solutions. The organic phase was dried with $MgSO_4$, the solvent removed and the product purified by column chromatography on silica, (hexane: ether = 1:1, R_f = 0.46), giving red/brown crystals (9.488 g; 81 %). IR ν/cm^{-1} = 1750 (C=O).

Ethyl-3-ferroceneylethenoate, **10**: Sodium (1.16g; 50.5 mmol) was dissolved in dry ethanol (120 ml) at 0 ^oC under argon. A mixture of triethylphosphonoacetate (6.78 g; 30.2 mmol) and ferrocene carboxaldehyde, **9** (6.1 g; 28.7 mmol) was added drop-wise to the sodium ethoxide solution and stirred for an hour. The ethanol was removed, the product purified using column chromatography (ethyl acetate: hexane = 5:95, R_f = 0.62). IR ν/cm^{-1} = 1750 (C=O), 3000 (aromatic C-H).

Ethyl-3-ferrocenylethanoate, **11**: Ethyl-3-ferrocenylethenoate, **10** (4.332 g; 15.4 mmol) and palladium on carbon (0.085 g; 10 % Pd/C) were suspended in absolute ethanol (80 ml) and stirred under a hydrogen atmosphere for 16 hours, followed by filtration through 5 cm of celite. Cold water was added to the filtrate and the product extracted with diethyl ether (3 x 150 ml), washed with distilled water, and dried over $MgSO_4$ and solvent removed, giving orange crystals (70.2 %). Melting point = 48 ^oC. IR ν/cm^{-1} = 1750 (C=O), 3000 (aromatic C-H).

4.5.3.2 4,4”-Di[methoxyethoxymethoxy]-3’-amino-[1,1’:4’,1”-terphenyl]-3,3”-di[methoxy-ethoxymethoxycarbonyl], 13 using Bechamp reduction process

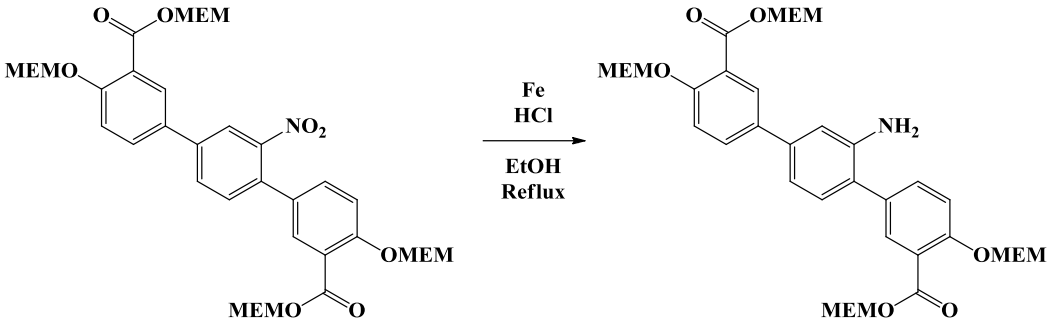

12 **13**

Iron powder (0.50 g; 8.970 mmol) was added to ethanol (50 ml) with 4,4”-di[methoxyethoxy-methoxy]-3’-nitro-[1,1’:4’,1”-terphenyl]-3,3”-di[methoxyethoxymethoxycarbonyl], **12** added dropwise to the ethanol mixture. The reaction was heated up to 60^{o}C whilst stirring. Hydrochloric acid (3 ml, conc.) was slowly added to the hot ethanol mixture and refluxed until all the iron powder was dissolved. The reaction mixture was cooled to room temperature, before adding distilled water (200 ml) and quenching the reaction with sodium hydroxide (2 M) until a pH of 6 is reached. The product was extracted with ethyl acetate (150 ml). The combined organic layers were washed with water (3 x 150 ml) and brine (3 x 150 ml), dried with $MgSO_4$ and concentrated in vacuo. The product was not purified and used as is in the next reaction step.

4.5.3.3 4,4”-Di[methoxyethoxymethoxy]-3’-[3-ferrocenylpropamide]-[1,1’:4’,1”-terphenyl]-3,3”-di[methoxyethoxymethoxycarbonyl], 14

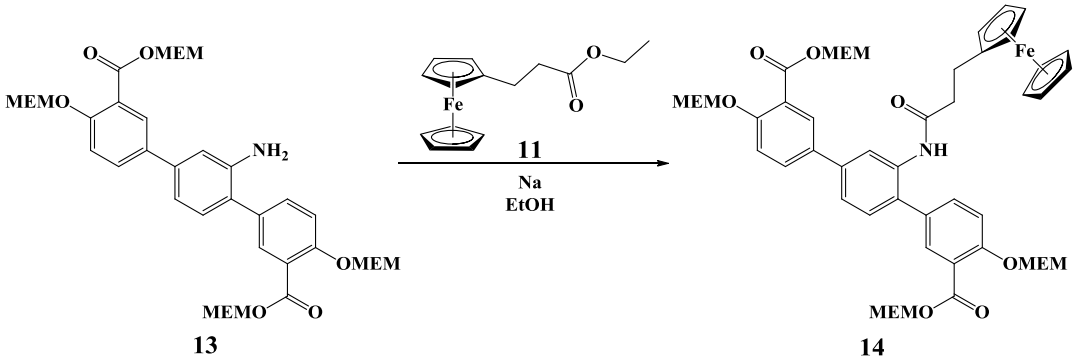

13 **14**

Sodium (0.105 g; 4.567 mmol) was completely dissolved in anhydrous ethanol (20 ml). Ethyl-3-ferrocenylpropanoate, **11** (0.704 g; 2.377 mmol) was slowly added to result in a light orange reaction mixture. Reaction mixture became a light orange colour. 4,4”-Di[methoxy–

ethoxymethoxy]-3'-amino-[1,1':4',1"-terphenyl]-3,3"-di[methoxyethoxymethoxycarbonyl], **13** (1.706 g; 2.377 mmol) was added dropwise to the reaction mixture. The reaction was stirred at room temperature for 16 hours, before removing the solvent under vacuo. Purification of the product was done by column chromatography on neutral alumina, (DCM: MeOH = 9:1, R_f = 0.35) to yield an orange oil (1.605 g; 70%). IR ν/cm^{-1} = 1620 (N-H), 1750 (C=O), 3000 (aromatic C-H), 3370 (N-H). ^{1}H NMR (400 MHz, $CDCl_3$) δ 7.68 (s, 1H), 7.50 – 7.30 (m, 2H), 7.08 (t, *J* = 8.9 Hz, 2H), 6.89 (s, 1H), 6.64 (t, *J* = 18.0 Hz, 1H), 6.52 (d, *J* = 5.3 Hz, 2H), 5.25 (s, 1H), 4.60 (m, 3H), 4.30 (m, 2H), 4.13 (s, 5H), 4.06 (s, 4H), 3.99 (m, 3H), 2.79 (s, 3H), 2.54 (m, 3H), 2.46 (m, 3H), Spectrum 1.2.10b, p. A8. ^{13}C NMR (600 MHz, $CDCl_3$) δ 173.20, 130.17, 118.81, 115.35, 87.51, 68.51, 67.92, 67.34, 60.39, 35.75, 24.89, 14.26; Spectrum 1.2.10c, p. A8. m/z = 825.74; found m/z = 830.633.

4.5.4 Deprotection of 4,4"-di[methoxyethoxymethoxy]-2',5'-dimethyl-[1,1':4',1"-terphenyl]-3,3"-di[methoxyethoxy-methoxycarbonyl], 3

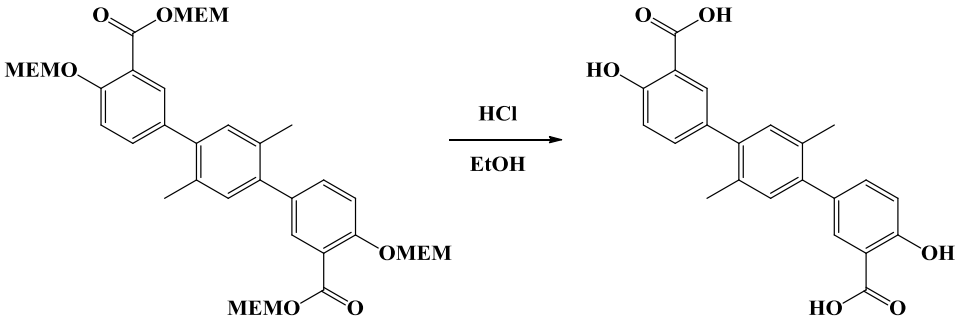

3 **4**

4,4"-Di[methoxyethoxymethoxy]-2',5'-dimethyl-[1,1':4',1"-terphenyl]-3,3"-di[methoxy-ethoxymethoxycarbonyl], **3** (0.950 g; 1.556 mmol) was dissolved in EtOH (25 ml). HCl (2 ml; 5 M) was added dropwise, and the solution refluxed with vigorous stirring for 2 hours. The reaction mixture was cooled to room temperature and extracted with DCM (3 x 60 ml). The combined organic extracts were extracted with 5% sodium bicarbonate solution. 5 % Hydrochloric acid was added to the combined water extracts, and then extracted with DCM (6 x 60 ml). The combined organic extracts was washed with Brine (3 x 60ml), dried with $MgSO_4$ and concentrated in vacuo to yield a white solid (300 mg; 60%). Melting point = 114^{o}C. IR ν/cm^{-1} = 1750 (C=O), 3000 (aromatic C-H), 3500 (O-H). ^{1}H NMR (600 MHz, $CDCl_3$) δ 10.44 (s,

2H), 7.84 (dt, *J* = 17.5, 8.7 Hz, 2H), 7.56 – 7.30 (m, 2H), 7.00 – 6.81 (m, 4H), 5.24 (s, 6H), Spectrum 1.2.3, p. A3.

4.5.5 Co-MOF-74-III solvothermal process

4,4”-Di[methoxyethoxymethoxy]-[1,1’:4’,1”-terphenyl]-3,3”-di[methoxyethoxymethoxy carbonyl] derivatives (**3**, **6**, **8**, **14**; 1 equivalent) was dissolved in DMF: MeOH: H_2O (1:1:1) by sonication. $Co(NO_2)_3.6H_2O$ (4 equivalents) was added to the solution and to ensure a homogeneity, the reaction mixture was sonicated for 30 minutes before it was transferred to a solvothermal reaction vessel, sealed and placed at 100^oC for 66 hours. After the vessel was cooled to room temperature, the solid product was obtained by centrifugation and washed with MeOH (3 x 60 ml). The product was purified in refluxing MeOH for 3 days with the MeOH being replaced once a day. The MeOH was first removed by evaporation and then under vacuum (8 x 10^{-1} Torr) at 100^oC for 16 hours. The characterization of the possible products is described below:

4.5.5.1 Co-MOF-74-III-Me

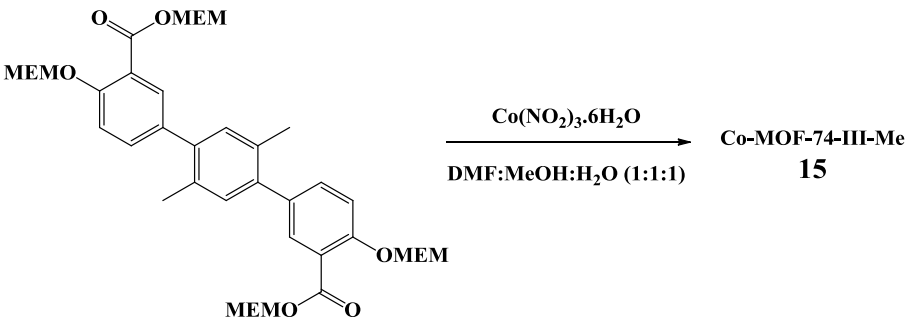

3

4,4”-Di[methoxyethoxymethoxy]-2’,5’-dimethyl-[1,1’:4’,1”-terphenyl]-3,3”-di[methoxy-ethoxymethoxycarbonyl], **3** (0.970 g; 1.327 mmol) and $Co(NO_2)_3.6H_2O$ (1.545 g; 5.309 mmol) were reacted to form a grey powder, 20 mg. IR ν/cm^{-1} = 3500 (O-H), 3000 (aromatic C-H), 1720 (C=O).

4.5.5.2 Co-MOF-74-III-OH

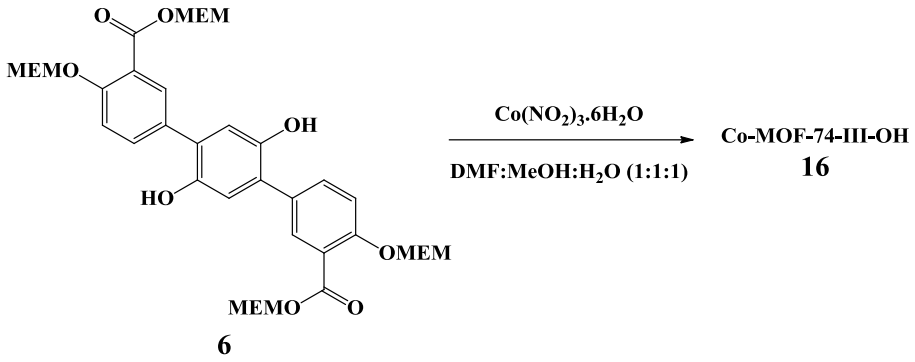

6

4,4”-Di[methoxyethoxymethoxy]-2’,5’-dihydroxy-[1,1’:4’,1”-terphenyl]-3,3”-di[methoxy-ethoxymethoxycarbonyl], **6** (4.36 g; 5.953 mmol) and $Co(NO_2)_3.6H_2O$ (6.93 g; 23.812 mmol) were reacted to form a black powder, 35 mg. IR ν/cm^{-1} = 3500 (O-H).

4.5.5.3 Co-MOF-74-III-OBn

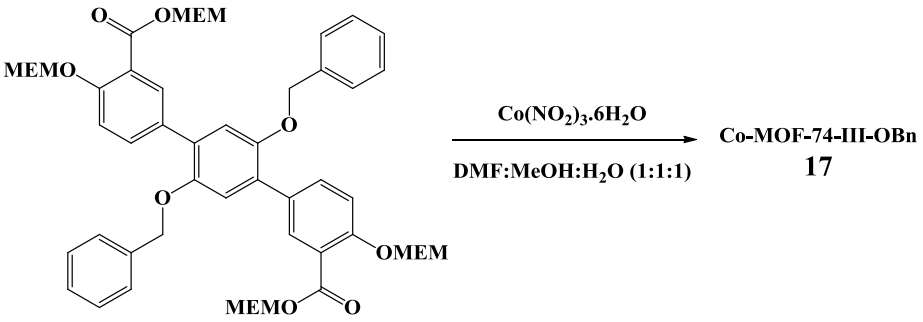

8

4,4”-Di[methoxyethoxymethoxy]-2’,5’-dibenzyloxy-[1,1’:4’,1”-terphenyl]-3,3”-di[methoxy-ethoxymethoxycarbonyl], 8 (1.15 g; 1.274 mmol) and $Co(NO_2)_3.6H_2O$ (1.483 g; 5.096 mmol) were reacted to form a grey powder, 5 mg. IR ν/cm^{-1} = 3500 (O-H).

4.5.5.4 Co-MOF-74-III-NHCOCH$_2$CH$_2$Fc

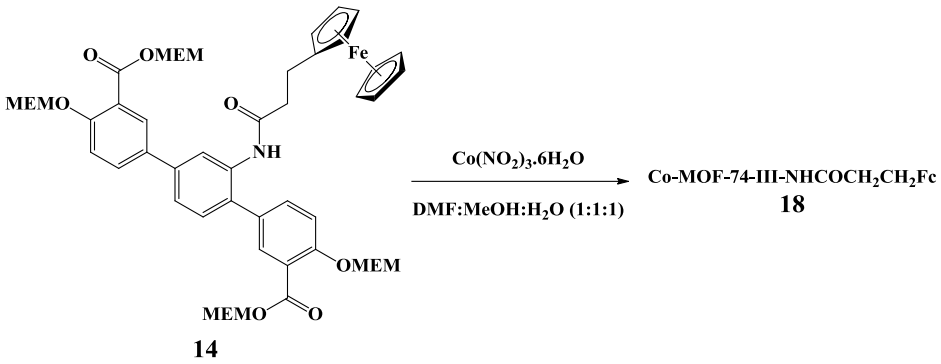

4,4''-Di[methoxyethoxymethoxy]-3'-[3-ferrocenylpropamide]-[1,1':4',1''-terphenyl]-3,3''-di[methoxyethoxymethoxycarbonyl], 14 (1.605 g; 1.663 mmol) and $Co(NO_2)_3.6H_2O$ (1.936 g; 6.654 mmol) were reacted to form a brown/grey powder, 2 mg. IR ν/cm^{-1} = 3500 (O-H), 3000 (aromatic C-H), 1750 (C=O).

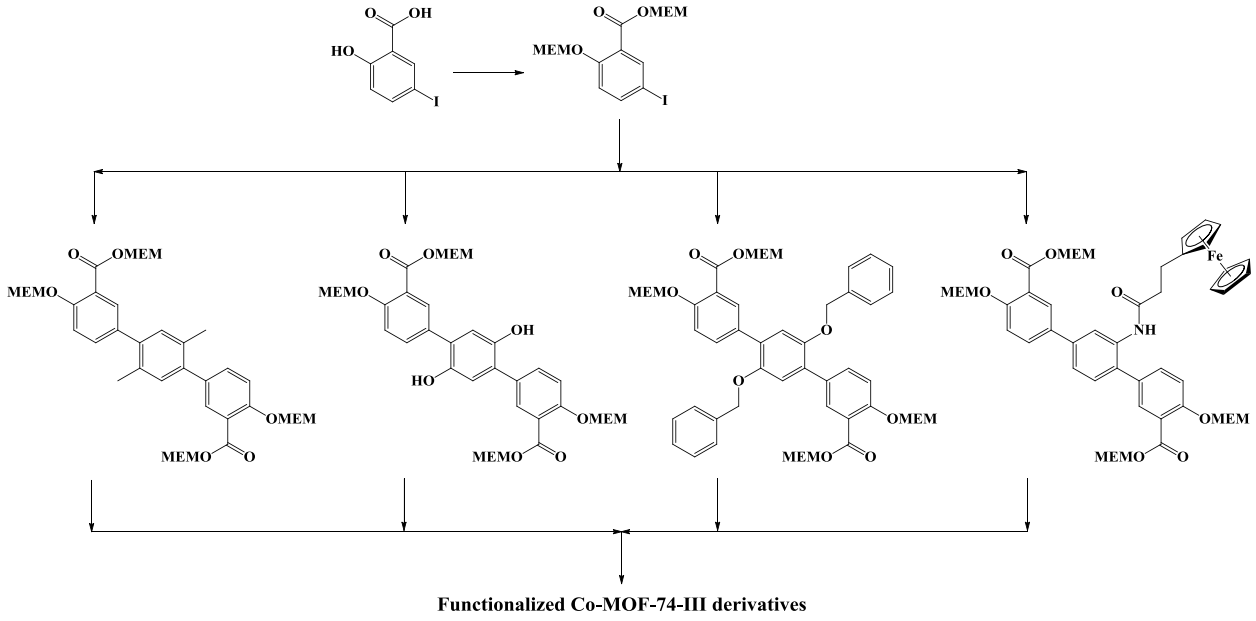

4.6 References

1. D. B. G. Williams, M. Lawton, *J. Org. Chem.*, **2010**, 75, 8351.

5 Conclusion and Future Perspectives

5.1 Conclusion

The general route for the synthesis of 4,4”-di[methoxyethoxymethoxy]-[1,1’:4’,1”-terphenyl]-3,3”-di[methoxyethoxymethoxycarbonyl] derivatives, starting with the protection of reactive sites, cross-coupling reaction and ending with the deprotection of reactive sites, consists of five steps. In this study the same basic route was followed, but with less synthesis steps. It was found the deprotection step, before MOF-74-III formation, was not nessecary if the correct protecting group was used. Methoxyethoxymethoxy chloride (MEMCl) was found to be such a general protecting group. While different protecting groups were previously used for the hydroxy- and carboxylic acid functionalities of the starting material, both these functionalities were protected with MEMCl in this study. When used for MOF-74-III synthesis, deprotection of the functionalized linkers is redundant since the MEM-protecting group can be easily cleaved by the acid present during the reaction.

For the formation of carbon-carbon bonds the Suzuki-Miyuara cross-coupling reaction was used. An excess base, KOAc, and excess catalyst, $(PPh_3)_2PdCl_2$, as well as a lower reaction temperature of 60 ^oC resulted in a high yield of the desired linkers. This correlates to literature which suggests that the base plays an important role in the transmetallation step of the catalytic cycle, and the appropriate catalyst results in the retardation of side-reactions. With these appropriate reaction conditions, the synthesis of 4,4”-di[methoxyethoxymethoxy]-2’,5’-dimethyl-[1,1’:4’,1”-terphenyl]-3,3”-di[methoxyethoxymethoxycarbonyl], **3** (90 %); 4,4”-di[methoxyethoxymethoxy]-2’,5’-dihydroxy-[1,1’:4’,1”-terphenyl]-3,3”-di[methoxyethoxy-methoxycarbonyl], **6** (90 %); 4,4”-di[methoxyethoxymethoxy]-2’,5’-bis-benzyloxy-[1,1’:4’,1”-terphenyl]-3,3”-di[methoxyethoxymethoxycarbonyl], **8** (60 %) and 4,4”-di[methoxyethoxymethoxy]-3’-nitro-[1,1’:4’,1”-terphenyl]-3,3”-di[methoxyethoxy-methoxy-carbonyl], **12** (90 %), was successful. These products were successfully characterized by means of FTIR transmission, NMR spectroscopy and MS spectrometry. Suzuki-Miyuara cross-coupling reaction is a versatile reaction and with the appropriate reaction conditions, this carbon-carbon

formation reaction was used to form all the linkers in this study. The reaction conditions is not that harsh and can accommodate a wide range of functional groups (-CH_3; -OH; -OBn; -NO_2; -NH_2; -$NHCOCH_2CH_2Fc$).

Modification of the nitro-functionality on 4,4”-di[methoxyethoxymethoxy]-3’-nitro-[1,1’:4’,1”-terphenyl]-3,3”-di[methoxyethoxymethoxycarbonyl], **12**, proceeded through utilization of the Buchamp reduction reaction, forming the 4,4”-di[methoxyethoxymethoxy]-3’-amino-[1,1’:4’,1”-terphenyl]-3,3”-di[methoxyethoxymethoxycarbonyl], **13** intermediate, which was further reacted with ethyl-3-ferrocenylpropanoate, **11** to give 4,4”-di[methoxyethoxymethoxy]- 3’-[3-ferrocenylpropamide]-[1,1’:4’,1”-terphenyl]-3,3”-di[methoxyethoxymethoxycarbonyl], **14** (70 %). This reaction demonstrates that bulky moieties can by successfully attatched via biodegradable amide bonds to MOF-74-III linkers. Other substituents can also be attached to the amine forming secondary, tertiary and quartenary amines, or the amine functionality can completely be converted to another functional group like an amide, imine, oxime, hydrazone, triflates, and an endless number of other options.

Thus the synthesis of structural isomers containing a different layout than that found in literature[6, 7] was successful. The synthesis of MOF-74-III from a structural different isomer was never attempted before and proved to reduce the cost of MOF-74-III synthesis. This is because the starting material used in literature, methyl-2-hydroxy-4-iodobenzoate, is more expensive than the starting material used in this study, 5-iodosalicylic acid. Synthesis expenditure was further reduced with the use of the same protecting group for the hydroxy- and carbonyl-functionalities.

Co-MOF-74-III-Me, **15** and Co-MOF-74-III-$NHCOCH_2CH_2Fc$, **18**, were successfully synthesized using solvothermal reaction conditions with the appropriate structural isomers, as proven by FTIR studies.

Accelerated Surface Area and Porosity Analysis (ASAP) showed that Co-MOF-74-III-Me, **15**, is mesoporous with a pore width of 32.6 Å. Due to insufficient sample amounts, the FTIR results of the other Co-MOF-74-III derivatives, could not be confirmed by ASAP.

Thermogravimetric Analyses (TGA) of Co-MOF-74-III-Me, **15** and Co-MOF-74-III-$NHCOCH_2CH_2Fc$, **18**, showed that these derivatives are stable up to 180 ^oC.

The Scanning Electron Microscopy (SEM) image of Co-MOF-74-III-Me, **15**, is similar to that found in literature, synthesised from the original structural isomer of 4,4”-di[methoxyethoxy-methoxy]-2’,5’-dimethyl-[1,1’:4’,1”-terphenyl]-3,3”-di[methoxyethoxymethoxycarbonyl], **3**. MOF formation could not be confirmed for the –OH and –OBn functionalized 4,4”-di[methoxy-ethoxymethoxy]- -[1,1’:4’,1”-terphenyl]-3,3”-di[methoxyethoxymethoxycarbonyl] derivatives, **6** and **8** respectively. The solid products obtained after Solvothermal synthesis with these ligands were both non-porous. The compounds have morphologies completely different from that of compound **15**, concluding that they are not MOF-74 derivatives.

Electrochemical analyses of the 4,4”-di[methoxyethoxymethoxy]-[1,1’:4’,1”-terphenyl]-3,3”-di[methoxyethoxymethoxycarbonyl] derivatives showed irreversible couples for the carbonyl functionality of the MEM-group (-1500 mV vs. FcH/FcH^{+}) and an extra couple for the carbonyl of the amide functionality on the 4,4”-di[methoxyethoxymethoxy]- 3’-[3-ferrocenylpropamide]-[1,1’:4’,1”-terphenyl]-3,3”-di[methoxyethoxymethoxycarbonyl], **14** linker. Solid state cyclic voltammetry of Co-MOF-74-III-$NHCOCH_2CH_2Fc$, **18**, shows clear reduction-oxidation peaks for the ferrocene moiety on the linker. This observation is possible due to the mesoporous material allowing fast enough electron transfer.

5.2 Future Perspectives

Optimization of the synthesis conditions during MOF formation could increase the yields. Using bench-top conditions does not generate the pressure and high temperatures of solvothermal conditions, and this might increase the reaction time, resulting in higher yields. Better purification procedures should be developed to clean the pores of the synthesized MOF-74-III derivatives. This would result in much higher observed surface areas and pore volumes.

The addition of other functional groups on the central phenylene ring need to be investigated like: SO_2; PO_3; $B_2(OH)_4$; just to mention a few. Post synthetic modification of the different functionalities on the MOFs can also be investigated. Co-MOF-74-III formation with an anime-functionality on the central phenylene ring should also be attempted and possible post synthetic modification of that functionality.

CONCLUSION AND FUTURE PERSPECTIVES

Low temperature Fischer-Tropsch (LTFT) synthesis using a Co-based catalyst produces long chain hydrocarbons and wax, which can be hydrocracked to give exceptional quality diesel.[2] Co-MOF-74-III-$NHCOCH_2CH_2Fc$, **18**, should be tested to determine the activity of this MOF as a catalyst for the low temperature Fischer-Tropsch synthesis of wax and long chain hydrocarbons. The combination of Co and Fe in the structure could even have a synergistic effect in this regard.

Boron- and ferrocene- containing compounds are known for their cancer therapy treatment.[8] By linking these compound to the central phenylene ring through a simple, biodegradable bridge, functionalized MOF-74-III derivatives can be effective in drug delivery. This could lead to a new field of study.

These linkers may also be combined with other metals, like Fe, Ni, Mg and Zn. These results could then be compared with the results obtained for the different Co-MOF-74-III derivatives, to identify the effect the metal have. Ni-Ga catalysts were recently used to reduce CO_2 to methanol at ambient temperatures.[4] Methanol is an excellent fuel and can be blended with gasoline. Direct methanol fuel cells, is much saver to the environment than other cells.[5] The linkers synthesized in this study can be used in a Ni-Ga mixed-metal MOF, and tested for CO_2 convertion to methanol.

5.3 References

1. A. Staniszewski, W. B Heuer, G. J. Meyer, *Inorg. Chem*., **2008**, 47, 7062.
2. R.L. Espinoza, A.P. Steynberg, B. Jager, A.C. Vosloo, *Applied Catalysis A: General*, **1999**, 186, 13.
3. P. F. Liu, S. Yang, B. Zhang, H. G. Yang, *ACS Appl. Mater. Interfaces*, DOI: 10.1021/acsami.6b12803.
4. F. Studt, I. Sharafutdinov, F. Abild-Pedersen, C. F. Elkjær, J. S. Hummelshøj, S. Dahl, I. Chorkendorff, J. K. Nørskov, *Nature Chemistry*, **2014**, 6, 320.
5. G. A. Olah, *Angew. Chem. Int. Ed*., **2005**, 44, 2636.
6. H. Deng, S. Grunder, K. E. Cordova, C. Valente, H. Furukawa, M. Hmadeh, F. Gándara, A.C. Whalley, Z. Liu, S. Asahina, H. Kazumori, M. O'Keeffe, O. Terasaki, J. F. Stoddart, O. M. Yaghi, *Science*, **2012**, 336, 6084, 1018.
7. A. M. Fracaroli, H. Furukawa, M. Suzuki, M. Dodd, S. Okajima, F. Gándara, J. A. Reimer, O. M. Yaghi, *J. Am. Chem. Soc*., **2014**, 136, 8863.
8. Hawthorne, M.F., Maderna, A., Chem. Rev., **1999**, 99 (12), 3421.

CONCLUSION AND FUTURE PERSPECTIVES

Appendix

1.1 NMR

1.1.1 Spectrum 1.2.1: 5-iodo-methoxyethoxymethoxy-2-methoxyethoxymethoxycarbonyl-phenyl, 1

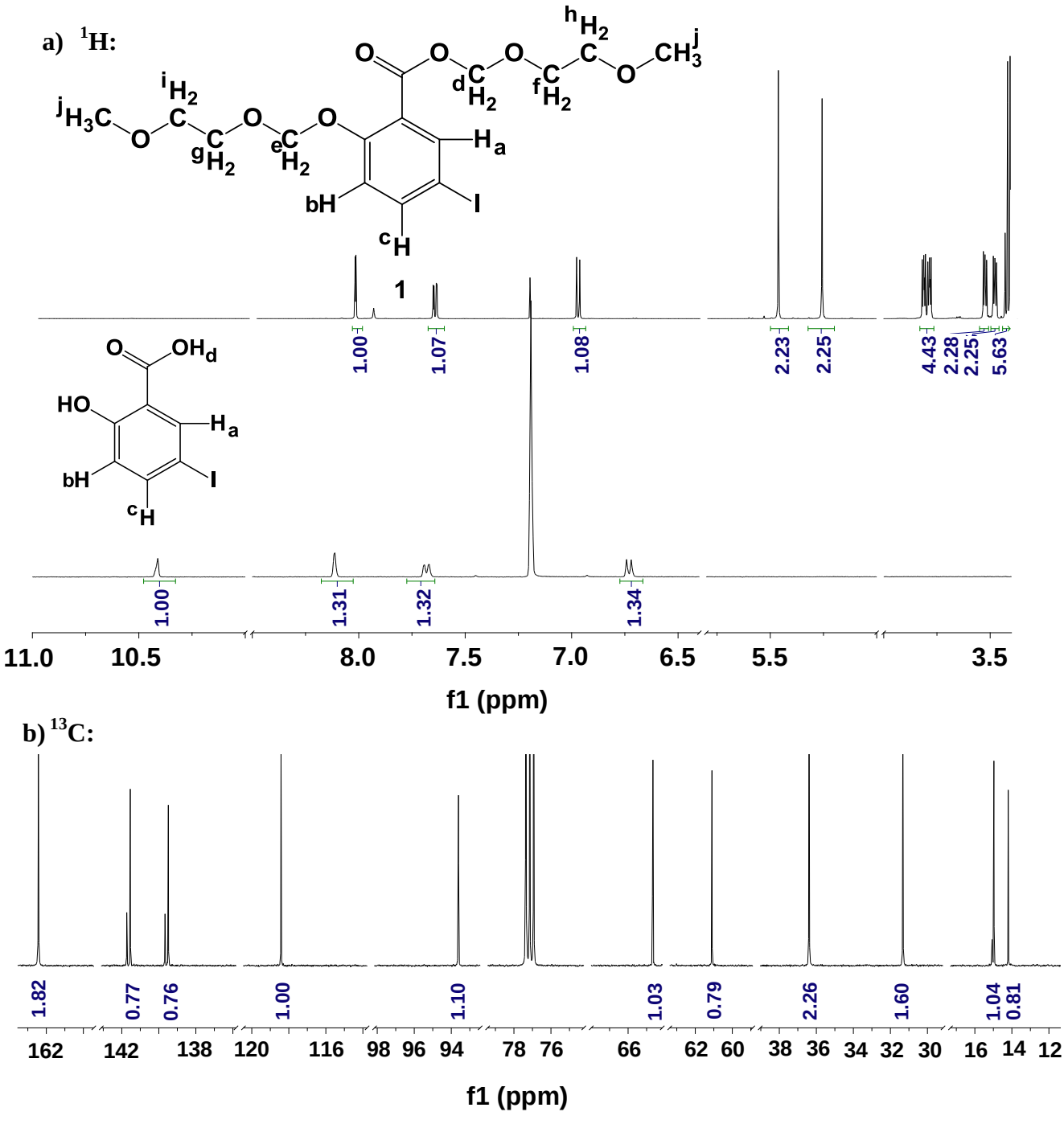

1.1.2 Spectrum 1.2.2: 4,4”-di[methoxyethoxymethoxy]-2’,5’-dimethyl-[1,1’:4’,1”-terphenyl]-3,3”-di[methoxyethoxymethoxycarbonyl], 3

a)

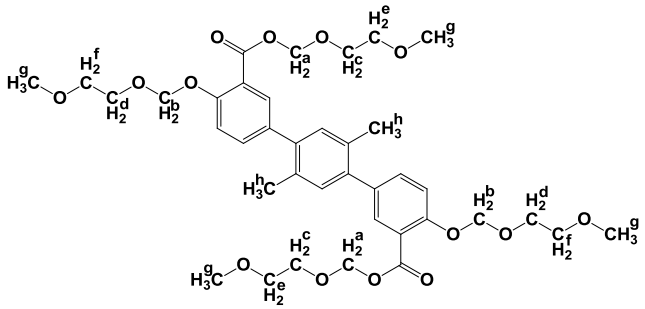

b) ^{1}H:

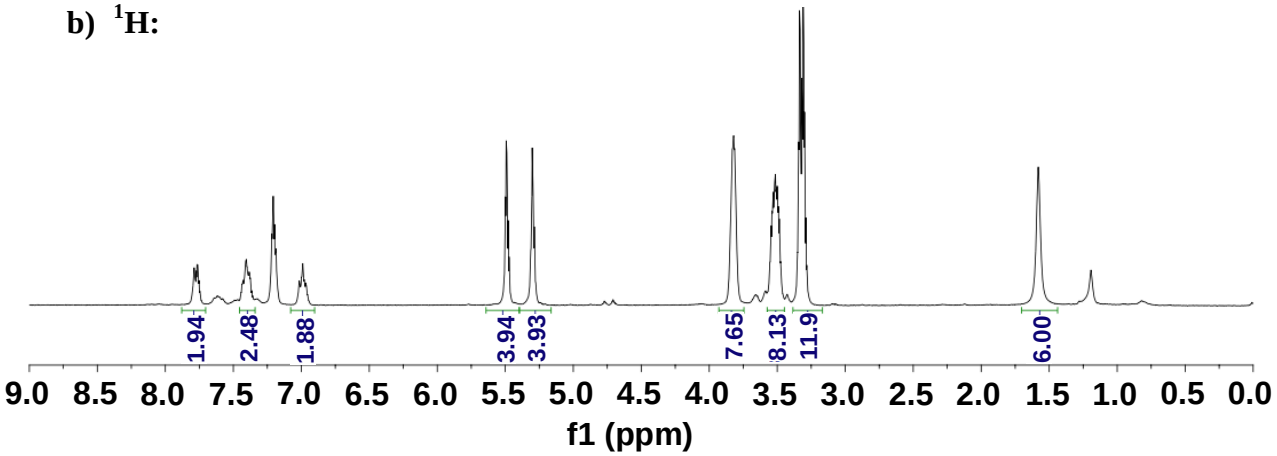

c) ^{13}C:

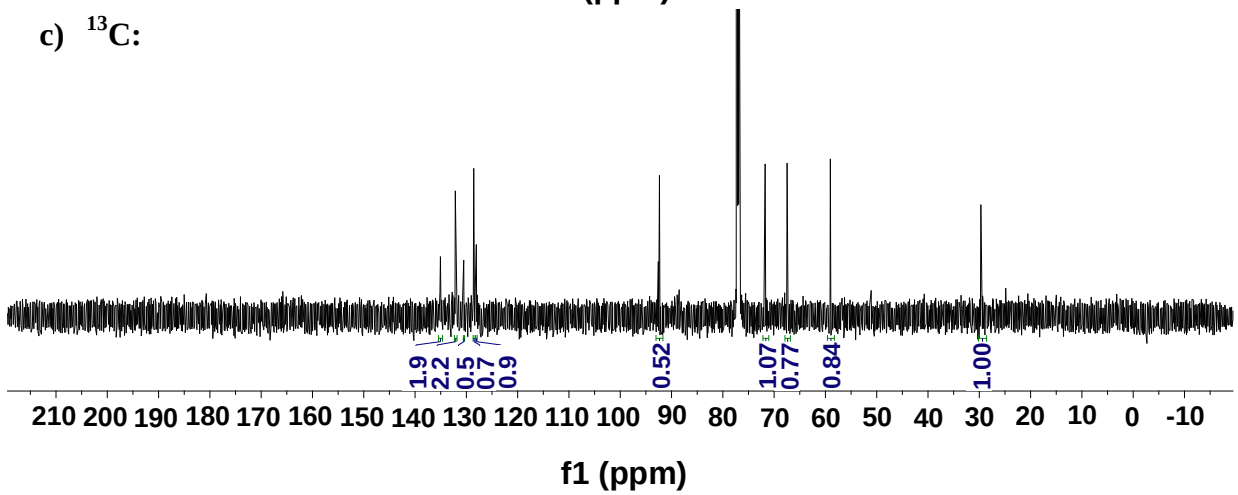

1.1.3 Spectrum 1.2.3: 4,4”-di[hydroxy]-2’,5’-dimethyl-[1,1’:4’,1”-terphenyl]-3,3”-dicarboxylic acid, 4

a)

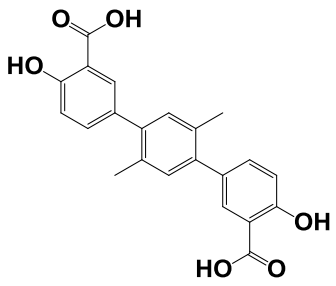

4

b) ^{1}H:

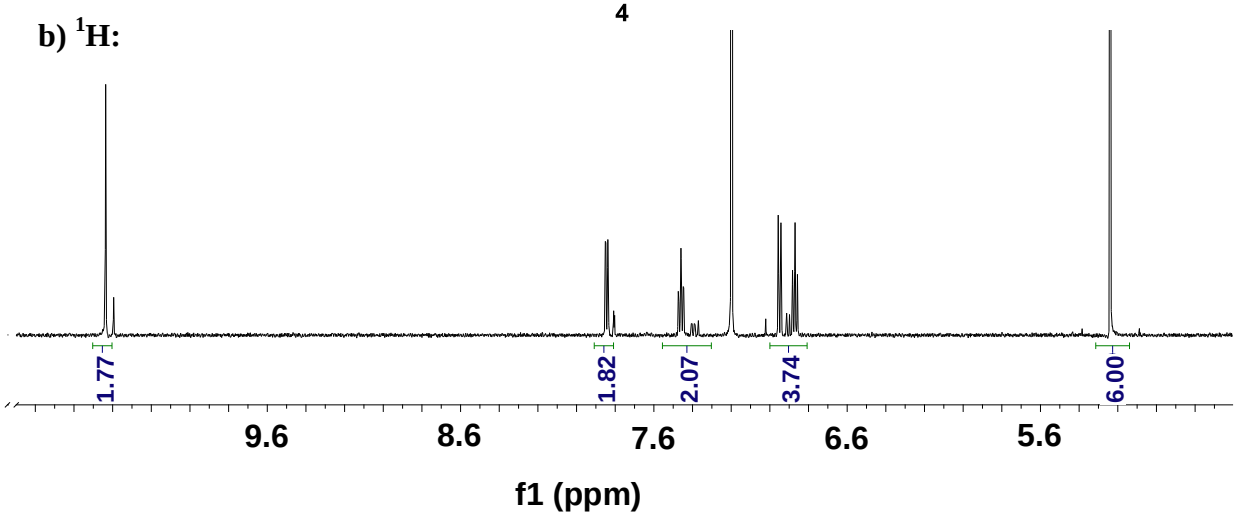

1.1.4 Spectrum 1.2.4: 4,4”-di[methoxyethoxymethoxy]-2’,5’-dihydroxy-[1,1’:4’,1”-terphenyl]-3,3”-di[methoxyethoxymethoxycarbonyl], 6

a)

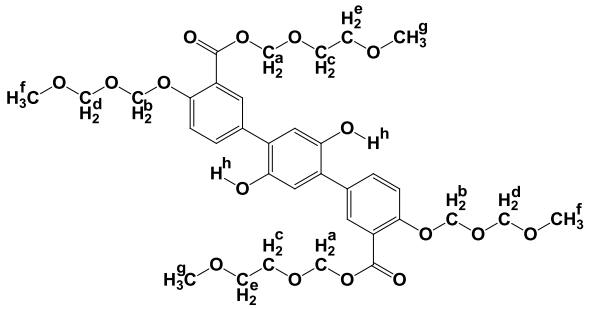

b) ^{1}H:

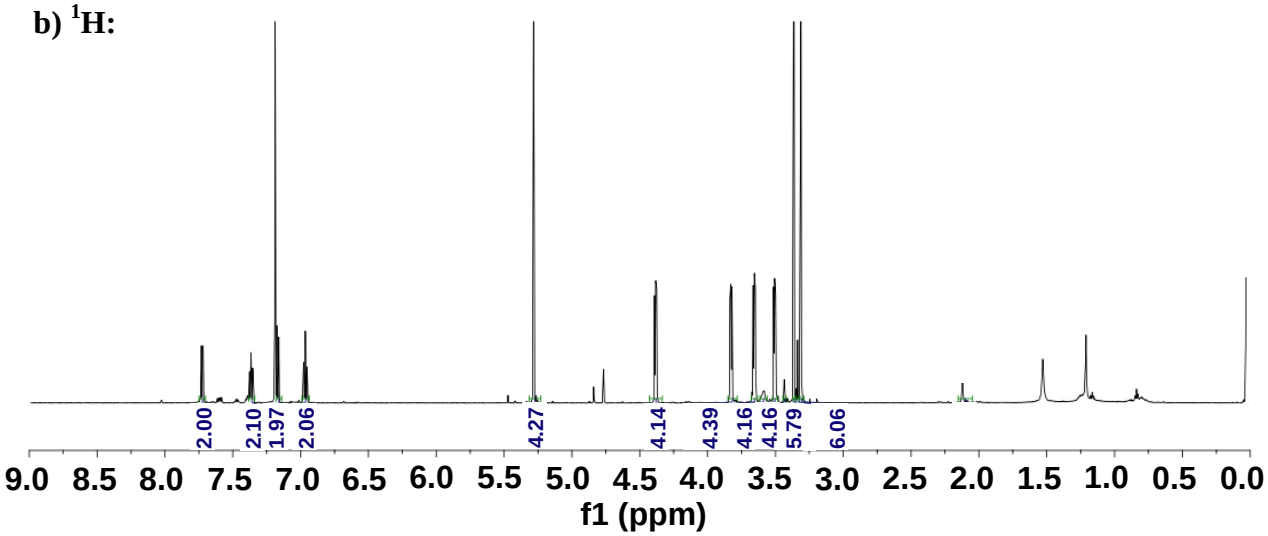

c) ^{13}C:

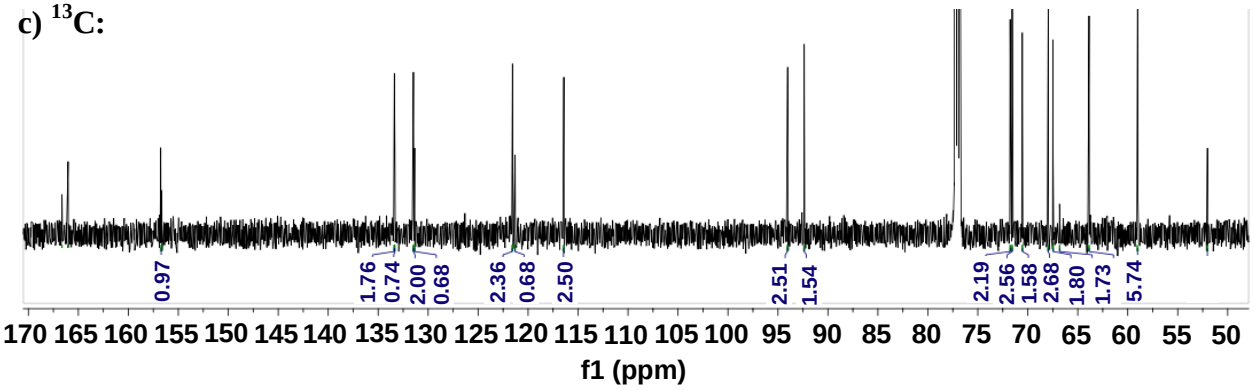

1.1.5 Spectrum 1.2.6: 1,4-bisbenzyloxy-2,5-dibromophenyl, 5

a)

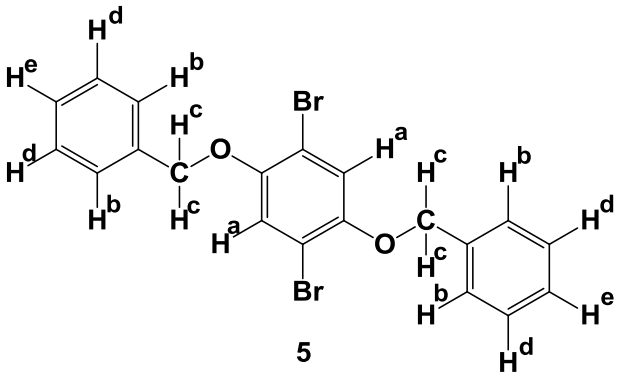

5

b) ^{1}H:

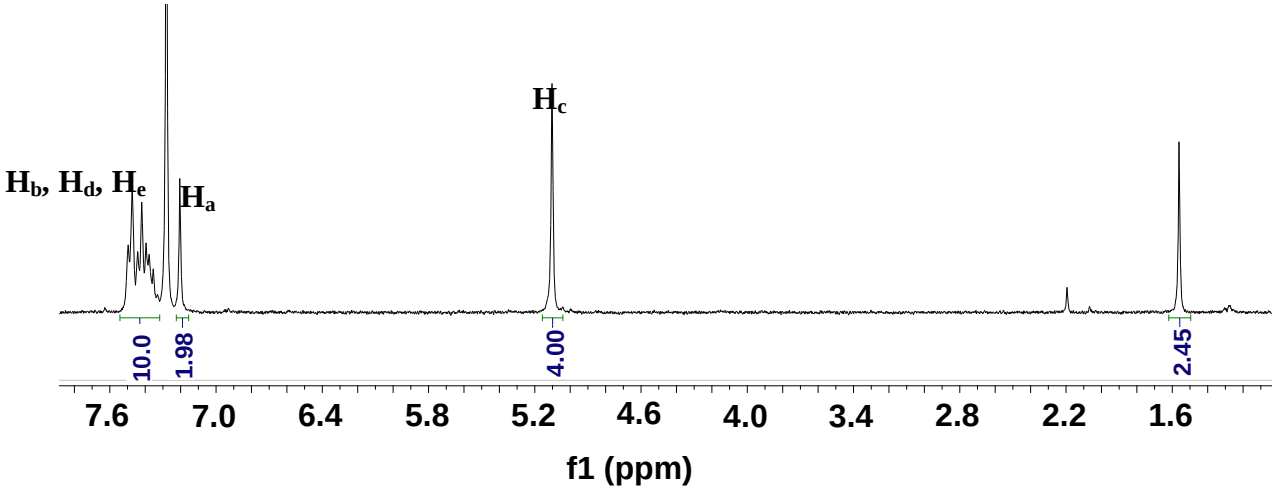

c) ^{13}C:

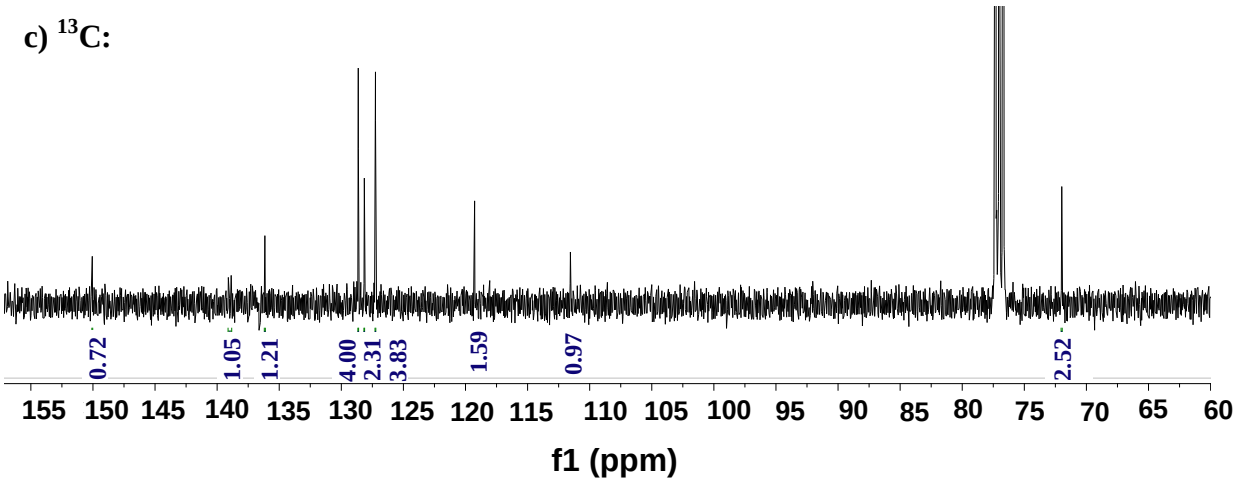

1.1.6 Spectrum 1.2.7: 4,4”- di[methoxyethoxymethoxy]-2’,5’-bis-benzyloxy-[1,1’:4’,1”-terphenyl]-3,3”-di[methoxyethoxymethoxycarbonyl], 8

a)

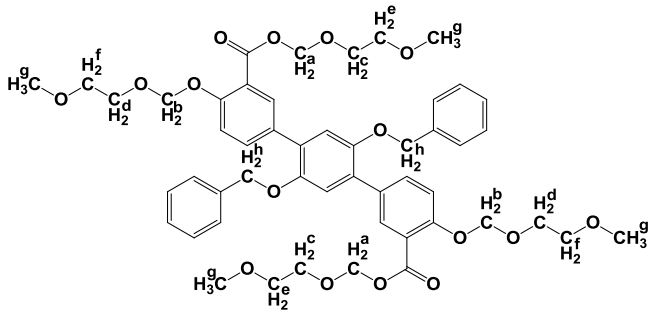

b) ^{1}H:

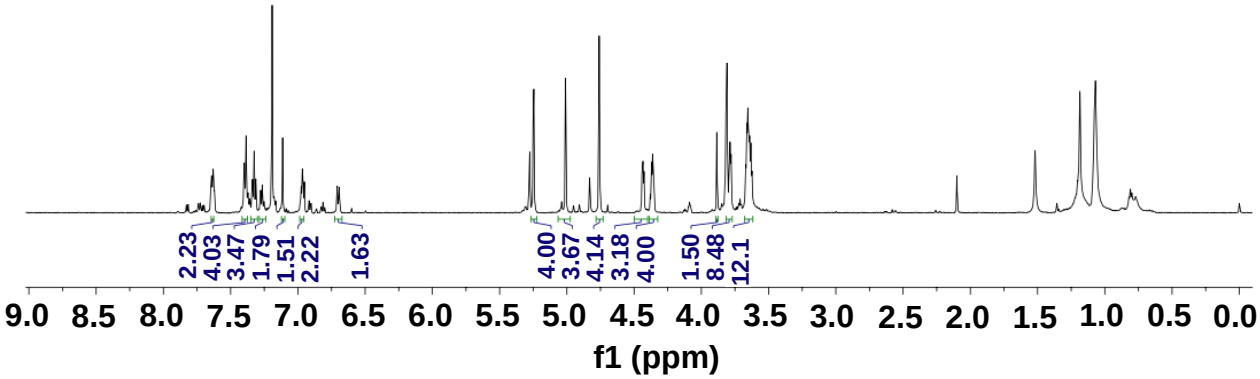

1.1.7 Spectrum 1.2.8: 4,4”-di[methoxyethoxymethoxy]-3’-nitro-[1,1’:4’,1”-terphenyl]-3,3”-di[methoxyethoxymethoxycarbonyl], 12

a)

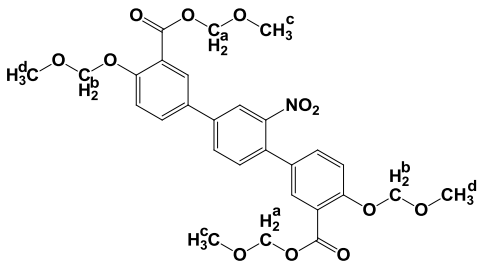

b) ^{1}H:

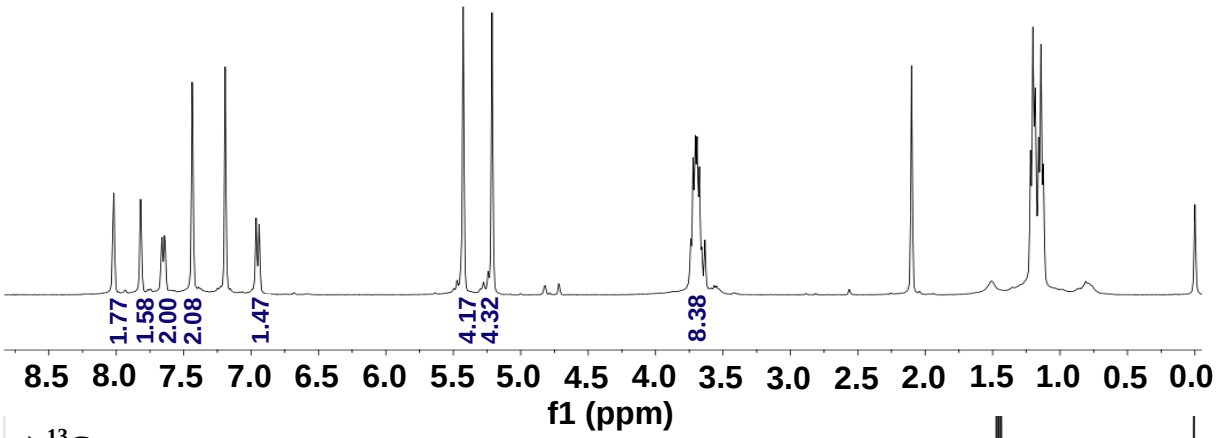

c) ^{13}C:

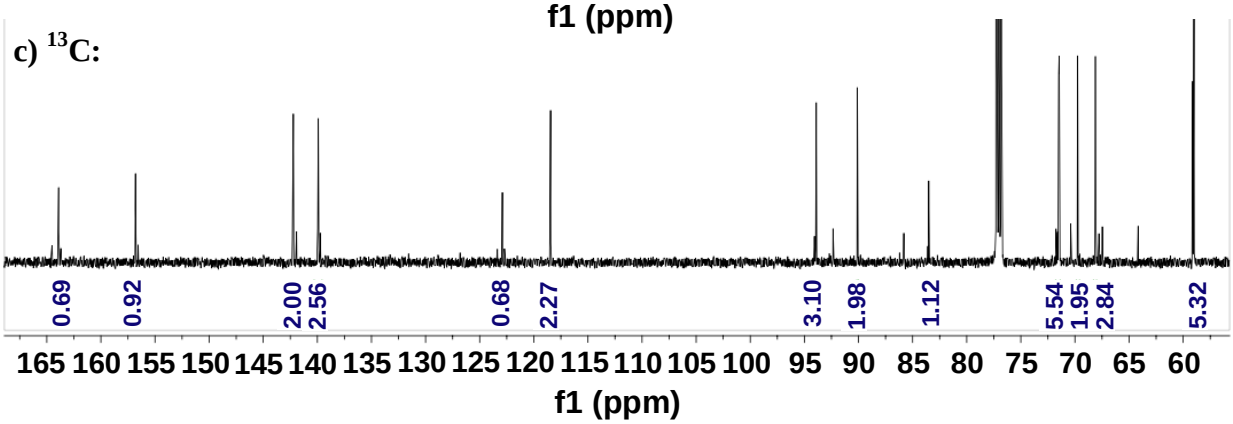

1.1.8 Spectrum 1.2.9: 4,4”-di[methoxyethoxymethoxy]-3’-[3-ferrocenylpropamide]-[1,1’:4’,1”-terphenyl]-3,3”-di[methoxy-ethoxymethoxycarbonyl], 14

a)

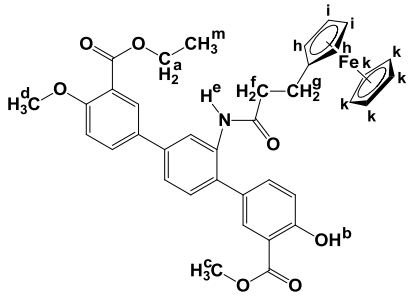

b) ^{1}H:

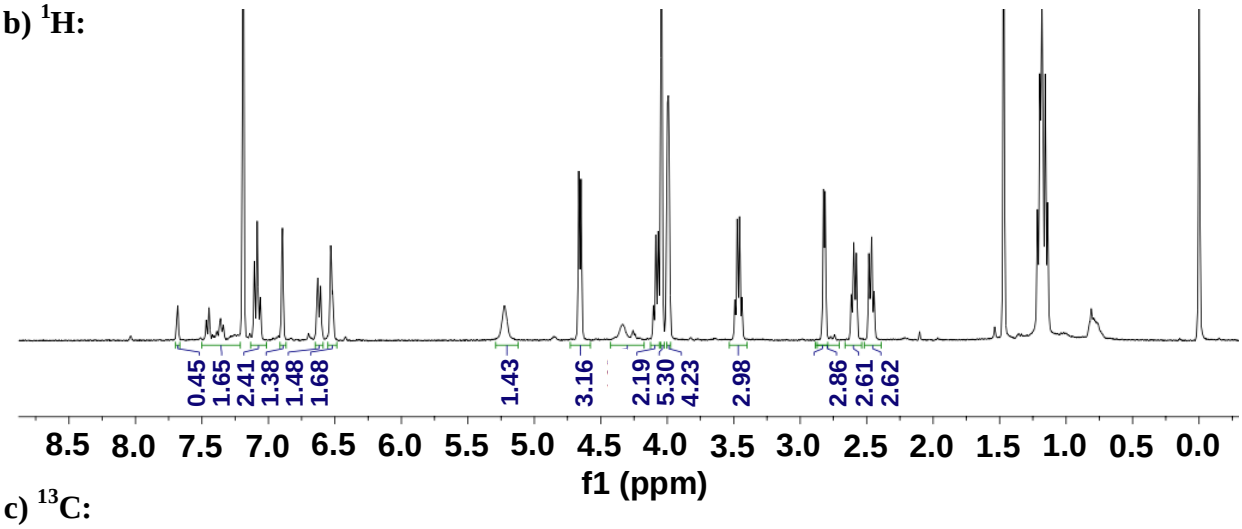

c) ^{13}C:

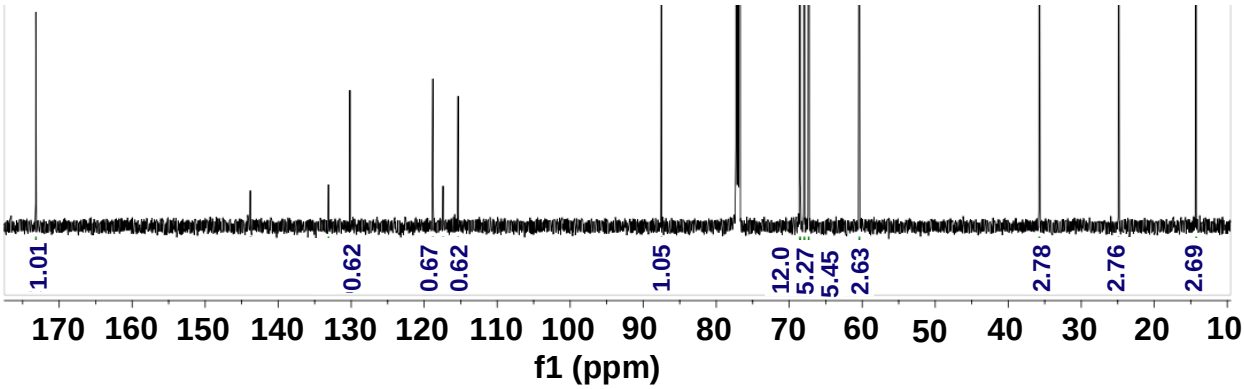

1.2 Electrochemistry

1.2.1 Spectrum 1.3.1: 5-iodo-methoxyethoxymethoxy-2-methoxy-ethoxymethoxycarbonyl-phenyl, 1

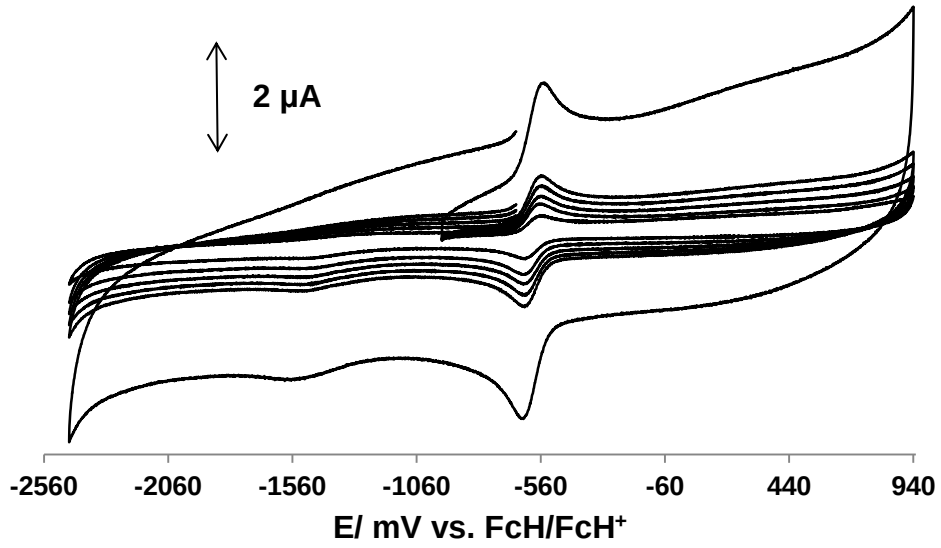

1.2.2 Spectrum 1.3.2: 4,4”-di[methoxyethoxymethoxy]-2’,5’-dimethyl-[1,1’:4’,1”-terphenyl]-3,3”-di[methoxyethoxy-methoxycarbonyl], 3

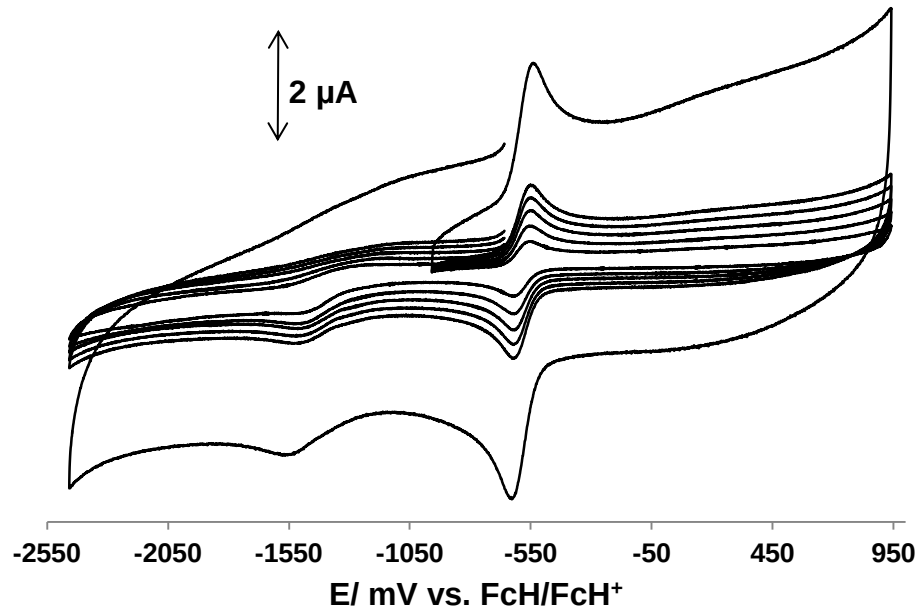

1.2.3 Spectrum 1.3.3: 4,4”-di[methoxyethoxymethoxy]-2’,5’-dihydroxy-[1,1’:4’,1”-terphenyl]-3,3”-di[methoxyethoxy-methoxycarbonyl], 6

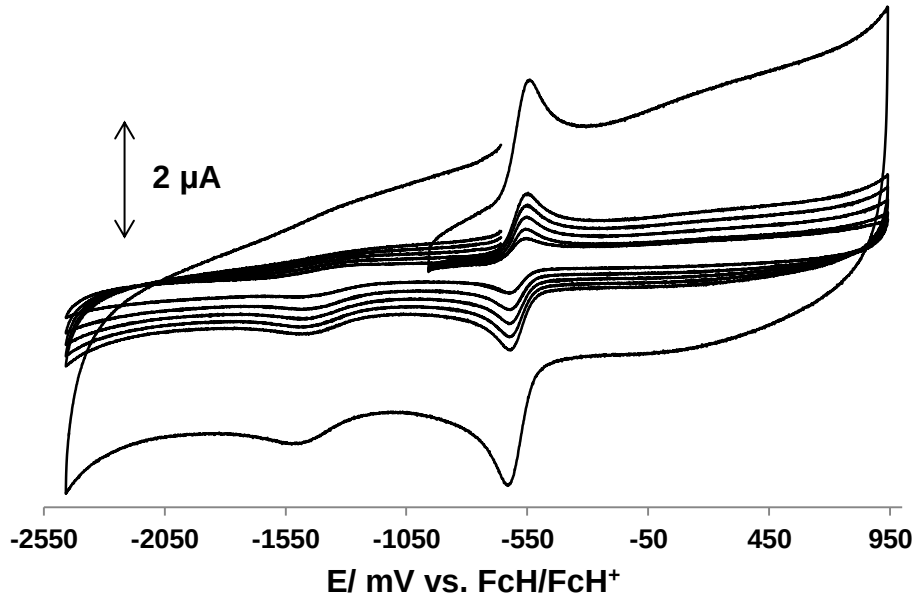

1.2.4 Spectrum 1.3.4: 4,4”-di[methoxyethoxymethoxy]-2’,5’-bis-benzyloxy-[1,1’:4’,1”-terphenyl]-3,3”-di[methoxyethoxy-methoxycarbonyl], 8

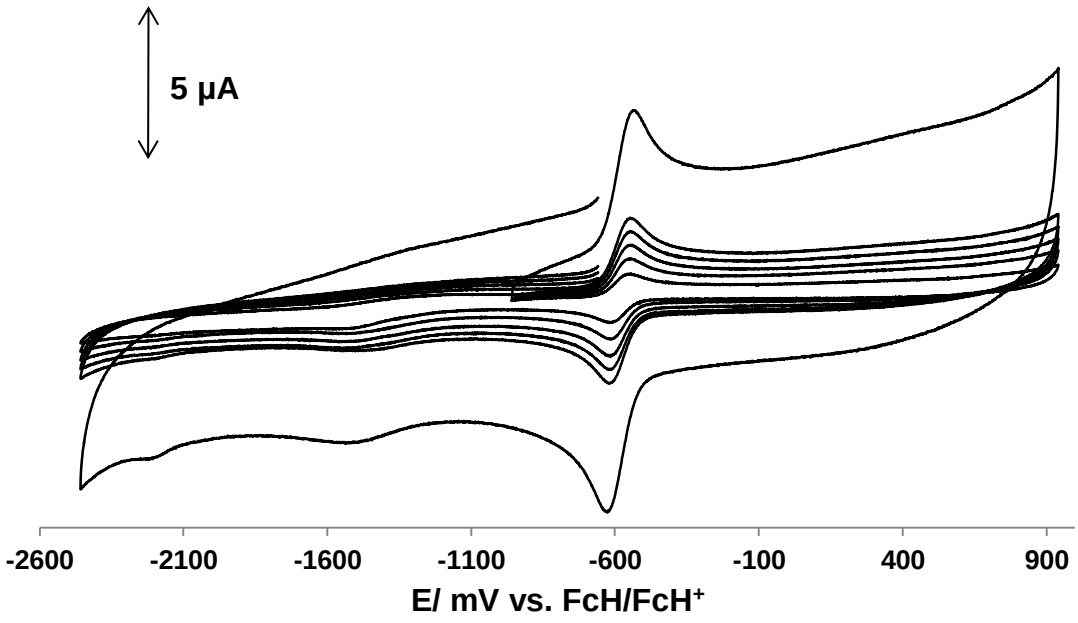

1.2.5 Spectrum 1.3.5: 4,4”-di[methoxyethoxymethoxy]-3’-[3-ferrocenylpropamide]-[1,1’:4’,1”-terphenyl]-3,3”-di[methoxy-ethoxymethoxycarbonyl], 14

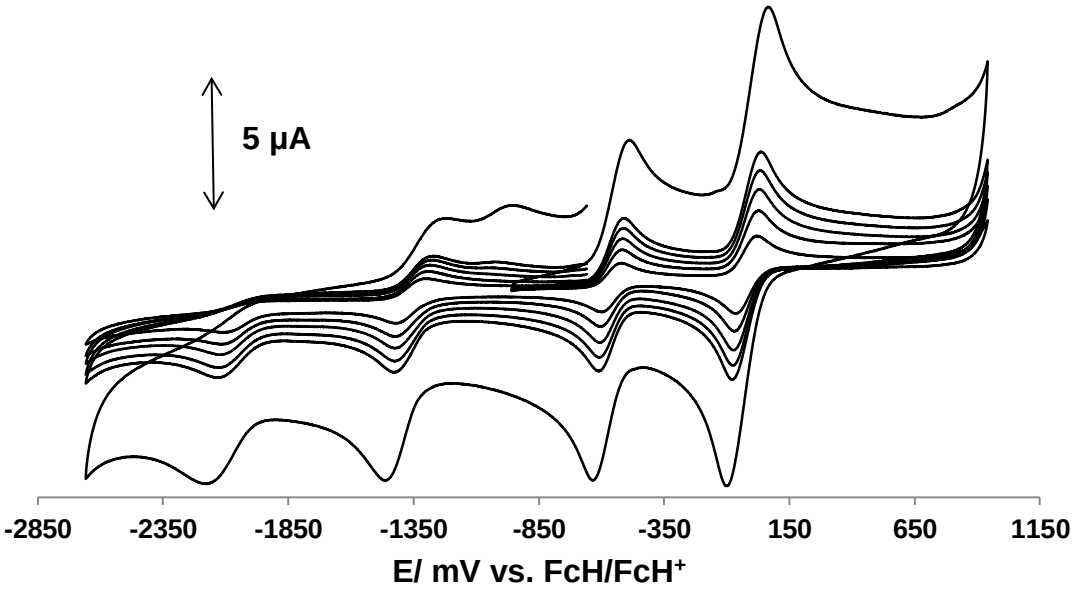

Declaration

(i) I, Annelmie Crause, declare that the Master's Degree research dissertation, that I herewith submit for the Master's Degree qualification, Magister Scientiae, at the University of the Free State is my independent work, and that I have not previously submitted it for a qualification at another institution of higher education.

(ii) I hereby declare that I am aware that the copyright is vested in the University of the Free State.

(iii) I hereby declare that all royalties as regards intellectual property that was developed during the course of and/or in connection with the study at the University of the Free State will accrue to the University.

Signed:  Date: 12 - 04 - 2017